THE UNIVERSITY *of* EDINBURGH

This thesis has been submitted in fulfilment of the requirements for a postgraduate degree (e.g. PhD, MPhil, DClinPsychol) at the University of Edinburgh. Please note the following terms and conditions of use:

- This work is protected by copyright and other intellectual property rights, which are retained by the thesis author, unless otherwise stated.
- A copy can be downloaded for personal non-commercial research or study, without prior permission or charge.
- This thesis cannot be reproduced or quoted extensively from without first obtaining permission in writing from the author.
- The content must not be changed in any way or sold commercially in any format or medium without the formal permission of the author.
- When referring to this work, full bibliographic details including the author, title, awarding institution and date of the thesis must be given.

Modification and Use of Polymeric Particles for Chemical Biology

Frank Thielbeer

Doctor of Philosophy

The University of Edinburgh

2012

Abstract

Polymeric nano and microparticles are important tools for an increasing variety of applications in the life sciences such as cellular delivery, sensing and imaging, with a fundamental requirement being particle functionalisation. Herein, the use of zeta potential measurements is described as a convenient tool to allow a variety of chemical reactions to be rapidly monitored on particles. To allow multi-functionalisations these particles need to be orthogonally modified. As part of this thesis, novel dual-functionalised aminomethyl and boronic acid particles were synthesised. These particles could be modified via amide formation and palladium-mediated cross coupling, with applications demonstrated in cellular delivery and cell-based cargo release. The requirement for bright fluorescent particles for applications in the life sciences was addressed by the synthesis and analysis of particles prepared using polymerisable fluorescein derivatives. Although nanoparticles are a promising technology to solve a variety of problems, their behaviour in biological systems is not fully understood. Herein, the effects of the particle's surface chemistry on cellular uptake and toxicity were investigated.

Table of Contents

Declaration

This thesis has been composed by the author, and describes research carried out by the author under the supervision of Professor Mark Bradley at the University of Edinburgh. Where work has been performed either jointly or wholly by others, this is clearly attributed. No part of this thesis has been previously submitted for any other degree or professional qualification.

Parts of this thesis were published previously or have been submitted as:

Thielbeer, F., Donaldson K. and Bradley M. Zeta Potential Mediated Reaction Monitoring on Nano and Microparticles. *Bioconjugate Chemistry* **2011**, *22*, 144-150.

Thielbeer, F. Fluorescein. *Synlett*, **2012**, *23*, 1703-1704.

Thielbeer, F., Chankeshwara, S. V. and Bradley, M. Polymerizable fluorescein derivatives: synthesis of fluorescent particles and their cellular uptake. *Biomacromolecules* **2011**, *12*, 4386-4391.

Thielbeer, F., Chankeshwara, S. V., Johansson, E. M. V. and Bradley M. Pd-mediated bio-orthogonal conjugation of nanoparticles for intracellular delivery and targeting. *Submitted* **2012**.

Cho, W.-S., Thielbeer, F., Duffin, R. Johansson, E. M. V., Megson, I. L., MacNee, W., Bradley, M. and Donaldson, K. Functionalization affects the zeta potential, coronal stability and membranolytic activity of polystyrene latex particles. *Submitted* **2012**.

Signed: Date:

Acknowledgements

First of all I would like to thank Prof Mark Bradley for giving me the opportunity to carry out my PhD in his research group. Throughout my PhD, he was supportive and encouraging to help me to overcome problems and the first time we met, he told me that 'I will have a lot of fun with my project and that is what the PhD is about' and he was absolutely right – it was fantastic.

I also would like to thank Dr Sunay Chankeshwara for his constant advice and help during my time in Edinburgh. He is a great source of knowledge and it was an absolute pleasure to work with him. Equally, Dr Emma Johansson was around all the time to answer questions and providing a helping hand if needed. In addition, I would like to thank Prof Ken Donaldson and Dr Wan-Seob Cho for their collaboration and giving me the insights into the field of nanotoxicology.

A enourmous thanks is reserved for the biolab team, Anne Hansen, Dr Annamaria Lilienkampf (also for her proof reading skills) and Emma, making the biological experiments in this thesis possible. I would also like to thank Dr Ron Brown (BET), Dr Nicola Cayzer (SEM), Dr Lorna Eades (ICP-OES) and Dr David Kelly (fluorescence microscope) for their assistance with the technical equipment.

Additionally; I would like to thank Dr Juanma Cardenas-Maestre, Dr Nicos Avlonitis and Dr Tashfeen Walton for spending time to answer all my questions. I would also like to thank the whole Bradley group for their support and help and the good times together in and outside the lab.

Finally, I would like to thank my family for their support during my stay here although I missed out so many gatherings. And I would like to thank Anne for all the support, advice and love she gave.

Abbreviations

AbC	Ammonium bicarbonate in acetonitrile
AU	Arbitrary units
BET	Brunauer-Emmett-Teller
B. fragilis	*Bacteroides fragilis*
Boc	^{t}Butyloxycarbonyl carbamate
BODIPY	Boron-dipyrromethene
BSA	Bovine serum albumin
calcd.	Calculated
CF	5(6)-Carboxyfluorescein
Cy5	Cyanine 5
DCC	Dicyclohexyl carbodiimide
DCM	Dichloromethane
d_{dry}	Dry diameter
d_{hyd}	Hydrodynamic diameter
DIC	*N*,*N´*-Diisopropylcarbodiimide
DIPEA	*N*,*N*-Diisopropylethylamine
DLS	Dynamic light scattering
DMEM	Dulbecco's modified Eagle medium
DMF	*N*,*N*-dimethylformamide
DMSO	Dimethyl sulfoxide

dPET	Donor-excited photoinduced electron transfer
DTNB	5,5'-Dithiobis-(2-nitrobenzoic acid)
DTPA	3,3′-Dithiopropionic acid
DTT	Dithiothreitol
DVB	Divinylbenzene
EDC	1-Ethyl-3-(3-dimethylaminopropyl)carbodimide
EDTA	Ethylenediaminetetraacetic acid
eGFP	Enhanced green fluorescent protein
ELSD	Evaporative light scattering detector
Equiv.	Equivalent(s)
EtOAc	Ethyl acetate
Et_2O	Diethyl ether
EtOH	Ethanol
FBS	Fetal bovine serum
Fmoc	Fluorenylmethoxycarbonyl
FmocHN-PEG_3-OH	Fmoc-4,7,10-trioxa-1,13-tridecaneediamine succinamic acid
Fmoc-AED-Suc-OH	1-(9*H*-fluoren-9-yl)-3,12-dioxo-2-oxa-7,8-dithia-4,11-diazapenta decan-15-oic acid
FSC	Forward scatter
Gd	Guanidnium
Glu	Glutamic acid
H	Hour(s)
HEK293T	Human embryonic kidney 293T cell line
HeLa	Cervical cancer cell line

His-tag	Polyhistidine tag
HOBt	1-Hydroxybenzotriazole
HPLC	High-performance liquid chromatography
ICP-OES	Inductively coupled plasma – optical (atomic) emission spectroscopy
I-FAM	5-Iodofluorescein
*i*PrOH	*iso*-Propanol
K_D	Dissociation constant
λ	Wavelength
λ_{em}	Emission wavelength
λ_{ex}	Excitation wavelength
LLF	Lung lining fluid
LUMO	Lowest unoccupied molecular orbital
MALDI	Matrix-assisted laser desorption/ionisation
MeCN	Acetonitrile
MEH-PPV	Poly[2-methoxy-5-(2-ethylhexyl-oxy)-1,4-phenylenevinylene
MeOH	Methanol
min	Minute(s)
µm	Micrometer
MS	Mass spectrometry
MTT	3-(4,5-Dimethylthiazole-2-yl)-2,5-diphenyltetrazolium bromide
mV	Milli Volt
µw	Microwave
nm	Nanometer

NMR	Nuclear magnetic resonance
NTA	*N*-(5-Amino-1-carboxypentyl)iminodiacetic acid
Oxyma	Ethyl 2-cyano-2-(hydroxyimino) acetate
PBS	Phosphate-buffered saline
[Pd]	Palladium catalyst
PDI	Polydispersity index
$Pd(OAc)_2$	Palladium acetate
PEG	Polyethylene glycol
PFBT	Poly[(9,9-dioctylfluorenyl-2,7- diyl)-*co*-(1,4-benzo-{2,1',3}-thiadiazole)]
pH	*Potentia hydrogenii*
pK_a	Negative decadic logarithm of acid dissociation constant
PLA	Polylactic acid
PLA_2	Phospholipase 2A
PLGA	Poly(lactic-*co*-glycolic) acid
PS	Polystyrene
PSD	Particle size distribution
Φ	Quantum yield
RAFT	Reversible addition/fragmentation chain transfer polymerisation
ROS	Reactive oxygen species
rt	Room temperature
SDS	Sodium dodecyl sulfate
SDS-PAGE	SDS polyacrylamide gel electrophoresis
SEM	Scanning electron microscopy

siRNA	Small interference RNA
SSC	Sideward scatter
^{t}Bu	*tert*-Butyl
TCEP	tris(-2-carboxyethyl)phosphine
TEA	Triethylamine
TFA	Trifluoroacetic acid
THF	Tetrahydrofuran
tlc	Thin-layer chromatography
TX-100	Triton X-100
V-50	2,2´-Azobis-(2-amidinopropane) hydrochloride
VBA	*para*-Vinylboronic acid
VBAH	*para*-Vinylbenzylamino hydrochloride
XPS	X-ray photoelectron spectroscopy
ZI	Zwitter ionic

Chapter 1

POLYMERIC PARTICLES IN THE LIFE SCIENCES

1.1 Nanotechnology

The European commission considers the progress and developments in the field of nanotechnology as paramount for all aspects of life in the European Union, with the belief that it will contribute to growth, competitiveness and sustainability of Europe and with far reaching implications for its citizens as well as people around the world.[1] A similar approach has been undertaken by a large number of global governments including the United Kingdom.[2] Indeed the market for nanotechnology already exists and has done for many years[3] and is expected to grow up to US$ one trillion by 2015.[4] How is nanotechnology able to evoke so many aspirations?

Nanotechnology describes the study and development of materials with at least one dimension having a size between 1 nm and 100 nm. Materials applying to this definition can have unique properties not seen for the same material at larger sizes. However, the size boundaries are fluid and materials can show size-related effects at larger sizes up to 500 nm.[5]

The electronic properties of molecules have been shown to be influenced by molecules in nanosize ranges resulting in previously unknown materials such as quantum dots (< 10 nm) which are used in optical imaging.[6] Furthermore, optical properties can also be changed, *e.g.* nano-sized pigments are transparent and widely applied as additives in cosmetics or paint coatings.[7] Due to the small size of nanoparticles they are also extensively used for biological and medicinal applications since they are small enough to cross biological barriers and offer novel techniques for diagnosis and therapy.[8]

Probably the most significant property of nanomaterials in contrast to their respective bulk materials is their extremely high surface area to volume ratio. The surface area grows exponentially with decreasing particle diameter by constant volume (Figure 1.1). This effect starts to dominate the properties of spherical particles with diameters smaller than approximately 200 nm. The high surface area implies also that an exceptional high number of atoms are present on the surface in comparison to the bulk resulting in amplification of the surface charges and forces while weakening the mass forces of the materials.[5]

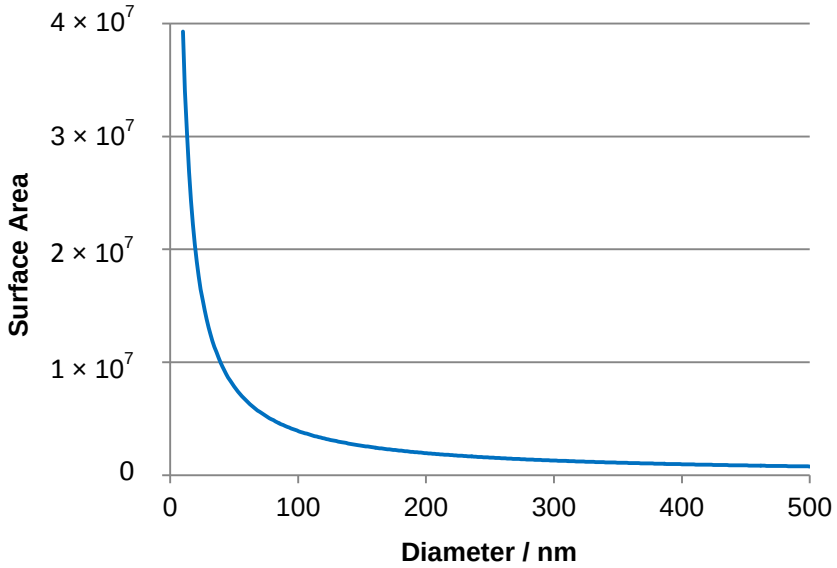

Fig. 1.1. Relation between surface area and the diameter of spherical particles with constant volume.

The high number of surface atoms makes nanoparticles very reactive[9] and has been used to accelerate heterogeneous catalysed reactions.[10] Furthermore, novel catalysts have been developed, for example gold showed chemoselective catalytic activity if smaller than 3 nm,[11] while iron atoms deposited on silica nanoparticles demonstrated selective oxidation of alkenes and arenes.[12]

However, nanomaterials and its exposure to humans are also of great concern. The properties of nanoparticles such as their small size and high reactivity are beneficial for a variety of applications but both are associated with an increased risk towards human health. Indeed, a number of nanomaterials have been assessed to be toxic although the same material in larger sizes was not. Hence, an understanding of the toxicological paradigms of nanomaterials is also part of nanotechnology and of utmost importance for continuing successful developments in this field.[13]

The above mentioned properties contribute to the high aspirations of nanotechnology, which may be able to contribute in solving a variety of problems

concerning healthcare, the environment and manufacturing processes. The number of novel materials prepared in nano-sized dimensions with ever new applications continuously increases. For example, nanodiamonds[14] and carbon dots[15] were developed in the previous decade and hold great promise for applications in the life sciences.

1.2 Applications of polymeric particles

POLYMERIC PARTICLES. Chemical structures consisting of polymers that form particulate structures are classified as polymeric particles, *e.g.* nanocapsules, micelles and nanospheres.[16] Nanocapsules have a characteristic inner compartment able to be loaded with a solid or liquid cargo.[17] Polymeric particles that originate from self-assembled polymers are known as micelles.[18] In contrast, nanospheres that form relatively rigid structures have been prepared as homo- or heterogenous polymeric particles. In addition inorganic nanoparticles are regularly enclosed by a polymeric shell to form hybrid nanoparticles. Here the shell has different functions, for example it may stabilise inorganic particles in water while avoiding the leakage of metals or allow surface modification.[19] Sometimes the metal core adds optical, magnetic or hyperthermic characteristics to the polymeric particle.[20] In this thesis, the term polymeric particle is used to represent solid polymeric nanospheres of approximately 200 nm. Moreover, the application of polymeric particles range from catalytic supports[21] to paints[22] to name but a few although uses in the life science are primarily addressed in here.

Polymeric particles can be divided into two classes with respect to their composition; biodegradable, and biostable particles. Biodegradable particles which

break down under physiological conditions have been investigated to improve the targeting of a variety of diseases. They support the bioavailibity, solubility and retention time of potent, but water insoluble drugs. Polylactic acid (PLA) and poly(lactic-*co*-glycolic) acid (PLGA) are the most common building blocks of biodegradable polymeric particles.[23] In contrast, biostable polymeric particles are mainly prepared from styrene and (meth)acrylate monomers and can be modified in a variety of ways, while not being degraded inside cells. As such, they are often suitable for a variety of applications as research tools in the life sciences.

The number of biomedical applications employing polymeric particles has increased dramatically over the last decades. This emanates from the particle's characteristics which can be fine-tuned to address chemical, physical and biological problems by varying the polymer composition.[24] Furthermore, particle surfaces can be modified by conjugation of bioactive molecules, drugs or fluorophores and importantly the particles are able to cross the cell membrane.

APPLICATIONS OF POLYMERIC PARTICLES. The ability of polymeric particles to cross the cell membrane was established many years ago[25] and has enabled the development of polymeric particles as carriers of bioactive compounds into cells. Those compounds range from small molecules such as sensors to large macromolecules, *e.g.* proteins and nucleic acids. The translocation of these compounds into cells can contribute to medicinal applications for therapy and diagnosis.[8]

The ability to measure a wide variety of cellular parameters reveals important information about the physiological state of a cell and has the potential for early diagnosis of diseases which would otherwise not be detected.[26] For example, the

concentration of ions such as calcium[27] and copper,[28] as well as pH[29] values have been determined inside cells using fluorescent sensor molecules attached to polymeric particles (Figure 1.2a). In addition oxygen[30] (on bacteria cell surfaces) and glucose[31] concentrations have been measured using polymeric sensor particles. The rational design of polymeric nanoparticles has also allowed the identification of apoptotic cells by enzymatic cleavage of a peptide sequence releasing a fluorophore which was previously quenched when attached to the particle.[32] Real-time measurement of protein kinase activity in cells has also been achieved by phosphorylation of a specific peptide sequence resulting in the dissolution of the particle and release of a previously quenched fluorophore (Figure 1.2b).[33]

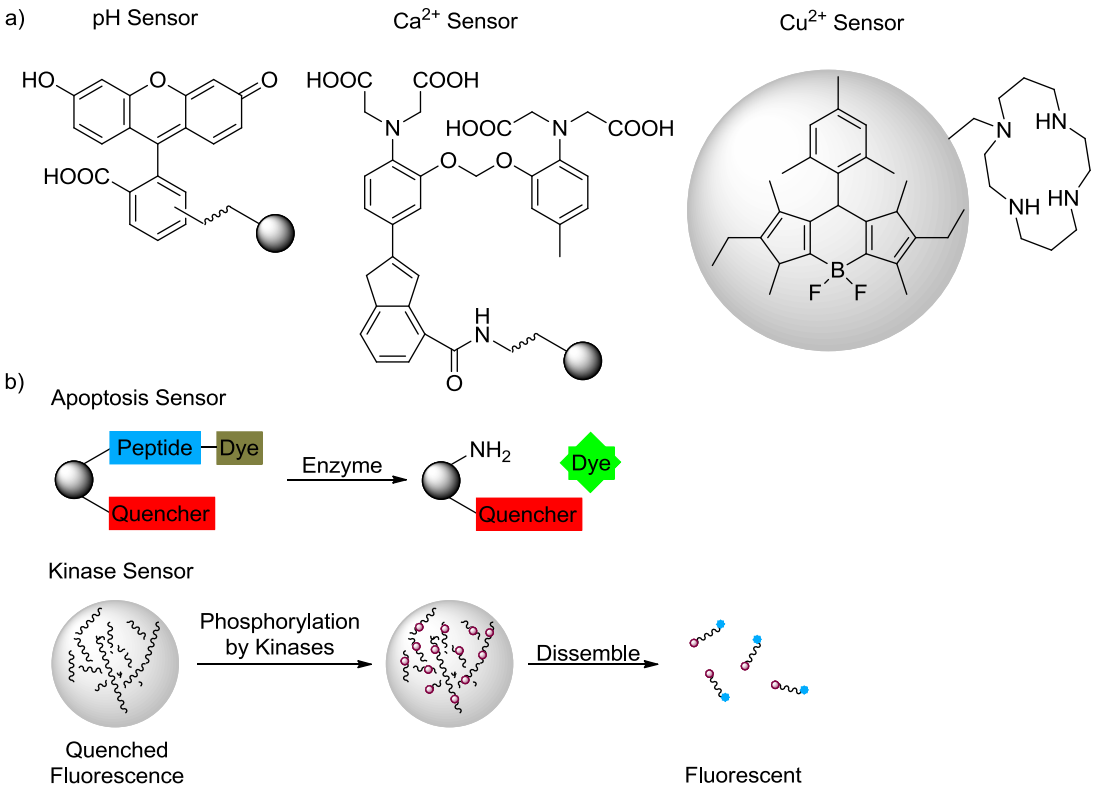

Fig. 1.2. Polymeric particles for sensing: (a) sensing of ions by dyes whose fluorescence is influenced by the presence of the respective ions; and (b) protein sensors releasing quenched fluorophores after enzymatic cleavage.

The delivery of macromolecules, *i.e.* proteins and nucleic acids, could contribute to improvements in the field of therapeutics, however they require a carrier to be internalised into cells.[34,35] Proteins have also been conjugated onto polymeric particles either in a covalent or non-covalent fashion followed by cellular delivery.[36,37] The delivery of nucleic acids is the foundation of gene therapy by which corrective DNA is introduced to replace mutant genes or introducing new or down-regulating genes to treat diseases.[35] Proteins can also be down-regulated in a process known as gene silencing requiring the delivery of small interference RNA (siRNA) into the cytosol. Alexander demonstrated the attachment of siRNA via disulphide bonds onto polymeric particles and subsequent cellular delivery and silencing of eGFP.[38] Analogous, biotin-labelled (non-encoding) DNA has been conjugated onto streptavidin-functionalised particles and internalised into cells.[39] The incorporation of plasmid DNA into biodegradable polymeric nanoparticles has enabled gene expression following the intracellular degradation of the particles and release of DNA.[40] Both techniques may provide promise in tackling a variety of currently incurable diseases.

The ability of the particles to cross biological membranes also opens the door to cellular imaging using fluorophore-labelled polymeric particles that can be tracked within mixtures of non-labelled cells.[41,42] Recently, non-fluorescent polymeric particles were prepared and demonstrated to turn-on fluorescence following cellular uptake.[43] The ability to employ polymeric particles in *in vivo* experiments was also demonstrated.[44]

1.3 Synthesis of polymeric particles

The technique employed in preparing polymeric nano and submicroparticles is mainly governed by the size of the required particles. The use of dispersion polymerisation yields particles with a size between 100 nm and 2,000 nm, smaller particles (50 nm – 300 nm) can be prepared by emulsion polymerisation, and particles smaller than 100 nm can be obtained using miniemulsion polymerisation.[45] The processes are free-radical polymerisations of hydrophobic monomers in either water and/or organic solvent mixtures. Dispersion polymerisation is characterised by an aqueous solution of monomer droplets mixed with organic solvents. By using a water-insoluble radical initiator, the particles are formed in the monomer droplets.[46] In contrast, the addition of an emulsifier to an emulsion polymerisation results in micelles and small amounts of monomer droplets, while water-soluble radical initiator facilitates particle formation inside the micelles rather than in the droplets. Furthermore, the number of monomer droplets can be dramatically increased and size decreased by external sheering forces to make a miniemulsion.[47]

EMULSION POLYMERISATION. The formation of particles via emulsion polymerisation has been described by the micelle-nucleation model developed by Harkins, Smith and Ewart.[48,49] The aqueous polymerisation mixture contains non-water soluble monomers, surfactant and a water-soluble initiator (Scheme 1.1). The surfactant forms micelles which contain a small amount of monomer but mainly the monomer is stored in large monomer droplets. Following the radical initiation, the radical starter reacts with monomer molecules dissolved in water thus increasing its hydrophobicity. Since the micelles vastly outnumber the monomer droplets, the oligomeric radicals formed enter the micelles and continue to polymerise with the

present monomers. Micelles containing a growing polymer chain are known as "particle nuclei" and are fed by monomers present in the droplets and micelles. Following the complete consumption of monomers, the polymerisation ends resulting in a dispersion of polymeric particles in water.[50]

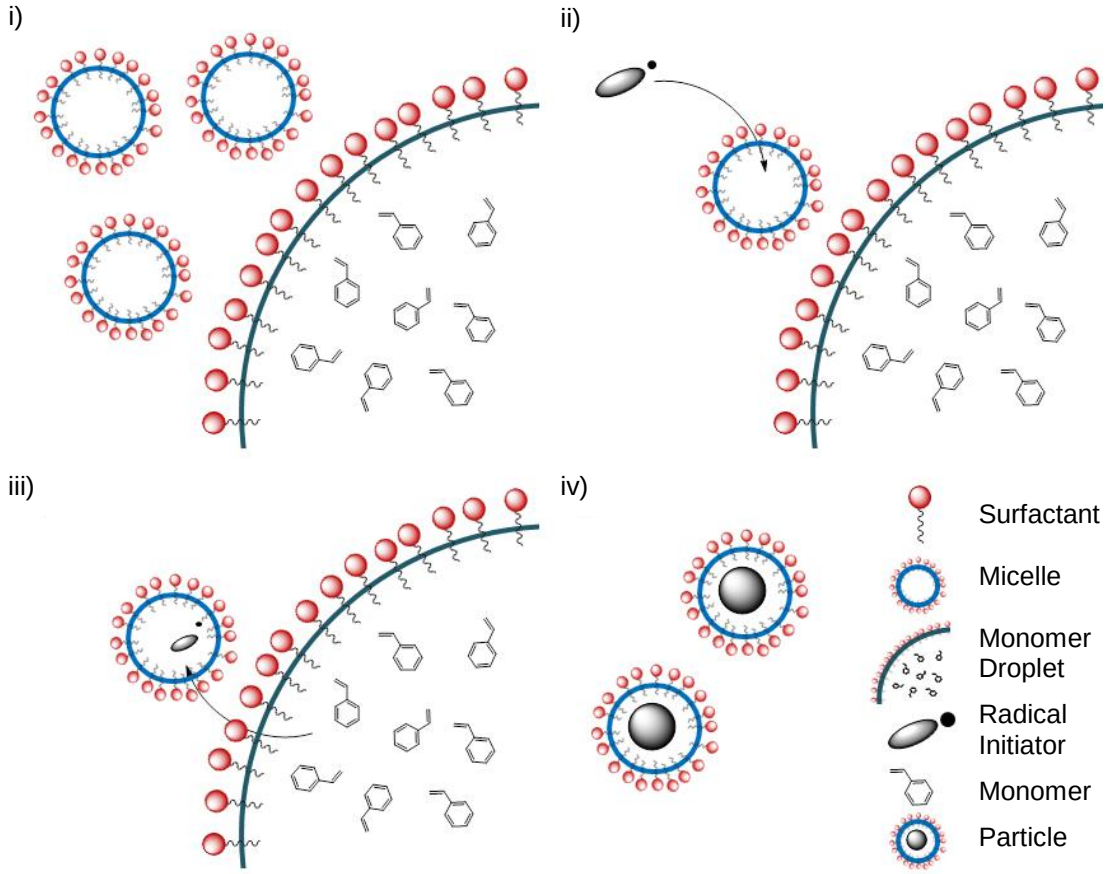

Scheme 1.1. Micelle nucleation model of the emulsion polymerisation: (i) formation of micelles and monomer droplets in water; (ii) water-soluble radical initiator reacts with the monomers dissolved in water before entering micelles (particle nuclei); (iii) the monomer transfers into micelles from the monomer droplets and polymerises; and (iv) particles stabilised by surfactants are formed.

A disadvantage of emulsion polymerisation is the excess of surfactant following the particle synthesis which is difficult to remove from the resulting dispersion. However, the surfactant is necessary for the formation of micelles, its concentration

is critical to gain the desired particle size and to stabilise the resulting particles. To avoid excess surfactant, emulsifier-free emulsion polymerisation can be used. The stability of the particles formed relies on the addition of charged monomers, such as acrylic acid[51] or *para*-vinylbenzylamine hydrochloride[52] resulting in negatively and positively charged particles, respectively. The charges provide the necessary repulsion forces to avoid agglomeration. An additional feature of these particles is the ability to modify the functional groups changing the properties of the particles or attaching additional functionality.[53]

1.4 Aims

Polymeric particles that can be modified with a wide range of compounds such as fluorophores, sensors and proteins have been developed for a broad range of intracellular applications within the Bradley group.[53] To broaden their application, the aims of this thesis were to further develop and study chemical and biological properties of the particles. Although the work presented in this thesis is restricted to polystyrene-based particles, these studies are exemplified using nanoparticles of all sizes and compositions.

The modification of nanoparticles with a variety of compounds to boost their function is now standard laboratory pratice. However, the determination of chemical transformations on a particle's surface is often limited and empirical in nature. One aim of this thesis was to use zeta potential measurements for the rapid analysis of particle functionalisations. Specifically, the ability to follow multi-step modifications was investigated.

In general, particle-based biological applications require fluorescent labelling of the particles. Thus, another aim of this thesis was the synthesis and application of novel polymerisable fluorophores to enable the comparison of particles which were fluorescently labelled during or following the polymerisation process.

To further improve the properties of nanoparticles and boost their applications, dual-functionalised surfaces are often required which allow orthogonal cargo conjugation. Novel dual boronic acid and aminomethyl-functionalised particles were developed allowing palladium-mediated Suzuki-Miyaura cross-coupling in combination with orthogonal amide conjugation onto the particles. The suitability of these dual-functionalised paticles for cellular loading was investigated.

Since nanoparticles are widely used, the effects of surface chemistry were analysed; of particular importance being the formation of a protein corona with respect to cellular uptake and toxicity.

Chapter 2

REACTION MONITORING ON NANO AND MICROPARTICLES

Parts of this chapter were previously published as:

Thielbeer, F., Donaldson, K. and Bradley, M. Zeta Potential Mediated Reaction Monitoring on Nano and Microparticles. *Bioconjugate Chemistry* **2011**, *22*, 144-150.

2.1 Reaction monitoring on particles

Nano- and microparticles are routinely functionalised to broaden the scope of their possible applications. For example, conjugation of cargos or sensors can add additional functionality on particles to allow cellular delivery or sensing in cells (Chapter 1). Although, the conjugation of molecules to particles is widely carried out and countless different method exists,[24] the monitoring and analysis of chemical modification *on-bead* remains a challenge.

REACTION MONITORING ON PARTICLES. Currently the most widely used analysis tool for reaction monitoring on particles are colorimetric tests which can identify and

at times quantify different functional groups. For example, the Kaiser test can be used to determine the levels of free amino groups.[54,55] Other colorimetric methods[56] include the Ellman test for thiols[57] and the Pomonis test for the detection of alcohols[58] to name but a few. Furthermore, surface-group quantifications are also available by a range of titration techniques including potentiometry and conductometry.[59] In addition, non-destructive colorimetric or fluorometric assays have been designed to correlate dye binding with functional group loading. In these assays a dye is adsorbed onto particle surfaces *via* charge-charge interactions with complementary functionalities such as amino[60] or carboxyl groups[61], generating quantitative information. Recent modifications allow surface interactions with metals[62] or macrocyclic host complexes[63] followed by visualisation with complementary dyes. Moreover, surface groups have also been quantified by peptide[64] or protein attachment.[65] The group of Whitesides demonstrated the ability of magnetic levitation to analyse chemical transformations on solid-phase resins.[66] However, these methods are laborious and typically have high material demands.

Alternatively, analytical methods, such as NMR have been applied to particle analysis based on the integration of NMR-active nuclei in the conjugated molecule.[67] Salvino *et al.* monitored solid-phase transformations by ^{19}F-NMR with ^{19}F part of the molecule that was conjugated to the solid support and a successful conjugation was identified by a ^{19}F-signal shift.[68] Furthermore, specifically designed NMR techniques, such as magic angle spinning, can be used to monitor reactions on particles.[69,70] Fourier-transform infra-red and Raman spectroscopy have also been used to monitor modifications on particles such as the transformation of an alcohol to an aldehyde.[71]

Mass spectrometry of compounds attached to the particles has been applied to gain information regarding its chemical composition. To achieve *on-bead* analysis a photocleavable linker[72] has to be attached to the particles prior to MALDI-MS. However, exposing the particles to cleavage solution has also been shown to be sufficient for mass spectrometric analysis.[73,74]

The surface composition, determined by X-ray photoelectron spectroscopy (XPS), can also be used to measure, qualitatively and quantitatively, the surface chemistry make-up of particles.[75] However, since XPS analysis gives information only of the top several nanometers of the surface, the avoidance of contaminations is crucial, which can be a major drawback if any compound binds non-specifically to the surface.[76] Finally, a simple way to verify successful conjugation is the incorporation of fluorescent labels into the coupled group, *e.g.* fluorescein[77] or rhodamine.[78]

Since various particles and modifications are commonly employed, there is an urgent need for a practical, inexpensive, and universal method to analyse chemical modifications on them. Herein, the usage of zeta potential measurements is described as a convenient tool which allows chemical reactions to be quickly monitored on particles with minimal sample preparation.

2.2 Synthesis and characterisation of polymeric particles

Polymeric particles were synthesised to investigate the ability of the particle's zeta potential to be used as an indicator of reaction progress on solid particles. In this thesis, aminomethyl-functionalised polystyrene-based particles were prepared by an emulsifier-free emulsion polymerisation, while the size of the particles used was approximately 200 nm representing nano as well as micro-sized solid particles.

PARTICLE SYNTHESIS. Polystyrene particles were synthesised by an emulsifier-free emulsion polymerisation. The process is similar to the emulsion polymerisation as described previously (Chapter 1).[41,52] However, this method has advantages over emulsion polymerisation as the emulsifier is incorporated into the particle structure.[79] The polymerisable emulsifier used was *para*-vinylbenzylamine hydrochloride (VBAH) **1** which generated an emulsion of the monomer styrene **2** in water. In addition, the incorporation of VBAH into the particle structure creates aminomethyl groups on the particle surface for further functionalisations of the particles. Furthermore, to improve the stability of the particles, particularly in organic solvents, polymer chains were cross-linked with divinylbenzene **3** (DVB).

Polymerisation of styrene **2**, crosslinker DVB **3** (2 mol% with respect to styrene) and functional monomer VBAH **1** (3 mol%) in water using the water-soluble radical initiator 2,2´-azobis-(2-amidinopropane) hydrochloride (V-50) gave particles **4a** (Scheme 2.1). On average, circa 40 wt% of the monomers were converted into aminomethyl functionalised polystyrene-based particles and stored in water at a solid content of 2%.

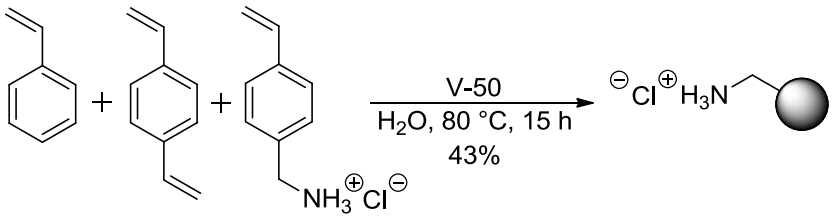

Scheme 2.1. Synthesis of aminomethyl-functionalised polystyrene-based particles.

FUNCTIONAL MONOMER SYNTHESIS. The monomer VBAH, which is an emulsifier, also introduces amino groups onto the particle's surface. It was

synthesised by a Gabriel synthesis followed by acidification in moderate overall yield (19%) (Scheme 2.2).[52] The first step of the Gabriel synthesis involved reaction of potassium phthalimide with *para*-vinylbenzylchloride **5** in DMF. The phthalimide **6** was isolated in 65% yield after recrystallisation in methanol. The phthalimide group was removed using hydrazine hydrate to yield *para*-vinylbenzylamine **7** in 64% yield, followed by generation of the salt (VBAH **3**) in 45% yield.

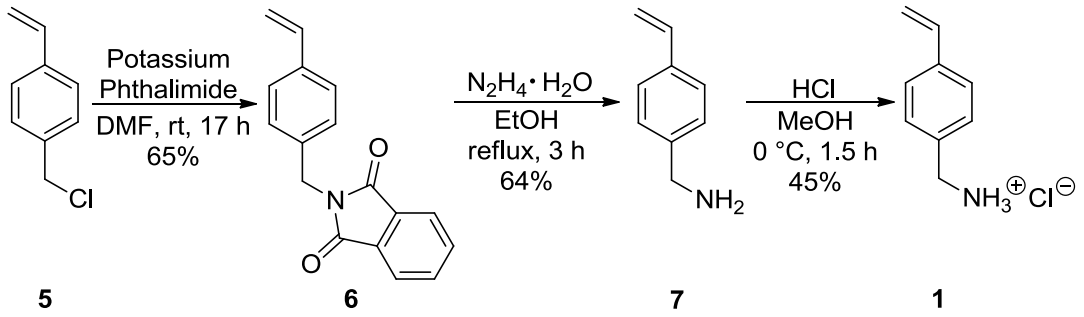

Scheme 2.2. Synthesis of the aminomethyl-bearing monomer *para*-vinylbenzylamine hydrochloride.

PARTICLE CHARACTERISATION. The main physical characteristics of solid particles are size, shape, density, porosity along with surface and chemical properties. These characteristics influence the behaviour of the particles within a biological environment and determine not only its uptake mechanism, but also whether particles could be internalised by cells (Chapter 5).[80]

SIZE AND SHAPE. Size measurements of a sample give the size distribution of particles (PSD) and can be determined by a variety of methods. The most common methods are dynamic light scattering (DLS), and analysis of images gained from methods such as electron microscopy. These approaches clearly influence the result as one is measured in solvent while the other is measured dry. Most sizing techniques

assume that particles have a spherical morphology to allow measurement of only one variable (diameter) in contrast to their actual three-dimensional shape which would require three variables (height, length, depth) to be determined. Depending on the technique used, the diameter determined is based on one of the three variables, hence, varying results can be obtained with different techniques.

Light scattering measures principally the velocity of particles in solution which is related to the particle size. If particles are dispersed in solution they move randomly due to Brownian motion. The velocity of this motion can be obtained by firing a laser onto the particles and analysing the resulting Rayleigh scattering. The scattered light of different particles interferes with each other and analysis of this generates information about the velocity of the particles. This velocity can be transformed into a diffusion coefficient which is directly related to particle size via the Stokes-Einstein equation (Equation 2.1).[81]

Equation 2.1. Stokes-Einstein equation.

$$D = \frac{k \cdot T}{6\pi \cdot \eta \cdot r}$$

D Diffusion coefficient in m^2/s

k Boltzmann constant (1.380×10^{-23} J/K)

T Temperature in K

η Viscosity coefficient in N s/m^{-2}

r Hydrodynamic particle radius in m

Sizes gained from particle dispersions are given as hydrodynamic diameter (d_{hyd}) since the technique cannot distinguish between the intimate ion-shell surrounding the

particle in solution and the solid particle core. In comparison, a dry diameter (d_{dry}) is measured by techniques such as electron microscopy. A further characteristic of the particle size is the polydispersity index (PDI) which can have a value between 0 (every particle in the suspension has exactly the same size) and 1 (the size of every particle differs). A value below 0.1 typically classifies dispersions as monodisperse.[42]

The shape, and additionally the dry diameter, of particles can be visualised by electron microscopy while the size of the particles determines the technique; scanning (SEM, above 200 nm) or transmission electron microscopy (below 200 nm). Particles **4a** are submicron-sized hence SEM was employed to investigate dry size and shape of the particles.

The size distribution of particles **4a** was determined by DLS (quantitatively), and SEM (qualitatively). The intensity-based distribution resulted in a hydrodynamic diameter of 232 nm with a PDI of 0.027 demonstrating monodisperse particles in the submicron range (Figure 2.1a). These results were verified by SEM with an expected slightly smaller dry diameter of (202 ± 10) nm and uniform particles with a spherical morphology (Figure 2.1b).

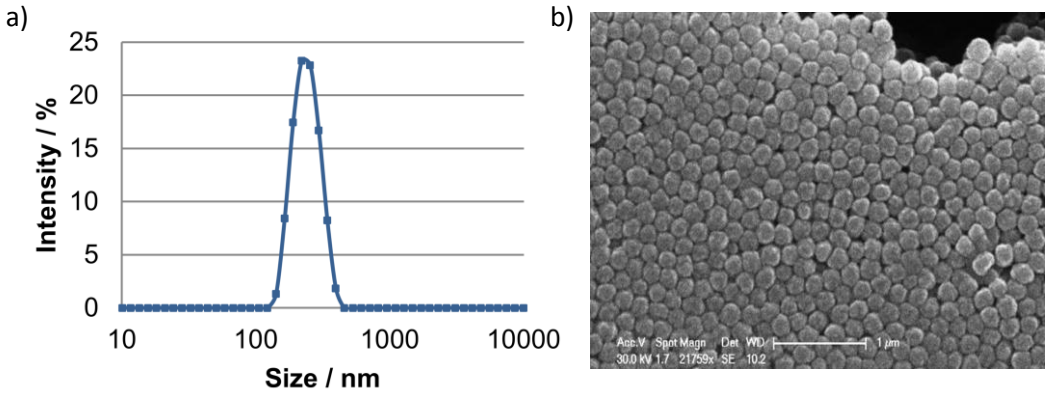

Fig. 2.1. Particle size distribution of aminomethyl functionalised polystyrene-based particles **4a**: (a) light scattering, d_{hyd} = 232 nm, PDI 0.027; and (b) scanning electron microscopy image, d_{dry} = (202 ± 10) nm, scale bar = 1 µm.

SURFACE. Solid particles can be further characterised by their surface properties which play a crucial role in the stabilisation of particle suspensions as well as being important for the ability to modify the particles as necessary for a particular application.

The surface of particles **4a** contains amino groups originating from VBAH which provide stabilisation of the particles by electronic repulsion between adjacent protonated amino groups. These groups can also be further modified via standard amide-bond formation chemistry. To evaluate the quantity of amino groups on the particles a quantitative Kaiser test was carried out[55] giving an amino group loading of (135 ± 2) µmol/g.

ZETA POTENTIAL. The particle surface was also characterised by its zeta potential which correlates to the charge of particles and can be simplistically described by the Gouy-Chapman-Stern model (Figure 2.2). A positively charged particle such as **4a** will affect nearby ions dissolved in the suspension medium. The surface of the particles is highly positively charged (quantified by the surface potential) and attracts negatively charged counter ions. These ions form a tightly adsorbed monolayer on the particle surface. This leads to a linear decrease of the potential resulting in the so-called Stern potential. A diffuse layer follows which contains ions which are still attracted by the particle and its surrounding Stern layer but are more loosely bound. A boundary exists between ions of the diffuse layer which will move with the particle and those which will not. The potential measured at this boundary is called the zeta potential which is also the only easily quantifiable potential using current techniques.[82]

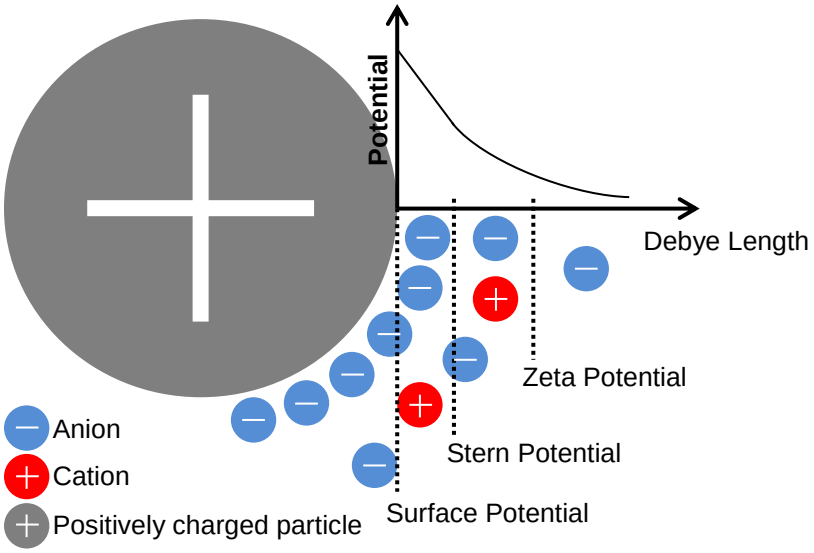

Fig. 2.2. A positively charged particle and its interaction with ions in the suspension medium.

Zeta potential measurements of particles depend in particular on the ionic strength and the pH of the suspension medium. The density of counter ions and possible multi-charged counter ions will influence zeta potential measurements. Multi-charged counter ions have a greater Coulombic attraction to the particle surface hence reducing the particle charge more than single charged ions which also affects the zeta potential. Furthermore, the pH of the suspension medium influences the zeta potential. For example, aminomethyl functionalised particles **4a** have a protonated amino group at pH 7 and therefore a positive zeta potential. An increase of the pH leads to a decrease of the zeta potential due to deprotonation of the amino groups (pK_a ~ 10).[83] The particle's isoelectric point was determined to occur at pH 10 (Figure 2.3). However, as shown in Figure 2.2 the loss of charge was measured by zeta potential which is dissimilar from surface and Stern potential, hence, there are still charged amino groups on the particle surface available which are neutralised by

surrounding counter ions. Therefore, an apparent isoelectric point of the particles appears although amino groups on the surface are still protonated.

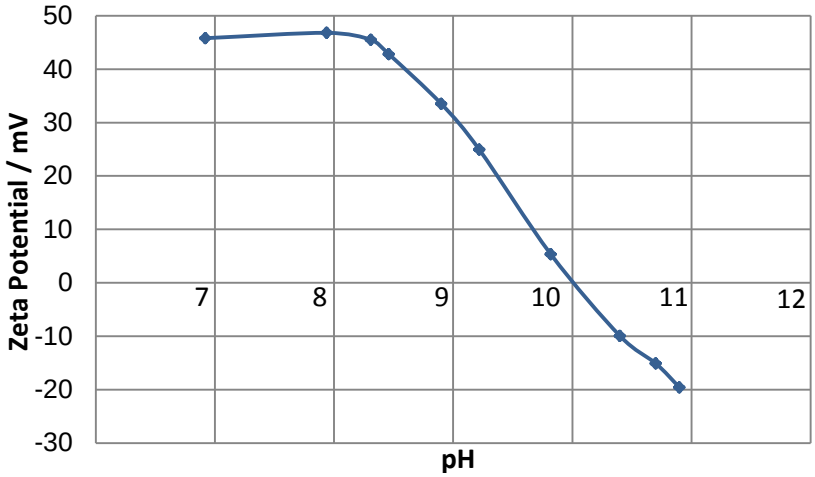

Fig. 2.3. Zeta potential dependency on pH (aminomethyl-functionalised polystyrene particles **4a** in de-ionised water were titrated against NaOH).

The importance of zeta potential is based on its simple determination via measurement of the electrophoretic mobility and its value for the prediction of suspension stability. As a rule of thumb zeta potentials higher than ±18 mV give stable polymer lattice suspensions.[84] Knowledge of suspension stability is required for a variety of dispersions such as consumer products (paints and adhesives) or the destruction of unwanted colloidal suspensions (water purification).[85]

Herein, zeta potentials were measured at pH 7.4 in 10% PBS to provide a stable environment and comparative measurements of different samples. Electrophoretic mobilities were determined by laser Doppler velocimetry. The basis of this technique is that the particles move in an electric field and are targeted with a laser beam. Due to the particle motion the scattered laser beam is phase shifted (Doppler-effect). This phase shift is transformed into electrophoretic mobility which in turn can be converted into a particle's zeta potential.

Aminomethyl-functionalised polystyrene-based particles **4a** had a zeta potential of +25 mV at pH 7.4 (Figure 2.4). Thus, according to the rule of thumb described above the determined zeta potential is higher than +18 mV hence the particles would be expected to form a stable dispersion. These results confirmed the low polydispersity and uniform size characteristics of the particle suspension while demonstrating a stable dispersion.

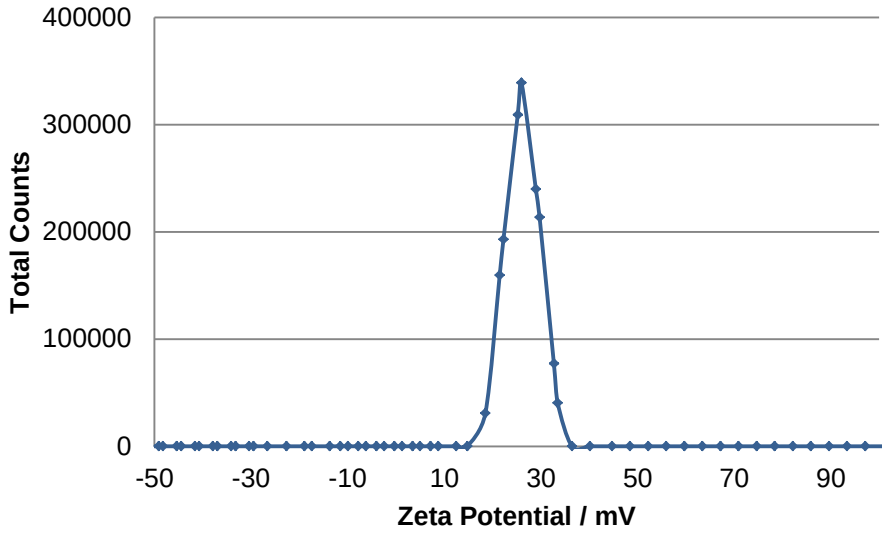

Fig. 2.4. Zeta potential distribution of aminomethyl-functionalised polystyrene-based particles **4a** (zeta potential +25 mV in 10% PBS, pH 7.4).

2.3 Monitoring of particle modifications

ZETA POTENTIAL OF FUNCTIONALISED PARTICLES. Initially, the zeta potential of particles bearing different surface functionalities were investigated. Particular attention was paid to the shift in zeta potential following chemical reactions. Since a particle's surface chemistry has a major effect on the zeta potential, the aminomethyl-functionalised particles **4a** were conjugated to different molecules resulting in a variety of surface chemistries (Scheme 2.3). All of the modifications were also bench-marked with the Kaiser test[54] to verify modification. A small

quantity of the particle suspension (20 µg) was dispersed in 10% PBS (pH 7.4) followed by zeta potential measurement (Table 2.1, Figure 2.5).

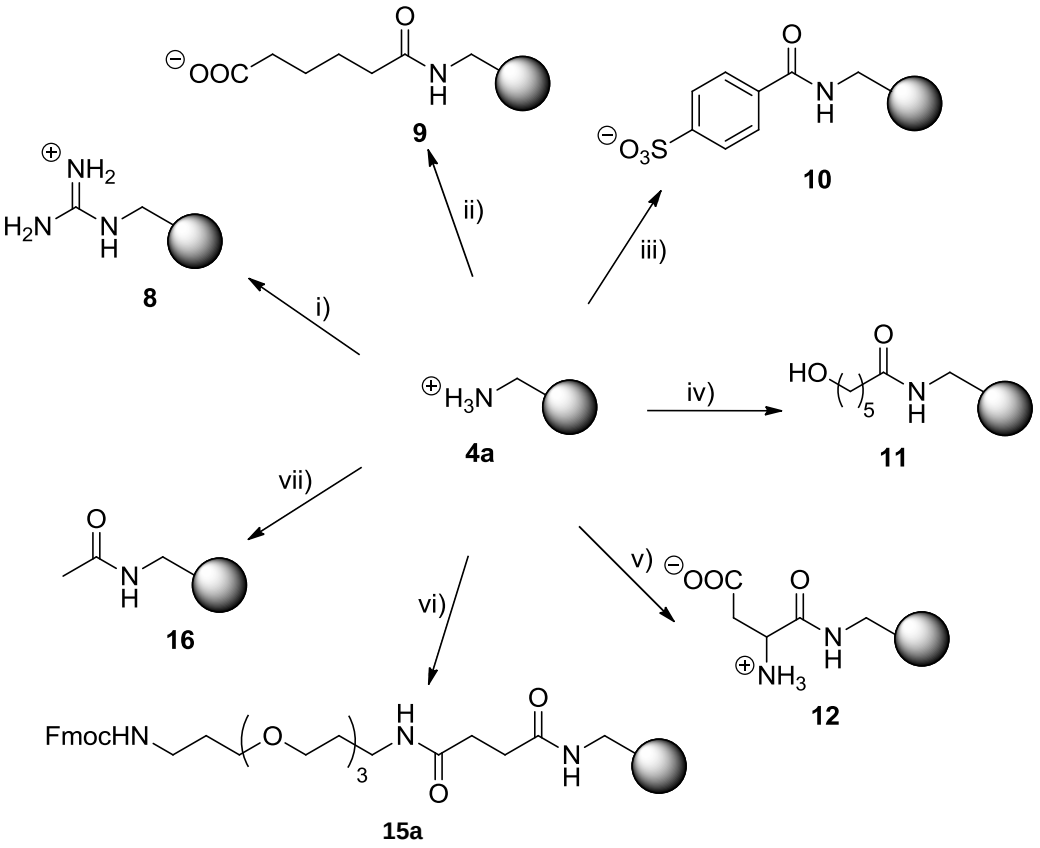

Scheme 2.3. Synthesis of functionalised particles: (i) *N´*,*N*-bis(*t*butoxycarbonyl)-*S*-methylurea, TEA in DMF, 60 °C (µw), 30 min; 20% TFA in DMF, 2 h. (ii) adipic acid, DIC in DMF, 60 °C (µw), 20 min. (iii) *para*-sulfobenzoic acid, oxyma, DIC in DMF, 60 °C (µw), 20 min. (iv) *ε*-hydroxycaproic acid, oxyma, DIC in DMF, 60 °C (µw), 20 min. (v) Fmoc-Glu(*t*Bu)-OH, oxyma, DIC in DMF, 60 °C (µw), 20 min followed by 20% TFA in DMF, 2 h and 20% piperidine in DMF, 2 × 20 min. (vi) Fmoc-4,7,10-trioxa-1,13-tridecaneediamine succinamic acid (FmocHN-PEG_3-OH), oxyma, DIC in DMF, 60 °C (µw) 20 min. (vii) acetic anhydride, pyridine, DMF, 2 × 20 min).

The starting aminomethyl particles **4a** were transformed to the more basic guanidinium group **8** by reaction with *N´*,*N*-bis-(*t*butoxycarbonyl)-*S*-methylurea followed by TFA-mediated *t*butyloxycarbonyl carbamate (Boc) deprotection. The zeta potential changed from +25 mV to +31 mV due to the increased basicity of the

surface. Due to this high zeta potential particles did not aggregate and formed a stable monodisperse solution (238 nm, PDI 0.056). Negatively charged surface groups were introduced by amide bond formation using diisopropylcarbodiimide (DIC) as an activator and adipic acid to generate a carboxylic acid functionality **9** and oxyma/DIC[86] with *para*-sulphobenzoic acid to generate sulphonic functionalities **10**, respectively. A strong negative zeta potential was found after conversion to carboxylic acid **9** (–44 mV) and, as expected, even stronger negative values were obtained after attachment of the more acidic sulfonic acid **10** (–65 mV). The size and PDI of the particles (279 nm and 252 nm, 0.056 and 0.030) were not affected as expected since the zeta potential values for both functions were large enough to stabilise the particles despite being negative.

Furthermore, a variety of neutral functionalities were coupled to the aminomethyl group. Hydroxyl groups **11** (via oxyma/DIC and ε-hydroxycaproic acid) resulted in a slightly negative zeta potential (–7 mV). An increased size of 463 nm was determined in combination with an increased PDI of 0.204 which resulted from the loss of charge. Conversion to a zwitterionic surface **12** by the attachment of glutamic acid was detected with a very broad zeta potential peak with a mean value of –10 mV. Furthermore, the size distribution was measured to be 1736 nm with a PDI of 0.901. Aggregation of the particles was expected since the stabilisation is based on a net charge and the zwitterionic-functionalised particles have no net-charge, thus they have a propersity to aggregate strongly.

The attachment of a short polyethylene glycol (PEG) spacer was achieved by reaction with FmocHN-PEG-OH **14** which was synthesised following the route of

Zhao *et al.* (Scheme 2.4).[87] Diamino PEG **13** was conjugated in a one-pot reaction with succinic anhydride and Fmoc-OSu in moderate yields (44%).

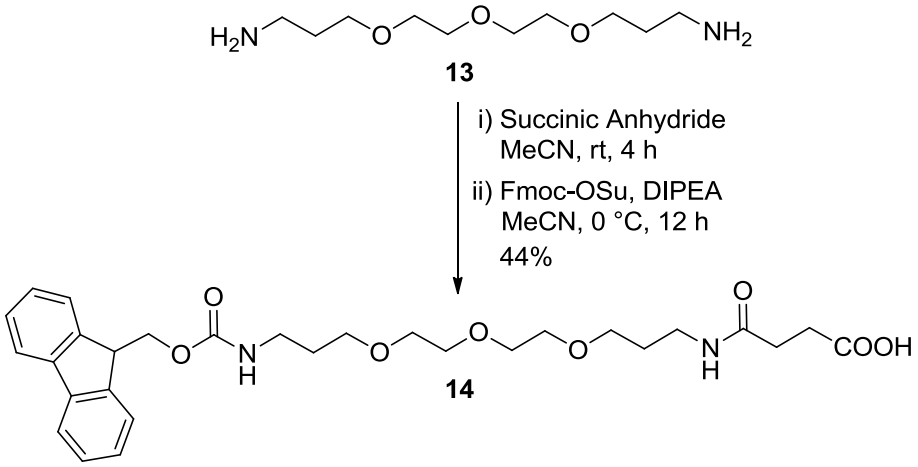

Scheme 2.4. Synthesis of FmocHN-PEG$_3$-OH **14**.

Conjugation of FmocHN-PEG-OH **14** resulted in a zeta potential of +3 mV for particles **15a** while acetylation of the amino group **16** produced a zeta potential of –5 mV. The zeta potential values close to zero mV demonstrated the lost charge on the particle surface after amino group capping. Moreover, capping induces strong aggregation of the particles measured as large particulate size values (1435 nm and 2270 nm) in combination with high PDI (0.566 and 0.424) representing differently sized agglomerates.

Table 2.1. Functionalised particles and their zeta potential, size and PDI.

Compound	Zeta Potential [mV]	Size [nm] (PDI)	Compound	Zeta Potential [mV]	Size [nm]
Amino **4a**	+25	232 (0.027)	Hydroxylated **11**	-7	463 (0.204)
Guanidinium **8**	+31	238 (0.056)	Zwitterionic **12**	-10	1736 (0.901)
Carboxylated **9**	-44	279 (0.103)	FmocHN-PEG **15a**	+3	1435 (0.566)
Sulphonated **10**	-65	252 (0.030)	Acetylated **16**	-5	2270 (0.424)

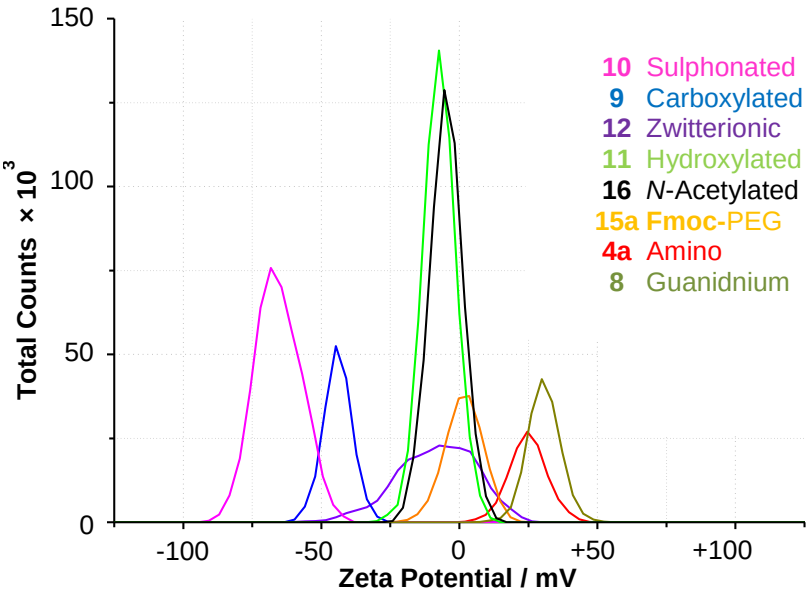

Fig. 2.5. Zeta potential of aminomethyl and subsequently functionalised polystyrene particles.

It should be noted, that the use of the zeta potential for reaction monitoring is based on the comparison between the zeta potentials of the initial particle and those of the reaction product. It was observed that different batches of aminomethyl-functionalised polymeric particles had slightly different initial zeta potentials (+25 ± 3) mV, however, the shifts in zeta potential were significantly greater after surface modification. The results demonstrated that zeta potential allows information to be

derived regarding the surface chemistry of the particle. Although a quantitative relationship between the number of surface groups and the zeta potential cannot be achieved, it proved to be a tool useful nonetheless.

MONITORING MULTI-STEP REACTION SEQUENCES VIA ZETA POTENTIAL. Nano and microparticles are increasingly used and modified with multistep reaction sequences to attach the desired linkers or functional molecules. It can be difficult to follow such sequences on polymeric supports due to the unknown coupling efficiencies of different reaction steps. In addition, the reactions are often performed in aqueous media involving highly charged biomolecules. To investigate if the zeta potential could also monitor multistep reactions, a reaction sequence on particles was analysed by zeta potential measurements.

A common coupling sequence on particles includes the addition of a spacer such as polyethylene glycol (PEG). Scheme 2.5 represents the ability to use zeta potential to directly follow such a reaction sequence. The initial charge-stabilised aminomethyl polystyrene submicron particles **4b** had a zeta potential of +26 mV. The amino groups were coupled to Fmoc-protected PEG_3-spacer. Treatment with acetic anhydride capped the remaining, non-accessible amino groups **15b**. A small reduction in zeta potential to –2 mV (before capping -1 mV) was observed. Fmoc deprotection gave particles with free amines on the particle's surface **17** and therefore a strongly positive zeta potential (+31 mV). Finally, coupling of adipic acid **18** onto the particle surface resulted in a negative zeta potential (–39 mV) representing the carboxylic functionality. The three-step reaction sequence was easily monitored by notable changes in zeta potential without significant sample preparation, loss of material, or chemical cleavage from the particles. This

demonstrates that zeta potential is an excellent tool to follow direct *on-particle* modifications without necessary cleavage or introduction of specific spectroscopic reporter groups for analysis.

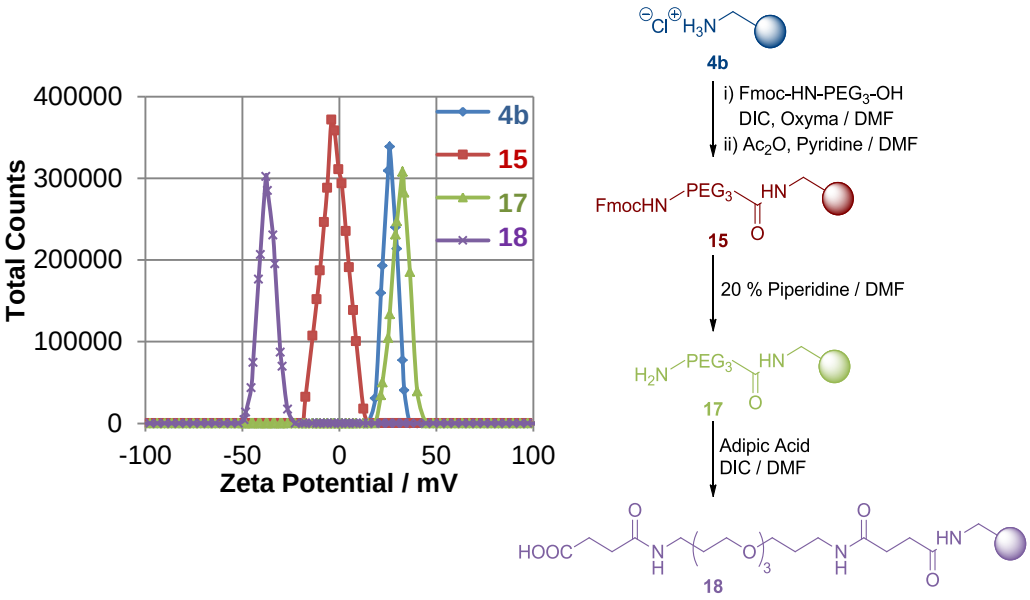

Scheme 2.5. A multistep reaction analysed by zeta potential monitoring of particles.

REACTION CONTROL. Commonly used functionalities in nano and microparticle bioconjugates are thiol and transition metal-bearing ligands. A thiol containing molecule can be easily coupled to a variety of biomolecules, *e.g.* via maleimides (Chapter 4), such as small interfering RNA (siRNA)[88] or proteins[89], metal-bearing functionalities are also used due to their ability to bind the widely-used His-tag and therefore non-covalently link proteins to particles.[90]

Thiols were generated on the particles by coupling 3,3′-dithiopropionic acid (DTPA) to the aminomethyl groups of particles **4b** followed by subsequent reduction with tris(-2-carboxyethyl)phosphine (TCEP). The first coupling resulted in a conversion from a positive zeta potential charge (+26 mV) to a negatively charged

surface **19** (–29 mV). The following reduction with TCEP in PBS gave free thiol groups **20** on the particle surface with a zeta potential value of –18 mV (Scheme 2.6). This value was close to that expected due to the relatively acidic nature of the thiol group (pK_a ~ 9).[91] The data from the zeta potential analysis was also verified by a positive Ellman test[57] proving the presence of free thiols, although not quantitative (Scheme 2.6).

Another reaction sequence, which is not easily monitored by current methods, is the introduction of carboxylic acid ligands, which are commonly used for binding transition metal bearing complexes. Initially, the synthesis of carboxylic acid bearing particles **18** was followed, yielding particles with a zeta potential of –39 mV. The commonly used *N*-(5-amino-1-carboxypentyl)iminodiacetic acid (NTA)-linker, containing three carboxylic acid moieties, was also introduced to give **21** with a notably decreased zeta potential of –48 mV (Scheme 2.6).

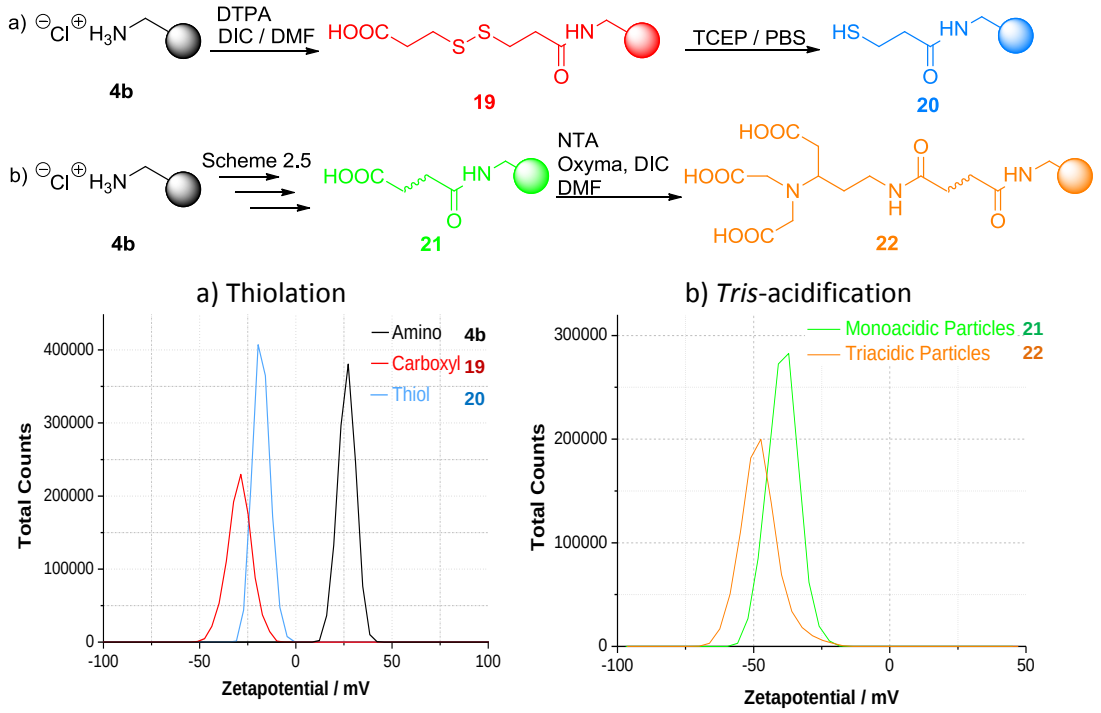

Scheme 2.6. Reaction control: (a) synthesis and zeta potential monitoring of thiol-functionalised and (b) tricarboxylated particles.

These two experiments show the ability of zeta potential to verify reactions which are difficult to analyse with other common techniques. A decrease in the strength of the surface acid, from carboxylic acid to thiol, was clearly observed as a change in zeta potential. Similarly, a notable difference in zeta potential values was detected when the number of carboxylic functionalities increased.

2.4 Conclusion

The use of nano and microparticles has increased dramatically with novel applications in chemistry and in the life sciences. An increasing number of particles are being chemically modified by attachment of different molecules including proteins and nucleic acids leading to a variety of functionalities. However, the

chemical analysis of the modified particles has been difficult and remains a challenge. Indeed, in many cases it is just assumed that the reaction has taken place. Herein, the ability of the zeta potential was demonstrated as a practical, easy method to follow conjugations on nano and microparticles. 200 nm aminomethyl-functionalised submicron polystyrene-based particles, representing nano and micro sized particles, were employed to couple a variety of different acidic, basic and neutral groups. The zeta potential values of different surface modified particles correlated to the nature of chemical modification and demonstrated the strength of the technique. Furthermore, a multistep coupling sequence was followed by zeta potential measurements. Finally, zeta potential was used to analyse modifications which are difficult to follow using conventional analysis techniques. Changing from amine to carboxylic acid or thiols as well as the number of presented acids was also verified by measuring the shift in zeta potential values on the respective particles.[92]

The presented method of reaction monitoring by zeta potential gives a qualitative analysis of reactions on particle surfaces. This technique could be applied to other areas such as reaction monitoring on non-polymeric particles[93] or bulk polymer surfaces for which zeta potentials are also obtainable as current titration or colour tests fail but a fast and easy quantitative analysis of surface modifications is desirable.

The presented zeta potential-based method is universal, fast, and convenient, and simplifies the analysis of reactions carried out on nano and microparticles. It has been demonstrated that zeta potential measurements are a useful method with the ability to directly analyse suspensions of nano and microparticles, and can easily be

used to validate chemical transformations and multistep reaction sequences on solid particles.

Chapter 3

FLUORESCENT POLYMERIC NANO AND MICROPARTICLES

Parts of this chapter were previously published as:

Thielbeer, F. Fluorescein *Synlett* **2012**, *23*, 1703-1704.

Thielbeer, F., Chankeshwara, S. V. and Bradley, M. Polymerizable fluorescein derivatives: synthesis of fluorescent particles and their cellular uptake. *Biomacromolecules* **2011**, *12,* 4386-4391.

3.1 Fluorescent particles

Nano and microparticles can be functionalised with a variety of compounds to boost their own or adjoin additional properties enabling them to be used in biological or medicinal studies. Standard modifications include labelling giving the ability to track the particles, verify their location and/or sense their environment. To achieve this, particles can be conjugated to imaging agents. The most common method of

particle detection is fluorescence, although numerous other methods such as magnetic resonance imaging,[94] or positron emission tomography[95] exist.

FLUORESCENCE. Fluorescence describes the emission of light (blue band), from a molecule following previous absorption of lower wavelength (higher energy) light (red) (Figure 3.1a). This is achieved when an electron moves from the ground state (S_0) into the multiple vibrational levels of the first excited state (S_1) (1→2, Figure 3.1b). Internal conversion reduces the energy of the molecule to the lowest vibrational state of S_1 (2→3, Figure 3.1b). The length of time the fluorophore remains in its excited state is known as its fluorescence life-time. Finally, the excited molecule decays with radiative emission of light (fluorescence) (3→1, Figure 3.1b). A fluorescent dye can be characterised by its absorption and emission profile, quantum yield and fluorescence life time. The quantum yield Φ describes how efficiently the molecule converts absorbed energy into emitted light.[96]

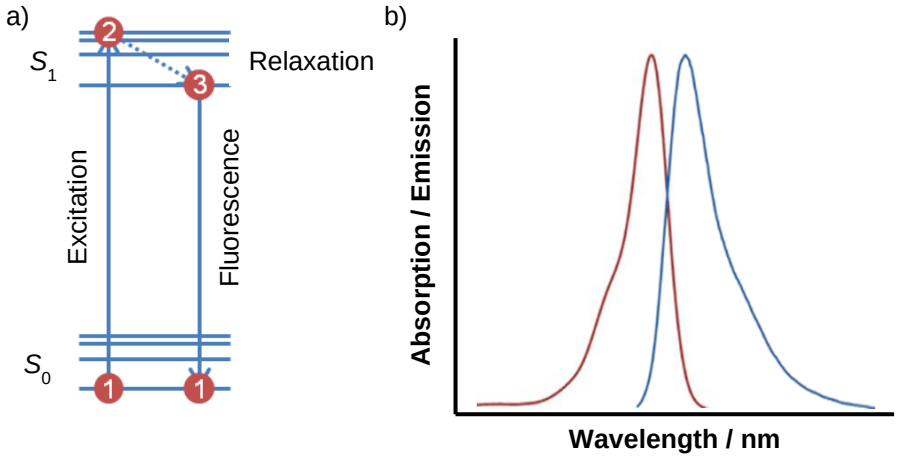

Fig. 3.1. Fluorescence: (a) excitation (red) and emission (blue) profile of a fluorophore; and (b) Jablonsky diagram of fluorescence.

FLUORESCEIN. Fluorescein is the probably most widely used fluorophore. Its numerous applications in particular in the life sciences are based on its robust and

biologically favourable properties. It has a high quantum yield (0.93), while the readily available argon-ion laser (λ = 488 nm) can excite fluorescein, it shows good water solubility, while commercially available derivatives allow biomodification. However, the fluorescence of fluorescein is strongly pH dependent. Neutral fluorescein is in equilibrium between the lactonised **22a** and open form **22b** (Scheme 3.1). The opened lactone ring is required for the fluorescent properties. However, neutral fluorescein (**22a**/**22b**) has a relatively low quantum yield of 0.30 which is even lower upon protonation (**22c**) (Φ = 0.18). In contrast, deprotonation yields the monoanionic species **22d** with an increased quantum yield of 0.37. Upon further deprotonation of **22d** the highly fluorescent dianion **22e** is formed with a quantum yield of 0.93. These characteristics are important for fluorescein-based applications with the pH-values crucial for the ability to form the highly fluorescent dianion with good fluorescent properties.[97] Indeed, it has been shown that modifications of the xanthine moiety which do not allow dianion formation reduce the fluorescence of fluorescein.[98]

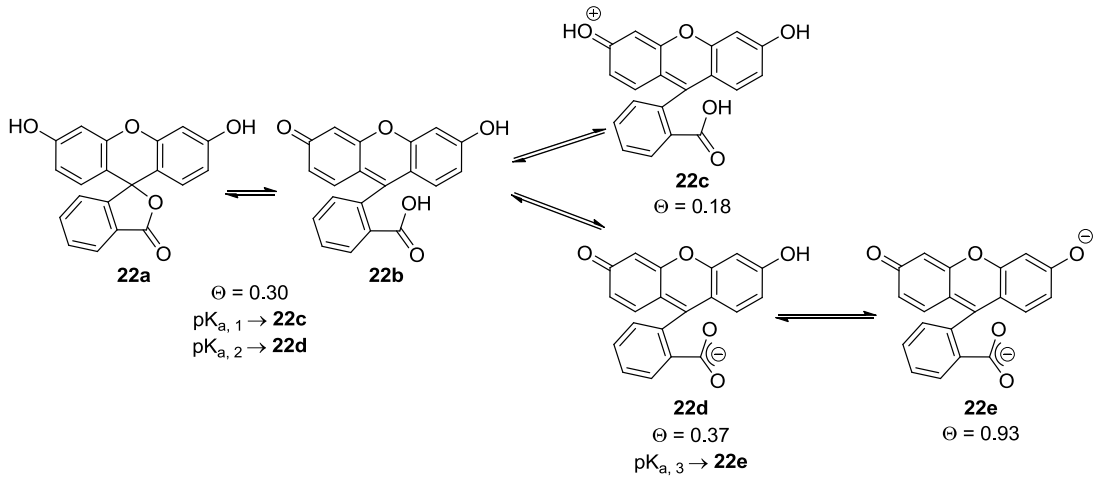

Scheme 3.1: Ionisation equilibria of fluorescein and fluorescence properties (p$K_{a,1}$ = 2.1; p$K_{a,2}$ = 4.3; p$K_{a,3}$ = 6.4).

PREPARATION OF FLUORESCENT PARTICLES. In general, the introduction of fluorescent dyes into or onto particles can be achieved by dye incorporation during the polymerisation or following the polymerisation process.

Most commonly, particle labelling occurs post-polymerisation where dyes can be deposited onto or into the particle by solvent evaporation,[99,100] or entrapped by particle swelling and subsequent shrinkage (Figure 3.2).[101] However, these types of particles are vulnerable to dye-leakage.[102] A route to reduce dye-leakage is the entrapment of dyes followed by polymer shell formation on top of the dye. Zhang[103] deposited dyes on the particle surface and subsequently trapped them by *on-surface* polymerisation of undecylenic acid **23** and crosslinker divinylbenzene **3** (Figure 3.2a). A conventional method is to fluorescently label polymeric particles by covalent attachment of dyes onto the surface groups, *e.g.* amine or thiol chemistry (Figure 3.2b).[104,105] This type of conjugation leads to covalent attachment and allows long-term use and storage without leakage of the fluorophores. However, covalent attachment reduces the number of surface functionalities available for conjugation of other cargos although this can be avoided by the application of bi-functional linkers that allow consecutive fluorophore binding and functional group conjugation.[106]

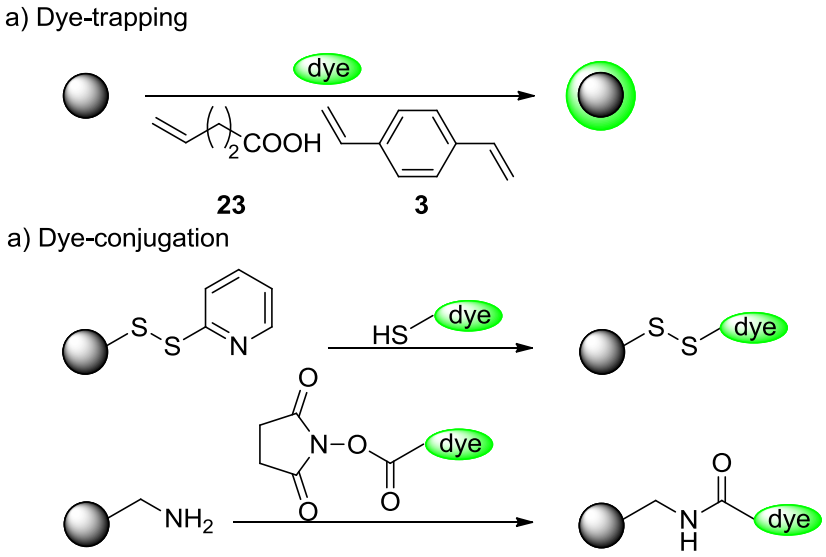

Fig. 3.2. Routes to generate fluorescent particles after polymerisation: (a) dye-trapping; and (b) dye-conjugation.

Alternatively, particle labelling can be achieved *in situ* during the polymerisation process (Figure 3.3). The simplest approach is the addition of a hydrophobic dye into the polymerisation mixture which is then trapped in the particle (Figure 3.3a).[107,108] However, due to lack of covalent bonds between dye and polymer, the dye can still leak out of the particle. This limits the conditions that a particle can be exposed to for chemical transformations. Another strategy uses fluorescent polymers, such as poly[2-methoxy-5-(2-ethylhexyl-oxy)-1,4-phenylenevinylene (MEH-PPV) **24**, poly[(9,9-dioctylfluorenyl-2,7-diyl)-*co*-(1,4-benzo-{2,1′,3}-thiadiazole)] (PFBT) **25** or polythiophene-based polymers **26** with fluorescent particles fabricated by direct entanglement[109,110] or interpenetration[111] of the fluorescent polymers into particles (Figure 3.3b). Another approach involves fluorescent monomers that can be added to the polymerisation process.[112] This approach has the advantage of generating a truly homogenous distribution of fluorescence giving particles with a high number of available surface functionalities and long-term fluorescent stability. In theory, a

broad range of fluorophores can be employed. However, the number of fluorescent particles which have been synthesised following this route is limited due to the small number of available polymerisable fluorophore monomers. These include rhodamine[113], fluorescein[113] and boron-dipyrromethene (BODIPY)[114] which have been conjugated to an acrylic acid unit to give **27a**, **27b** and **28**, respectively or nitrooxabenzodiazole linked to a methylmethacrylate to give **29**[115] and vinyl derivatised naphthalimide **30** (Figure 3.3c).[116]

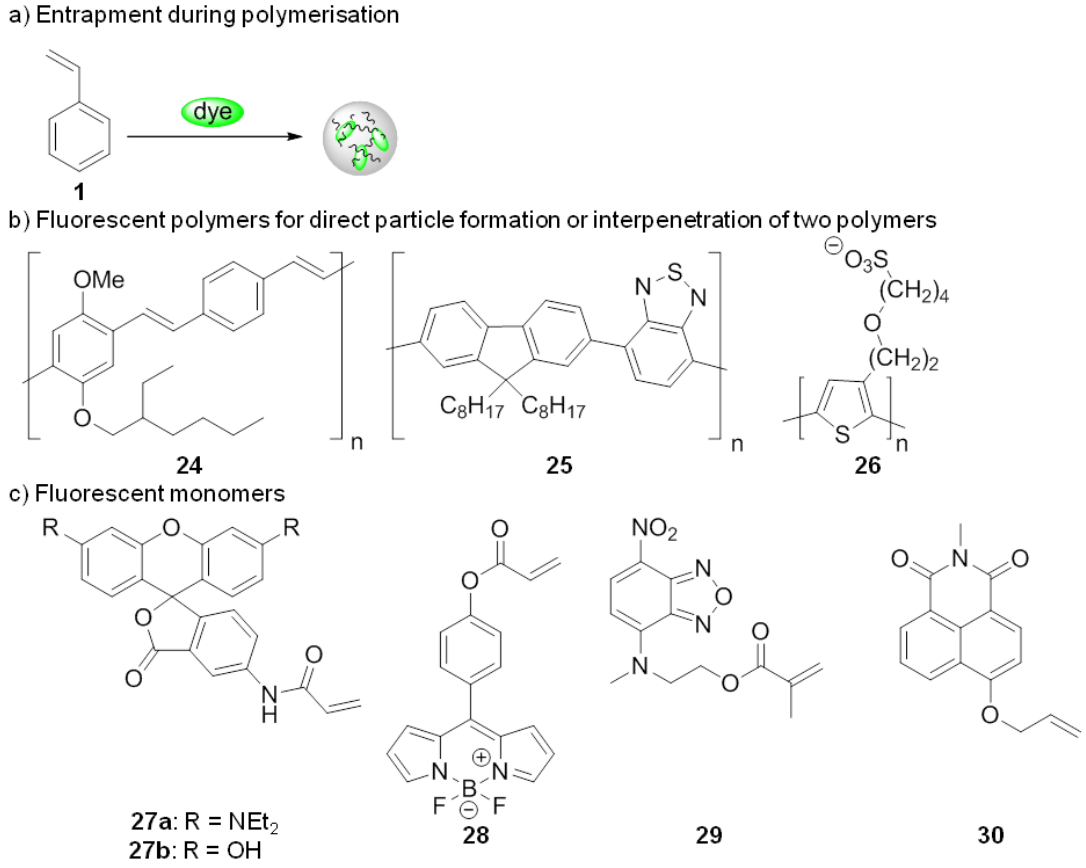

Fig. 3.3. Strategies for generating fluorescent particles during polymerisation: (a) entrapment; (b) use of fluorescent polymers; and (c) via addition of fluorescent monomers.

However, the incorporation of fluorescent monomers has not been studied systematically with an analysis of the influence of fluorescence intensity following modifications of the dye, or comparison of particle fluorescence when prepared with different polymerisable monomers. Herein, the preparation and investigation of highly fluorescent particles dependent on varying the fluorescein-based monomers is shown. Furthermore, the abilty of these particles to cross cell membranes to allow a variety of applications in biology is investigated.

3.2 Polymerisable fluorescein derivatives and their properties

To form fluorescent particles with direct attachment of the dye, fluorophores with a polymerisable functional group were used. The ability to achieve direct particle synthesis was investigated by modifying fluorescein **22** with a styryl group. Since the fluorescent properties of fluorescein depend strongly on the ability to form the dianionic species, three novel fluorescein monomers were synthesised with the styryl-functionality in a number of different locations (Scheme 3.2).[*]

MONOMER SYNTHESIS. The styryl group was introduced on the xanthine moiety of fluorescein **22** by transformation of the hydroxy group into an *O*-triflate **31** followed by Suzuki-Miyaura cross-coupling with *para*-vinylphenylboronic acid to give xanthine-styryl fluorescein **32** in moderate overall yield (46%). An alternative attachment of the styryl group was achieved by alkylation of fluorescein **22** with 4-vinylbenzyl chloride giving **33**. Saponification of this product selectively removes the ester to give *O*-styryl fluorescein **34** in good overall yield (72%). Since it is well established that modifications of the xanthine moiety influence fluorescence,[98,117–119]

[*] Fluorescein derivatives were jointly synthesised with Dr S. V. Chankeshwara.

the styryl group was also introduced on the phthalic moiety. This fluorescein derivative was synthesised by Suzuki–Miyaura cross-coupling of *para*-vinylphenylboronic acid and 5-iodofluorescein **35**[115] (synthesised by a Sandmeyer reaction of 5-aminofluorescein **36**) to give phthalic-styryl **37** in moderate overall yield (45%) (Scheme 3.2).

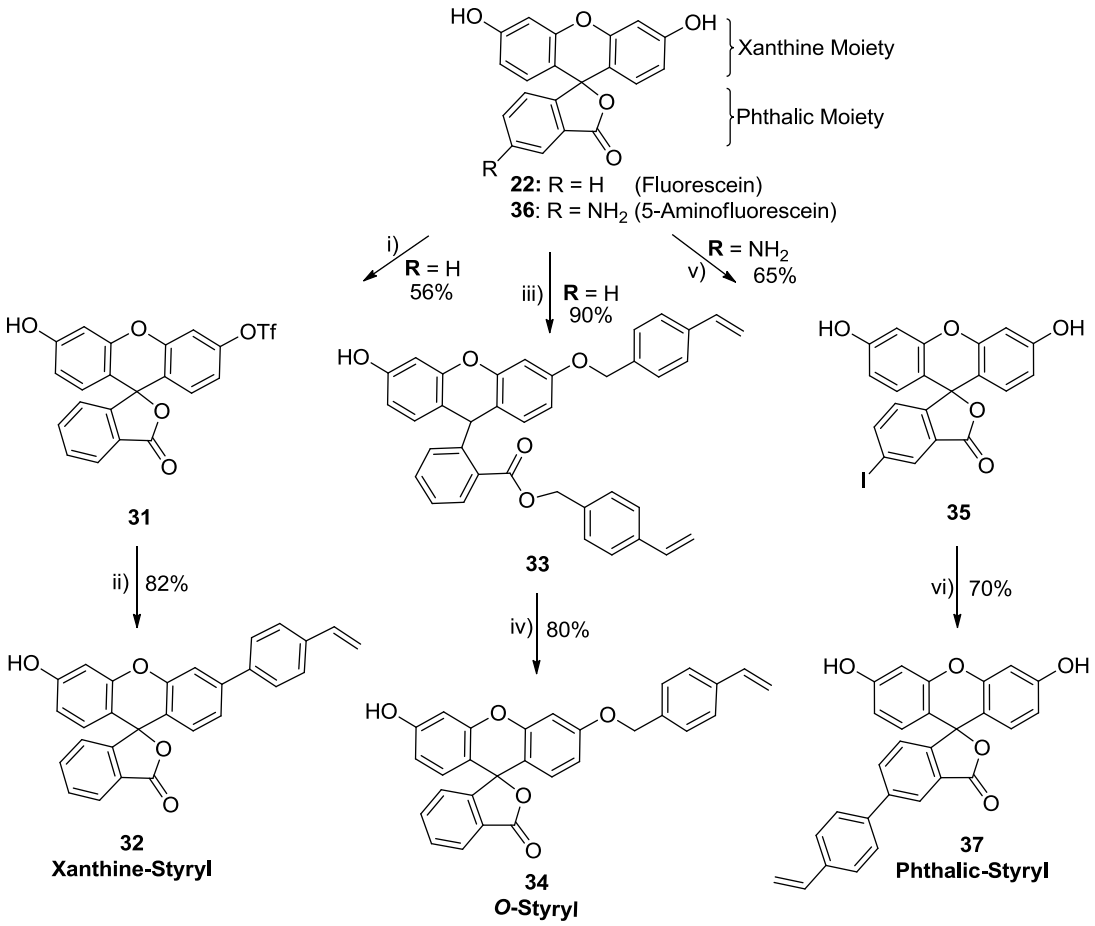

Scheme 3.2: Synthesis of polymerisable fluorescein-based monomers. (i) $PhNTf_2$, K_2CO_3, DMF, 80 °C (μw), 30 min; (ii) 4-vinylphenylboronic acid, $Pd(OAc)_2$, PPh_3, K_2CO_3, dioxane/water (9:1), 120 °C (μw), 30 min; (iii) 4-vinylbenzyl chloride, K_2CO_3, DMF, 60 °C, 12 h; (iv) LiOH, THF/water (1:1), 50 °C, 6 h; (iii) pH 3, conc. HCl; (v) conc. HCl, $NaNO_2$, KI, 0 °C to rt; 2 h; (vi) 4-vinylphenylboronic acid, $Pd(OAc)_2$, PPh_3, K_2CO_3, dioxane/water (9:1), 120 °C (μw), 30 min.

FLUORESCENT PROPERTIES OF THE MONOMERS. Modification of the fluorophores, in particular altering their conjugated system, may affect their fluorescent properties. Figure 3.4 shows the fluorescence spectra of monomers **32**, **34** and **37** in comparison to 5(6)-carboxyfluorescein. The fluorescence spectra were recorded in phosphate buffered saline (PBS) at pH 7.4 with an excitation wavelength of 488 nm. As expected, the change in the xanthine moiety had a dramatic effect on fluorescence, showing undesirable interference with the conjugated system by suppressing the fluorescent anionic quinone form. Transformation of the hydroxyl group to the styryl group **32** reduced fluorescence by over 30-fold. The conjugation of the styryl moiety as ether **34** restored some of this fluorescence but this was still 4-fold lower than that of 5(6)-carboxyfluorescein. It is known that modifications on the phthalic anhydride functionality generally have a minor effect on the fluorescence intensity. In fact, the attachment of the styryl group to the 5-position of fluorescein gave comparable fluorescence to 5(6)-carboxyfluorescein. An image of the four compounds at 10 μM in PBS clearly demonstrated the different effects of the styryl modifications. 5(6)-carboxyfluorescein and **37** gave very bright yellow solutions, **34** was only slightly yellow, while **32** had more of a brown coloration (Figure 3.5).

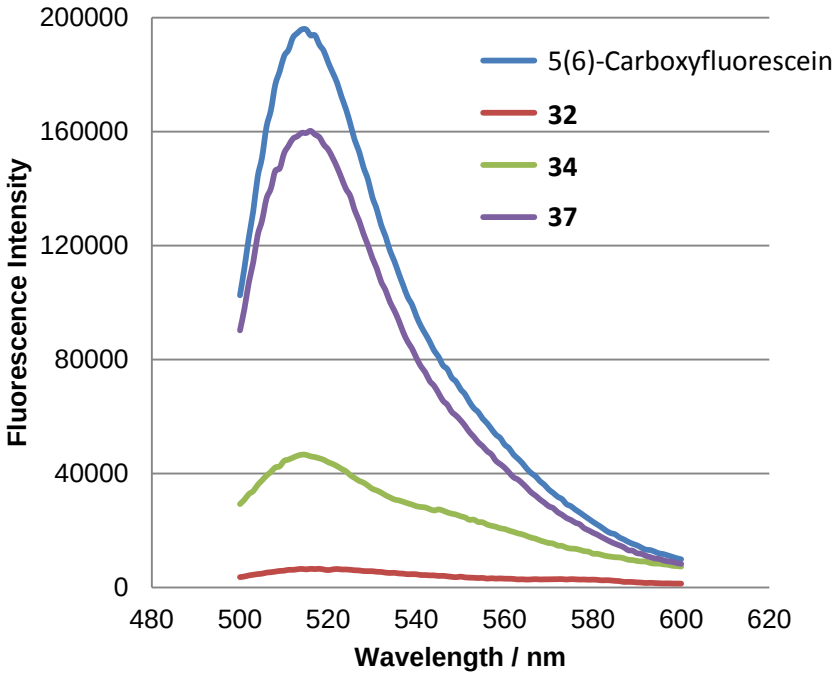

Fig. 3.4. Fluorescent properties of fluorescein monomers **32**, **34**, **37** and 5(6)-carboxyfluorescein (λ_{ex} = 488 nm, 10 nM solution in PBS, pH 7.4).

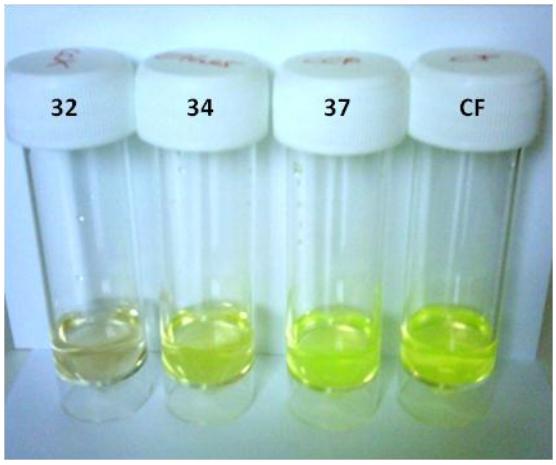

Fig. 3.5. Solutions of fluorescein monomers **32**, **34**, **37** and 5(6)-carboxyfluorescein (CF) (10 µM solutions in PBS, pH 7.4).

3.3 Synthesis of fluorescent polymeric particles and their properties

PARTICLE SYNTHESIS AND CHARACTERISATION. The fluorescent monomers were used to prepare fluorescent polymer particles to investigate the effects of the monomers on the fluorescent properties of the particles. Aminomethyl-functionalised

polystyrene-based particles were synthesised by an emulsifier-free emulsion polymerisation using styrene **2** and the crosslinker divinylbenzene (DVB) **3** with functionality introduced by addition of *para*-vinylbenzylamine hydrochloride (VBAH) **1**[41,52] with the addition of fluorescent monomers **32**, **34** or **37** (3%) (Scheme 3.3a). Polymerisation gave monodisperse particles (average diameter of 200 nm) with a polydispersity index (PDI) below 0.1 for all particles (Table 3.1).

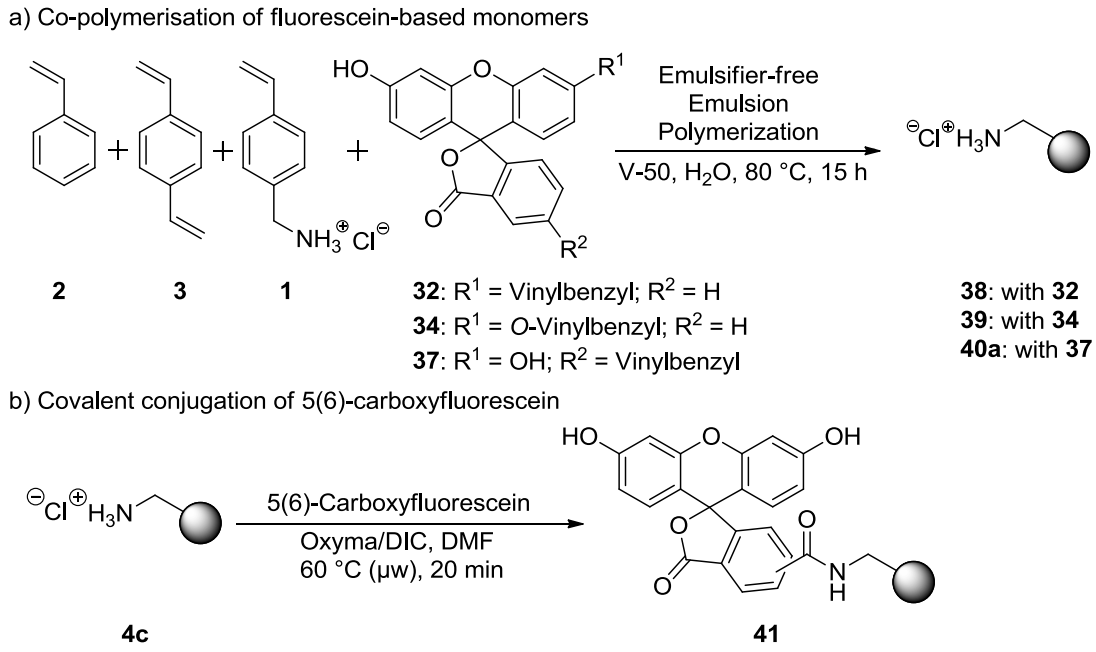

Scheme 3.3. Synthesis of fluorescent polymeric particles: (a) co-polymerisation of fluorescein-based monomers; and (b) covalent conjugation of 5(6)-carboxyfluorescein.

Table 3.1. Particle size, PDI and amine loading of fluorescent particles.

Particles	Size	PDI	Amine Loading
4c	224 nm	0.014	78 μmol/g
38	189 nm	0.099	121 μmol/g
39	217 nm	0.043	114 μmol/g
40a	187 nm	0.041	105 μmol/g

SEM images demonstrated that all particles had a uniform spherical morphology with particle sizes determined by dynamic light scattering (Table 3.1 and Figure 3.6). Quantification of the aminomethyl groups on the particles demonstrated that these were present at similar levels to those found on unlabelled particles indicating that the fluorescent monomers did not alter the loading levels of the particles (Table 3.1).

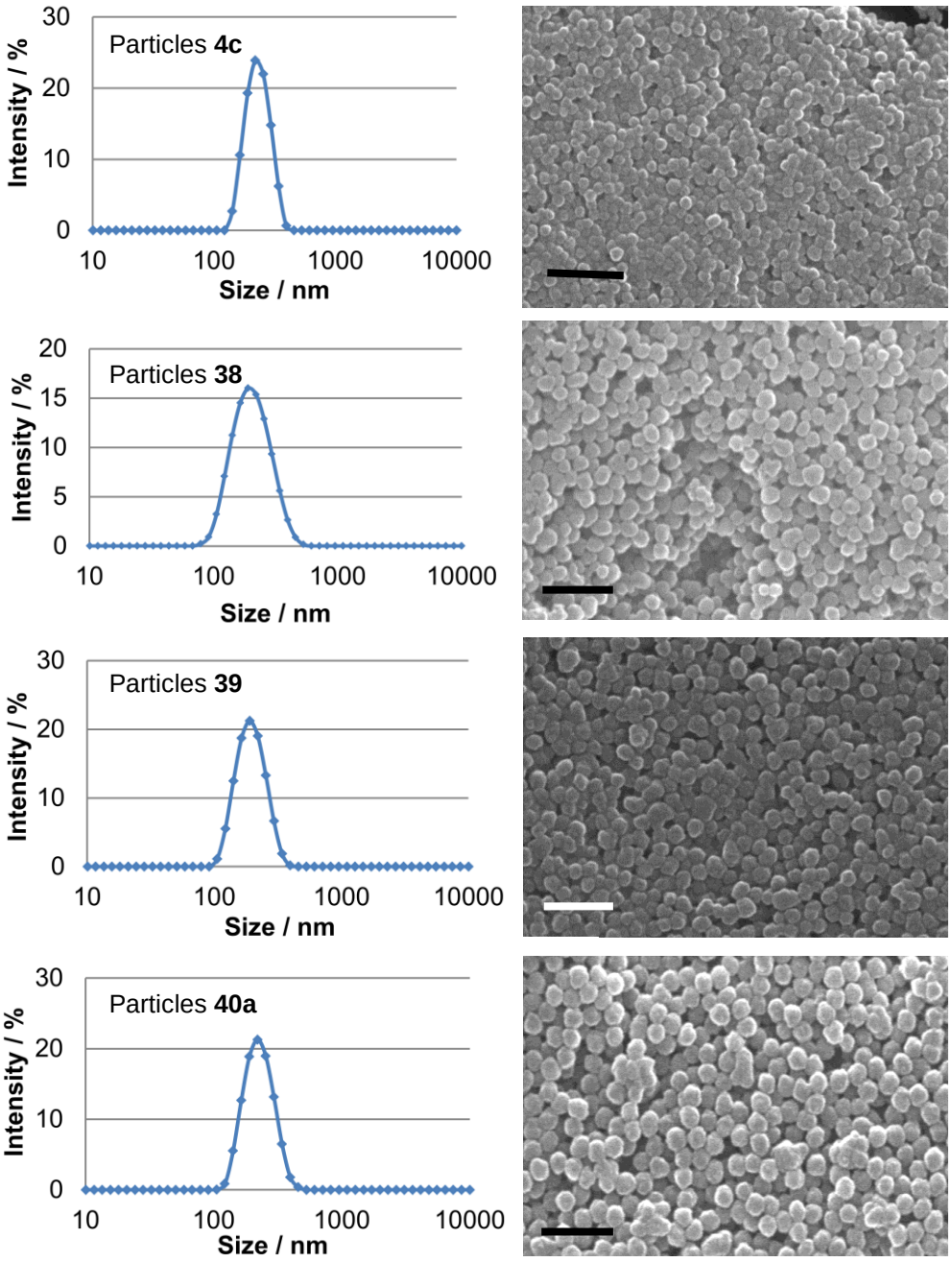

Fig. 3.6: Sizes of the fluorescent polymeric particles **4c**, **38**, **39** and **40a** (**4c**: 224 nm, PDI: 0.014; **38**: 189 nm, PDI 0.099; **39**: 217 nm, PDI 0.043; and **40a**: 187 nm, PDI: 0.041. Scale bar equals 1 µm).

FLUORESCENT PROPERTIES OF THE PARTICLES. Analysis of the fluorescent properties of the particles was carried out with a flow cytometer which is normally used for analysing cells but also analyses the morphology and fluorescent properties

of any three-dimensional object. In principal, one object at a time flows through a laser beam and scatters it. The scattered light is detected, separately, as forward (FSC) and sideward (SSC) scatter which carries information about size and granularity, respectively. Typically the received data are important for cellular analysis to distinguish cell-types and even identify properties of cell populations such as viability. Moreover, laser light irradiation can also be used to measure fluorescence intensities of objects or cells containing fluorescent dyes. A flow cytometer is generally equipped with monochromatic light sources of different wavelengths to allow measurement of a variety of fluorescence signals simultaneously.

The fluorescent particles prepared herein were excited at 488 nm and the emission filter was set to 515-545 nm to quantify the fluorescein-based fluorescence intensity of the particles. The two-dot plot (SSC versus FSC) of unlabelled particles **4c** (grey) and fluorescent particles **40a** (green) demonstrates that the morphology was similar for both types of particles (Figure 3.7a). Following gating of the particles, a two-dot plot (fluorescein fluorescence versus FSC) demonstrates the fluorescence shift of fluorescein-styryl polymerised particles in comparison to unlabelled particles (Figure 3.7b). The fluorescence was quantified and determined to be not significant for unlabeled particles **4c** (< 150 AU) (Figure 3.7c). As a positive control, unlabelled particles **4c** were conjugated to 5(6)-carboxyfluorescein to give **41** (Scheme 3.3b) with a fluorescence intensity of approximately 10^4 AU. The xanthine-styryl particles **38** (8000 AU) had a lower fluorescence than the secondary conjugated particles **41**. However, the fluorescence intensity approximately doubled for **39** (24,000 AU) which incorporated the *O*-styryl monomer. A further 5-fold fluorescent enhancement

resulted from the use of the fluorescein derivative functionalised via the phthalic moiety with styryl **40a** (50,000 AU). This demonstrated the advantages of polymerisation of fluorescent monomers versus secondary dye attachment (Figure 3.7c).

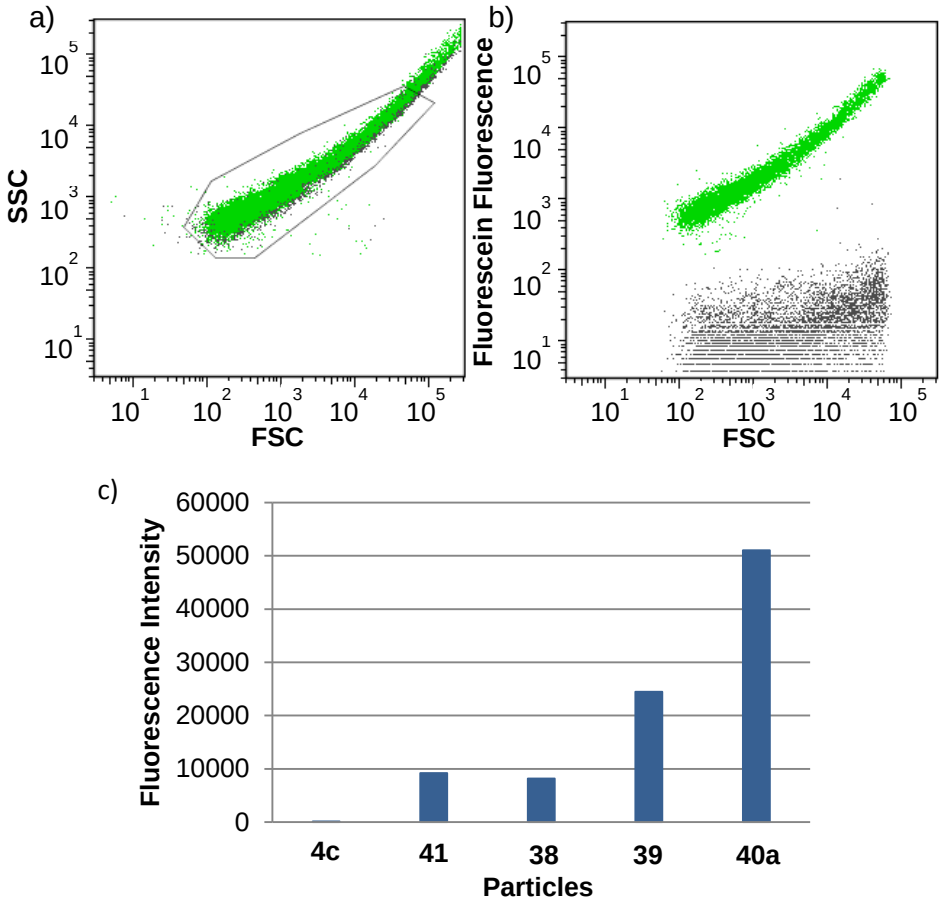

Fig. 3.7. Fluorescent properties of polymeric particles: (a) two-dot plot (sideward scatter vs. forward scatter) of unlabelled particles **4c** (grey) and **40a** (green); (b) two-dot plot (fluorescein fluorescence vs. forward scatter) of unlabelled particles **4c** (grey) and **40a** (green); and (c) fluorescence quantification (**4c**: unlabelled particles; **41**: 5(6)-carboxyfluorescein secondary functionalised particles; **38**: xanthine-styryl polymerised particles; **39**: xanthine-*O*-styryl polymerised particles; **40a**: phthalic-styryl polymerised particles).

It has been shown previously that surface attachment of fluorophores can lead to self-quenching[120,121] which can be avoided using fluorescent monomers that distributed uniformly throughout the particle's structure (Figure 3.8a). Moreover, the

fluorescent intensity of 5(6)-carboxyfluorescein is reduced following amide bond attachment.[119,122] This attachment increases the donor-excited photoinduced electron transfer (dPet) effect. Herein, the excited molecule (xanthine moiety of fluorescein) donates its energy via an electron transfer into the acceptor molecule (phthalic moiety of fluorescein) resulting in loss of fluorescent emission (Figure 3.8b).

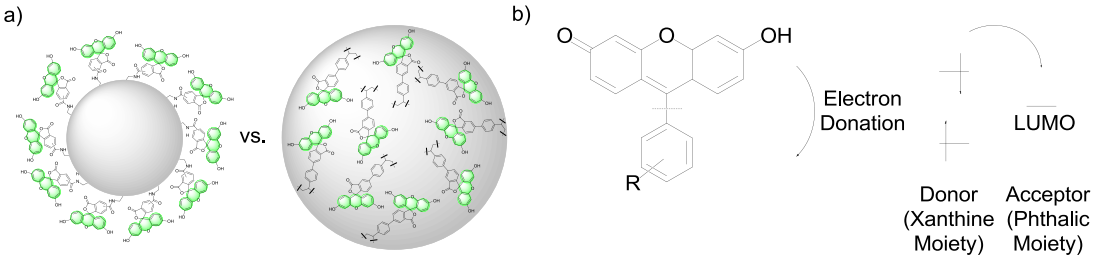

Fig. 3.8. Advantages of polymerised fluorescein and surface-attached fluorescein: (a) illustration of the self-quenching surface with attachment and homogenous distribution of fluorescein; and (b) dPET-effect in fluorescein.

PARTICLE MODIFICATION. An additional feature of the fluorescein particles generated here is the availability of the amino groups for conjugation. Particles **40a** were further investigated and coupled to FmocNH-PEG_3-OH **14** followed by Fmoc-removal with the reactions monitored by the particles' zeta potential (Figure 3.9).[92] Initially, particles **40a** had a zeta potential of +18 mV which after FmocHN-PEG-OH coupling **42** was reduced to -6 mV due to the loss of charge. A zeta potential of +6 mV was measured after Fmoc-deprotection **43a**. Spacer coupling was carried out with maintenance of fluorescence throughout the synthesis.

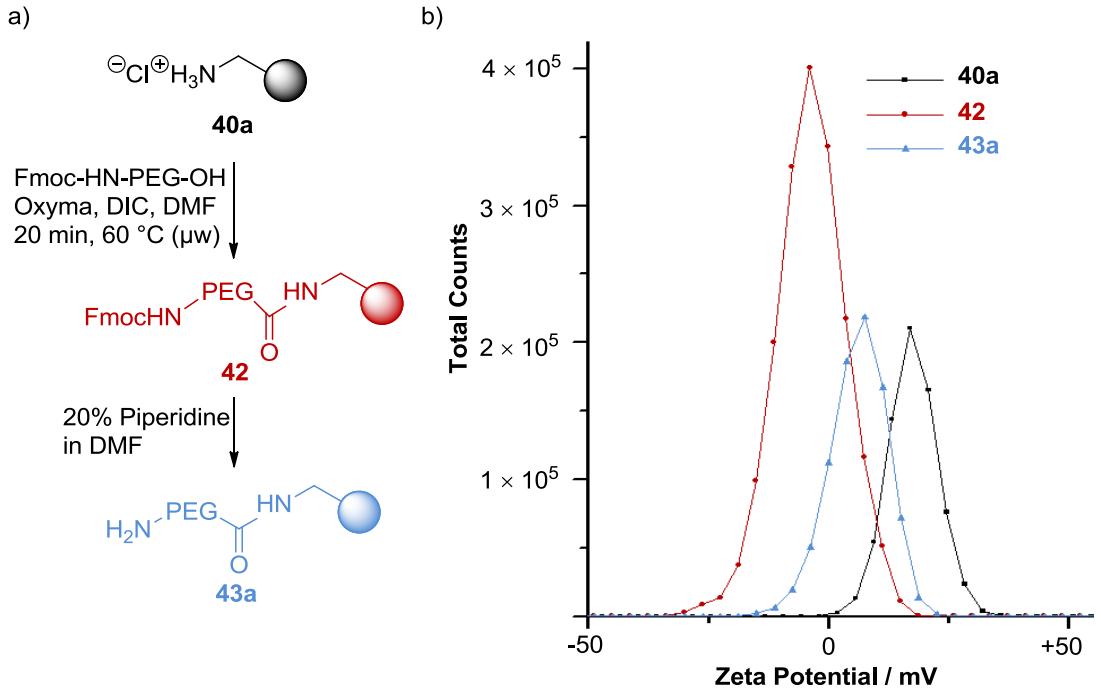

Fig. 3.9. Reaction monitoring on fluorescent particles: (a) reaction sequence; and (b) zeta potential mediated reaction monitoring.

3.4 Cellular uptake of fluorescent polymeric particles

The cellular uptake of particles was investigated by flow cytometry and fluorescence microscopy. The principal to determine the fluorescence of cells following particle internalisation is identical to the above described method for analysis of fluorescent particles. Human embryonic kidney 293T cells (HEK293T) and cervical cancer cells (HeLa) were used since they are regularly used in biological experiments. Therefore, a good cellular uptake would indicate compatibility with a wide range of potential applications in the life sciences.

The influence of particle uptake on cells is shown in the two-parameter plots (FSC versus SSC and FSC versus fluorescein intensity) in Figure 3.10. The healthy, untreated population of HEK293T cells was identified by its granularity (SSC distribution) and volume (FSC distribution) as shown by the gated image (Figure 3.10a). Following internalisation of particles **40a**, granularity was seen to be affected

due to the intracellular presence of the particles (Figure 3.10b). The cellular uptake of particles is size-dependent, amongst other factors (Chapter 5), and up to approximately 1,000 large nano to submicron-sized particles can be taken up by each cell.[123] These particles also scatter light and, hence, shift the SSC signal, however this shift does not indicate an unhealthy cell population.[124,125] Therefore, the control gate was enlarged to include cells with high particle internalisation with the healthy cell population identified by cell volume (Figure 3.10b). The cellular uptake of fluorescent particles was identified by a significant shift to higher fluorescence following exposure to particles **40a** (Figure 3.10c). The same results were determined for HeLa cells with particles demonstrating high cellular uptake in combination with high cellular fluorescence (Figure 3.10d – f).

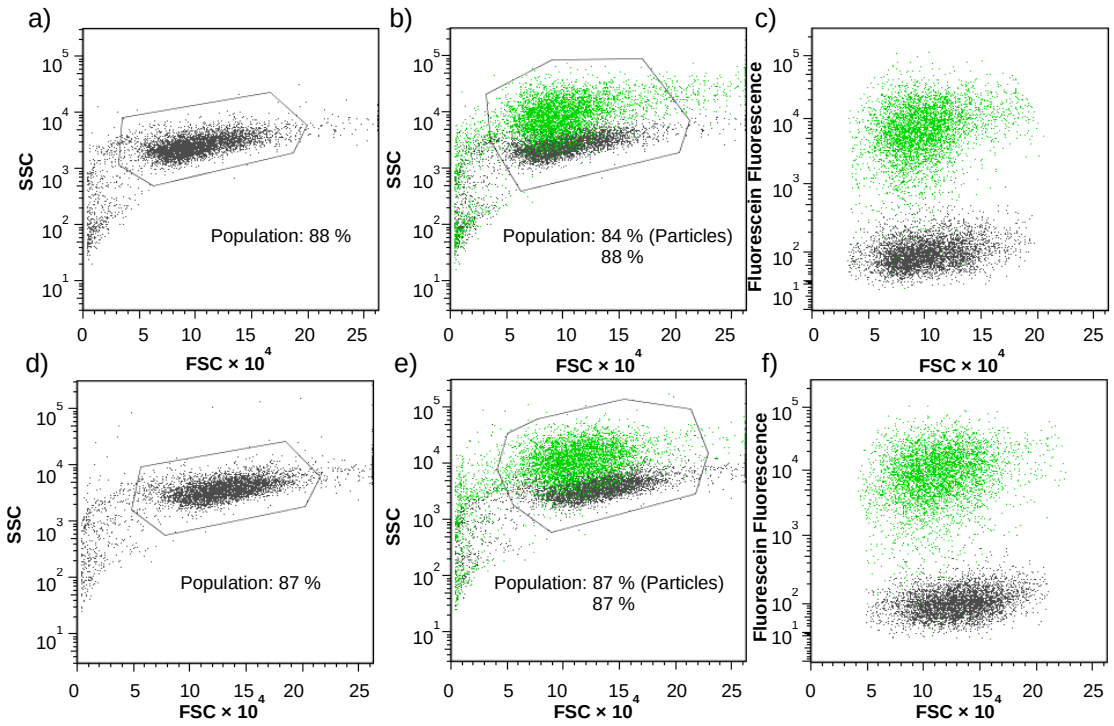

Fig. 3.10. Two parameter plot of flow cytometric analysis of particle uptake: (a) untreated HEK293T cells and gating (FSC vs. SSC); (b) untreated HEK293T cells (grey) and HEK293T cells with particles (green) **40a** (FSC vs. SSC); (c) untreated HEK293T cells (grey) and HEK293T cells with particles **40a** (green) (FSC vs. fluorescein fluorescence); (d) untreated HeLa cells and gating (FSC vs. SSC); (e) untreated HeLa cells (grey) and HeLa cells with particles (green) **40a** (FSC vs. SSC); and (f) untreated HeLa cells (grey) and HeLa cells with particles **40a** (green) (FSC vs. fluorescein fluorescence).

Figure 3.11 (HEK293T) and 3.12 (HeLa) summarises the results of cellular uptake of *in situ* polymerised fluorescein-containing particles **40a** and 5(6)-carboxyfluorescein-conjugated particles **41**. The fluorescent intensity of the cells increased gradually with higher particle concentrations for both sizes. However, the fluorescence of phthalic styryl particles was approximately 4-5-fold higher in comparison to 5(6)-carboxyfluorescein coupled particles at the same concentration. Representative histograms verified the good cellular uptake and high fluorescent intensities at varying concentrations. The cellular uptake data were in accordance with the fluorescence measurements of the particles which demonstrated a 4-5-fold

increase in fluorescence of the phthalic styryl particles **40a** in comparison to particles **41** which fluorophore coupled using more conventional methods. Microscopy of particle treated cells verified cellular uptake (Figure 3.11d and 3.12d).

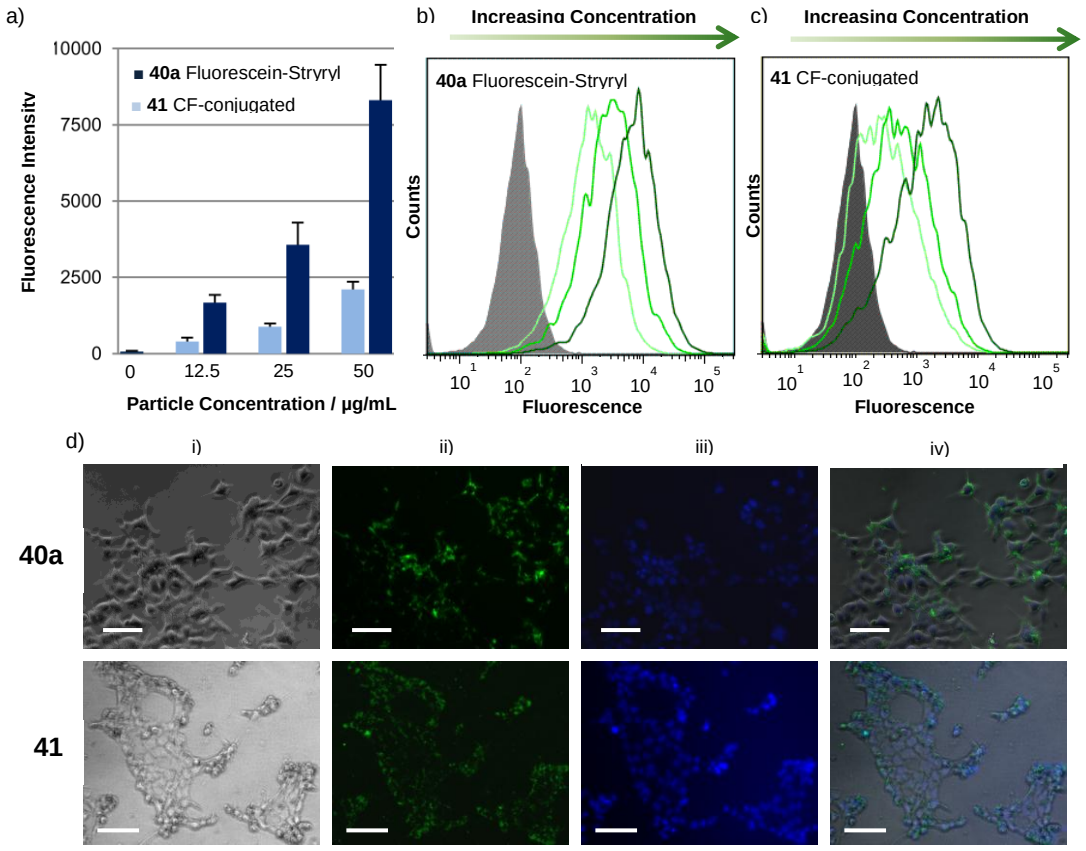

Fig. 3.11: Cellular uptake of fluorescent particles by HEK293T cells: (a) fluorescence intensity of cells treated with particles **40a** (dark blue) and **41** (light blue) (n = 3); (b) fluorescence histograms of cells treated with particles **40a** (particle concentration increases with shade); (c) fluorescence histograms of cells treated with particles **41** (particle concentration increases with shade); and (d) microscopy images following internalisation by HEK293T cells. (i) bright-field; (ii) green: fluorescent particles **40a** or **41** (λ_{ex} = 488 nm); (iii) blue: nuclei stain Hoechst 33342 (λ_{ex} = 405 nm) and (iv) composite image. Scale bar = 100 µm.

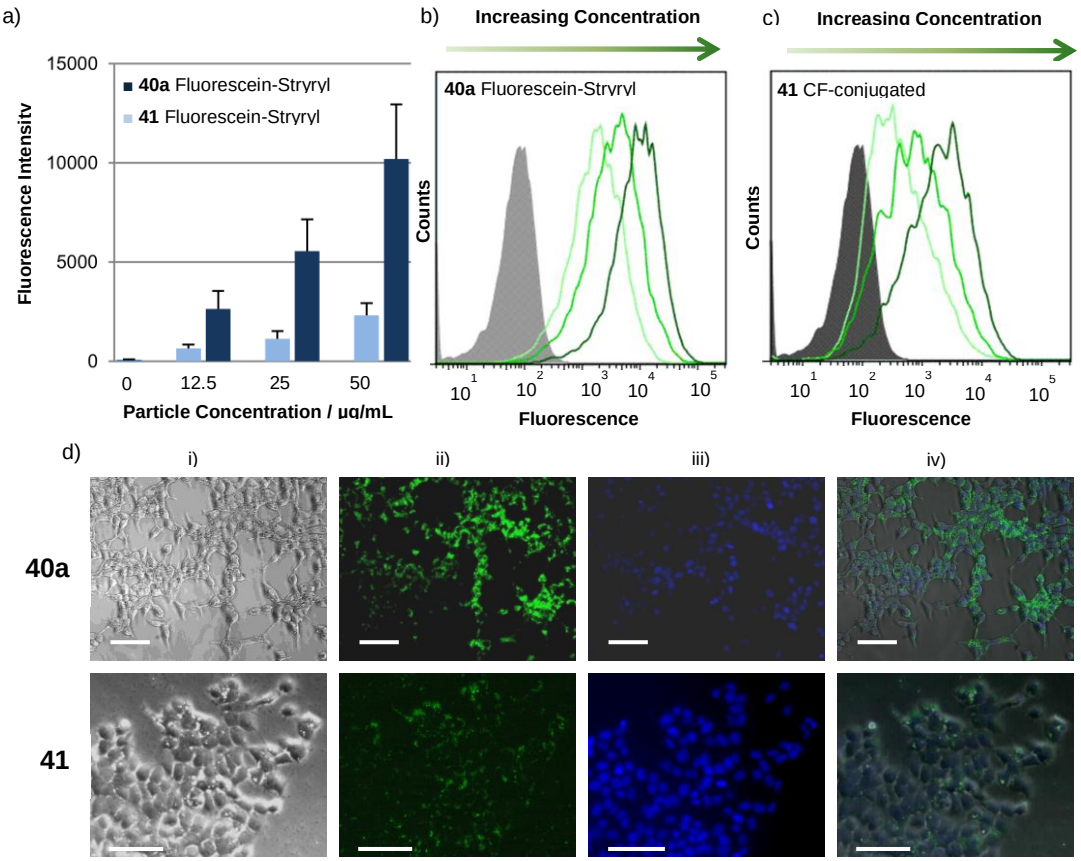

Fig. 3.12: Cellular uptake in HeLa cells: (a) Fluorescence intensity of cells treated with particles **40a** (dark blue) and **41** (light blue) (n = 3); (b) fluorescence histograms of cells treated with particles **40a** (particle concentration increases with shade); (c) fluorescence histograms of cells treated with particles **41** (particle concentration increases with shade); and microscopy images following internalisation in HeLa cells (i) bright-field; (ii) green: fluorescent particles **40a** or **41** (λ_{ex} = 488 nm); (iii) blue: nuclei stain Hoechst 33342 (λ_{ex} = 405 nm); and (iv) composite image. Scale bar = 100 µm.

3.5 Conclusion

Three novel fluorescein monomers in which the polymerisable styryl groups were attached in different positions were synthesised and their fluorescent properties analysed. Conjugation to the xanthine moiety of fluorescein considerably reduced fluorescence for both carbon-carbon and ether linkages. The modification via the phthalic anhydride moiety resulted in a similar fluorescence to 5(6)-carboxyfluorescein. The monomers were used to prepare monodisperse polymer

particles of ca. 200 nm with inherent fluorescent properties arising from the fluorescent monomers. Particles with xanthine-styryl fluorescein **38** had the lowest fluorescence, the fluorescence of ether-styryl-based particles **39** doubled, and a further increase was seen for particles using the phthalic-styryl monomer **40a**. However, in comparison to secondary conjugated 5(6)-carboxyfluorescein particles, fluorescent particles **39** (2-fold) and **40a** (4-5-fold) had improved fluorescence. The polymerisation resulted in evenly distributed fluorophores throughout the particle structure thereby avoiding self-quenching effects which resulted from the surface attachment of 5(6)-carboxyfluorescein. Moreover, styryl fluorescein polymerised particles **40a** were also taken up by cells and these exhibited a 4-5-fold increase in fluorescence signal over 5(6)-carboxyfluorescein-conjugated particles **41**.[126]

The herein synthesised particles are useful for a variety of applications in particular if particle tracking is required. A further enhancement could be achieved by amplifying the number of fluorescent dyes and using near infrared dyes which can be incorporated by direct polymerisation. This could allow the fluorescent particles to be used for *in vivo* applications.[127] Moreover, the monomeric fluorophores are not limited to particle-based applications. Polymeric surface functionalisation with fluorescent dyes[128] allows, for example, the fluorometric measurement of pH values of solutions without addition of compounds.[129] Moreover, the release of fluorescein monomers from a polymer by an external impulse could be used as a highly sensitive detection method.[130]

Chapter 4

DUAL-FUNCTIONALISED POLYMERIC PARTICLES

Parts of this chapter have been submitted for publication as:

Thielbeer, F., Chankeshwara, S. V., Johansson, E. M. V. and Bradley M. Pd-mediated bio-orthogonal conjugation of nanoparticles for intracellular delivery and targeting. *Submitted* **2012**.

4.1 Biomolecule conjugation to nano and microparticles

Nano and submicron polymeric particles have gained a prominent position in the life sciences due to their wide variety of applications, namely as carriers of intracellular sensors or as tools for cellular delivery. Crucial in the preparation of these constructs is the controlled attachment and display of bioactive molecules.

PARTICLE CONJUGATION. A wide variety of bioactive compounds with interesting intracellular applications cannot pass through the cell membrane and need a carrier to do so (Chapter 5). Increasingly, polymeric particles which have been

shown to deliver conjugated compounds into the cytosol are used as carriers.[131] To achieve successful delivery, the cargo can be attached to the particles either via a cleavable or non-cleavable bond. Herein, a mild conjugation method compatible with biomolecules is sought after. An additional desired feature is the controlled conjugation of several bioactive molecules onto the same particle but this requires orthogonally compatible reaction conditions.[24] There is increasing demand for *bio*orthogonal coupling, *i.e.* the ability to carry out chemoselective reactions in the presence of functionalities such as amino, carboxyl or thiol groups under physiological conditions and/or in the environment of cells.[132]

The most common way to conjugate biomolecules is via amino or carboxyl groups and the formation of amide (peptide) bonds (Figure 4.1a, b). The acid functionality is typically activated to form an active ester which undergoes nucleophilic attack by the amine to yield the amide bond. Standard routes to activated acids employ carbodimides such as 1-ethyl-3-(3-dimethylaminopropyl)carbodimide (EDC)[133] which can be used under aqueous conditions, or diisopropyl-carbodimide (DIC) in combination with hydroxybenzotriazole (HOBt)[134] if organic solvents are applicable. Otherwise, the acid can be activated via the formation of a succinimidyl ester to react directly with free amines. The presence of aldehydes has also been used to generate a secondary amine linkage by imine formation and subsequent reductive amination (Figure 4.1c).[36] Aldehyde-containing molecules have been conjugated to hydrazine-functionalised particles via hydrazone ligation (Figure 4.1d).[135]

A further well-known reaction in the field of bioconjugation generates thioethers from maleimides and thiols (Figure 4.1e).[136] In addition, thiol-functionalised

particles can be linked via disulphide bridges to bioactive compounds giving an intracellular cleavable disulphide linker (Figure 4.1f).[137] Recently, transition metal-catalysed bioconjugations, namely copper-catalysed Huisgen cycloadditions, have been employed for the funtionalisation of azide-containing particles (Figure 4.1g).[138] Moreover, cargos have been bound to particles by non-covalent bond interactions, *e.g.* NTA-bearing particles bound via nickel and a His-tag modified protein[90] or biotin functionalisation and the attachment of streptavidin-conjugated cargos.[39]

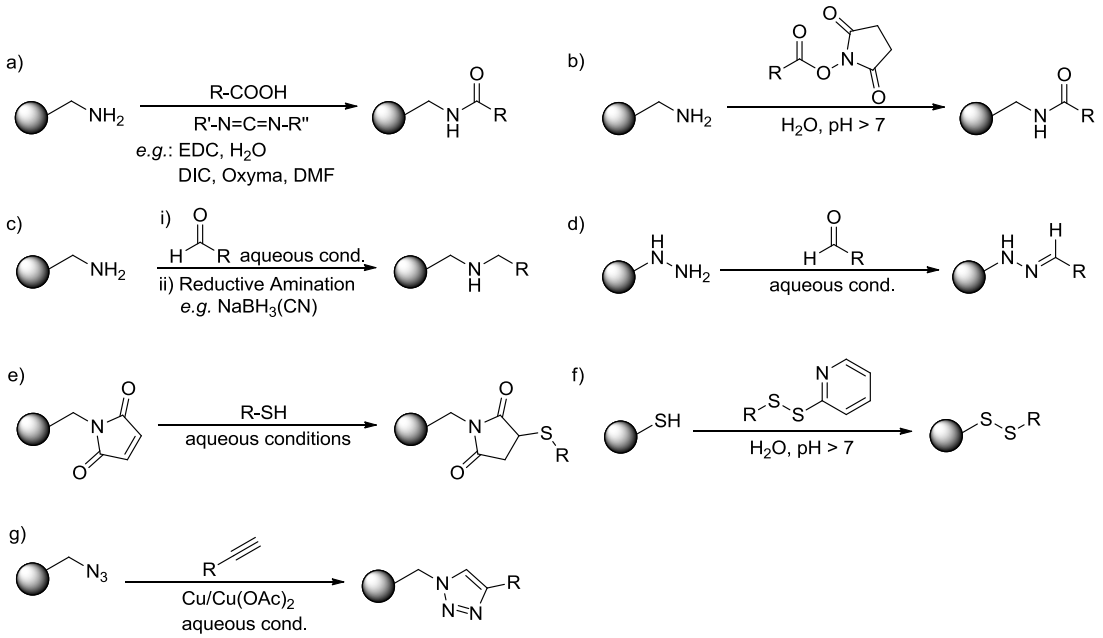

Fig. 4.1. Attachment of biomolecules onto particles: (a) carbodiimide mediated coupling; (b) *N*-hydroxysuccinimide ester mediated coupling; (c) imine formation; (d) hydrazone ligation; (e) maleimide mediated coupling; (f) pyridyl disulfide mediated coupling; and (g) Huisgen cycloaddition.

An emerging field in particle technology is theranostics,[139] a combination of therapy and diagnostic, which generally requires the incorporation of two functions on a particle. A common route is based on the introduction of one function into the particle's interior, while the additional property is attached after polymerisation, *e.g.*

a fluorescent core and a bioactive surface modification.[101] Another route can be followed by attaching spacers incorporating two functional groups which can be orthogonally deprotected and subsequently modified.[38]

However, a more elegant route involves the incorporation of two or more orthogonal functional groups on the particle's surface during the polymerisation process, in addition to core loading. The group of Boons has prepared gold-core nanoparticles with a block-copolymer containing acylhydrazide, amine and azide moieties on the particle surface. They also demonstrated the chemoselective functionalisation of the particles in addition to non-covalent drug loading.[140] Polymeric particles containing azide or alkyne and carboxyl functionalities have also been reported and successfully modified.[141] Azide-functionalised particles have been prepared by reversible addition/fragmentation chain transfer polymerisation (RAFT) with the agents subsequently functionalised via Michael addition and azide groups by Huisgen cycloaddition.[142]

Recently, a variety of palladium-mediated metal-catalysed reactions have been optimised to be used in biological conditions for protein modification in particular,[143] such as Suzuki-Miyaura,[144,145] Heck-Mizoroki[146] or Sonogashira[147,148] reactions (Figure 4.2). The Suzuki-Miyaura cross-coupling has even been performed inside cells[149] and for directly labelling bacteria *in vitro*.[150]

In this chapter the preparation of novel dual-functionalised polymeric particles containing aminomethyl and boronic acid groups are reported. These particles offer the ability to chemoselective functionalisation via amide bond formation and/or Suzuki-Miyaura cross-coupling.

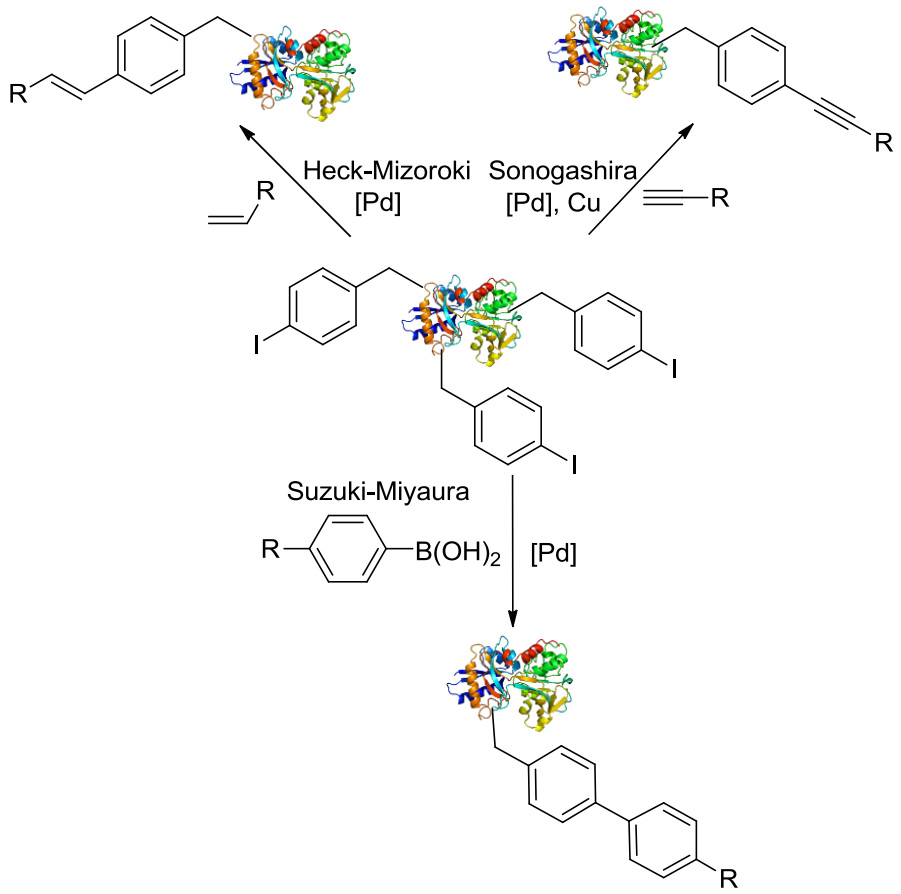

Fig. 4.2. Palladium-mediated protein functionalisation.

4.2 Boronic acid particles and Suzuki-Miyaura cross coupling

PARTICLE SYNTHESIS. The attachment of molecules *via* palladium-mediated Suzuki-Miyaura cross coupling requires the incorporation of either an aryl boronic acid or aryl halide functionality into the particle structure. Previously, polymers functionalised with boronic acid have been prepared to investigate their behaviour towards external stimuli. Kataoka prepared a hydrogel containing boronic acid groups whose swelling was induced by glucose to release insulin.[151] This technique was also used to detect glucose by viscosity measurements.[152] A further feature of boronic acid polymers is their ability to self-assemble into particles[153] and

disassemble following a glucose or pH stimulus.[154] Based on this boronic acid functionalised polymers, the effects of co-polymerising *para*-vinylbenzylboronic acid **44** (VBA) with styrene **2**, divinylbenzene **3** (DVB) and *para*-vinylbenzylamine hydrochloride **1** (VBAH) was investigated (Scheme 4.2).

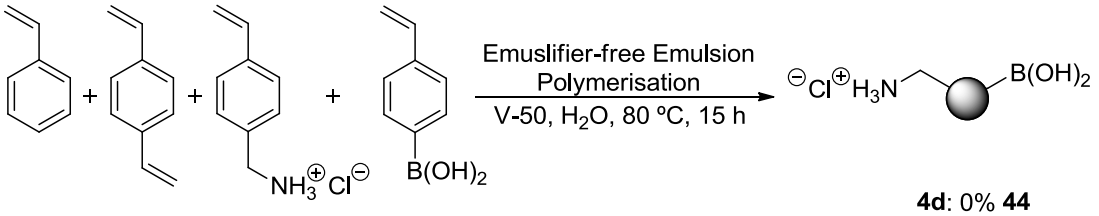

4d: 0% **44**
45: 3% **44**
46: 6% **44**
47: 7% **44**

Scheme 4.1. Synthesis of boronic acid- and aminomethyl-functionalised polystyrene-based polymeric particles for Suzuki-Miyaura-mediated attachment.

The particles were prepared by an emulsifier-free emulsion polymerisation of styrene **2**, cross-linker dinvinylbenzene **3** (2%), *para*-vinylbenzylamine hydrochloride **1** (3%) in water using the water soluble radical initiator V-50. To investigate the effects of the incorporation of $(HO)_2B$-functionalities onto the particle surface, varying amounts (3% **45**, 6% **46** and 9% **47**) of VBA were included and compared to $(HO)_2B$-free particles **4d** (Table 4.1). These had a size of 230 nm and a polydispersity index (PDI) of 0.060 demonstrating a monodisperse distribution and spherical morphology in addition to aminomethyl functionalisation (82 µmol/g). The addition of VBA resulted in a similar size distribution (240 nm) which was also classified as monodisperse with a PDI of 0.071. Scanning electron microscopy images verified these results and showed the spherical morphology of these particles **45** (Figure 4.2). These results are in accordance with the ability to co-polymerise

fluorescein-based monomers, without detrimental effects on the quality of the particle dispersion (Chapter 3).[126]

A further increase in VBA led to a degradation of the particle quality, although the size was still in the 200 nm range. The polydispersity was determined to be 0.190 for 6% VBA and 0.313 for 9% VBA. The rational for this is probably due to an acid-base interaction between VBAH and VBA which disturbed micelle formation thus lowering the quality of the required micelles in which the particles were formed (Table 4.1 and Figure 4.2).[50]

Table 4.1. Influence of VBA concentration on particle properties.

Particles	**Size [nm] (PDI)**	**H_2N-Group [µmol/g]**	**$(HO)_2B$-Group [µmol/g]**
4d (0% VBA)	229 (0.060)	(82 ± 14)	(2 ± 1)
45 (3% VBA)	240 (0.071)	(129 ± 15)	(62 ± 1)
46 (6% VBA)	260 (0.190)	(163 ± 5)	(116 ± 2)
47 (9% VBA)	211 (0.313)	(76 ± 3)	(204 ± 1)

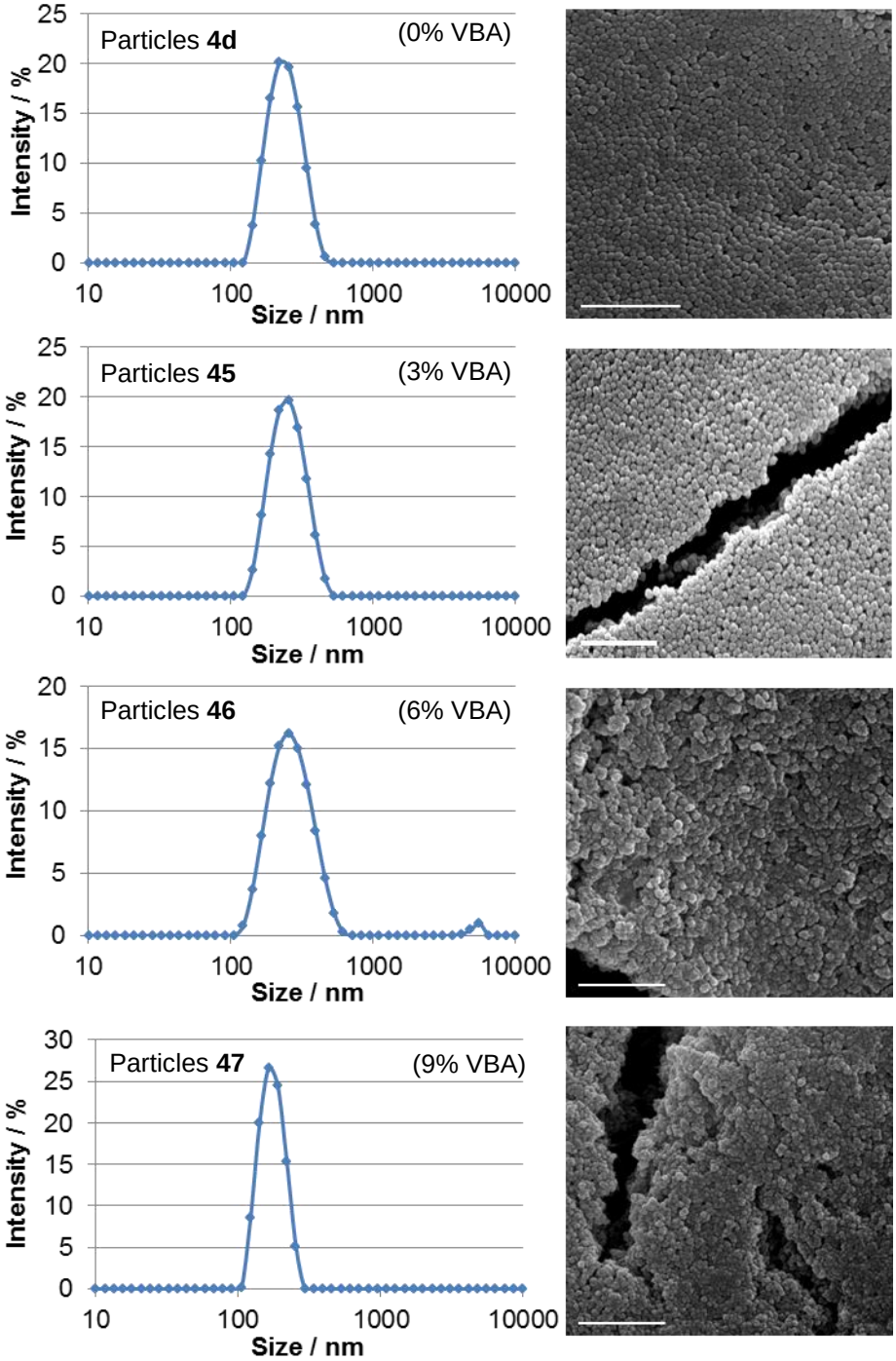

Fig. 4.2. Comparison of particles co-polymerised with *para*-vinylbenzylboronic acid (**4d**: 229 nm, PDI: 0.060; **45**: 240 nm, PDI 0.071; **46**: 260 nm, PDI 0.190; and **47**: 211 nm, PDI: 0.313. Scale bar equals 2 µm).

In addition to the size and morphology of the particles, verification of the surface functionalisations was essential to validate their potential for use in various applications. The loading with amino groups was determined by a quantitative Kaiser

test[55] and was compared to $(HO)_2B$-free particles **4d** (80 µmol/g). Similar loadings were found for $(HO)_2B/H_2N$-particles (80-130 µmol/g) (Table 4.1). Loading fluctuations were also observed following the synthesis of different $(HO)_2B$-free particle batches. To quantify the amount of incorporated boronic acid groups, the particle dispersion was directly analysed by inductively coupled plasma – optical (atomic) emission spectroscopy (ICP-OES).[155] In principal, the dispersion is nebulised and transferred into the plasma where it decomposes into its atomic constituents. As expected, particles prepared without the addition of VBA did not contain boron. However, particles prepared with 3% VBA contained approximately 60 µmol/g boron which gradually increased to 120 µmol/g (6%) and 200 µmol/g (9%), respectively. This demonstrated that boronic acid was incorporated into the particles in a controlled manner and gave particles with boronic acid groups in addition to amino groups (Table 4.1).

Palladium-mediated conjugation. Palladium-mediated Suzuki-Miyaura cross coupling is a mild way to form carbon-carbon bonds. However, so far particle modifications by Suzuki-Miyaura cross couplings have not been reported. It was investigated if a palladium-mediated Suzuki-Miyaura cross coupling specifically takes place between $(HO)_2B/H_2N$-particles and an aryl halide. 5-iodofluorescein[126] **35** was chosen as substrate to investigate the conjugation reaction. This compound enabled the Suzuki-Miyaura reaction to be followed via loss of the $(HO)_2B$-functional groups on the particle as well as fluorescence measurement of the particles after successful coupling.

Previously, the groups of Davis[145] and Lin[148] reported a water soluble palladium catalyst for the palladium-mediated cross coupling and demonstrated the ability to

functionalise iodinated proteins. The palladium catalyst **48** was prepared by basification of 2-amino-4,6-dihydroxypyrimidine **49** to give the sodium salt **50** followed by addition of $Pd(OAc)_2$ (Scheme 4.3a). The Suzuki-Miyaura cross coupling was carried out using a suspension of particles **45**, 5-iodofluorescein **35** and palladium catalyst **48** in PBS at 37 °C (Scheme 4.3b). Herein, 50 equiv. of 5-iodofluorescein were used in combination with a palladium catalyst concentration of 5% with respect to the aryl halogene.

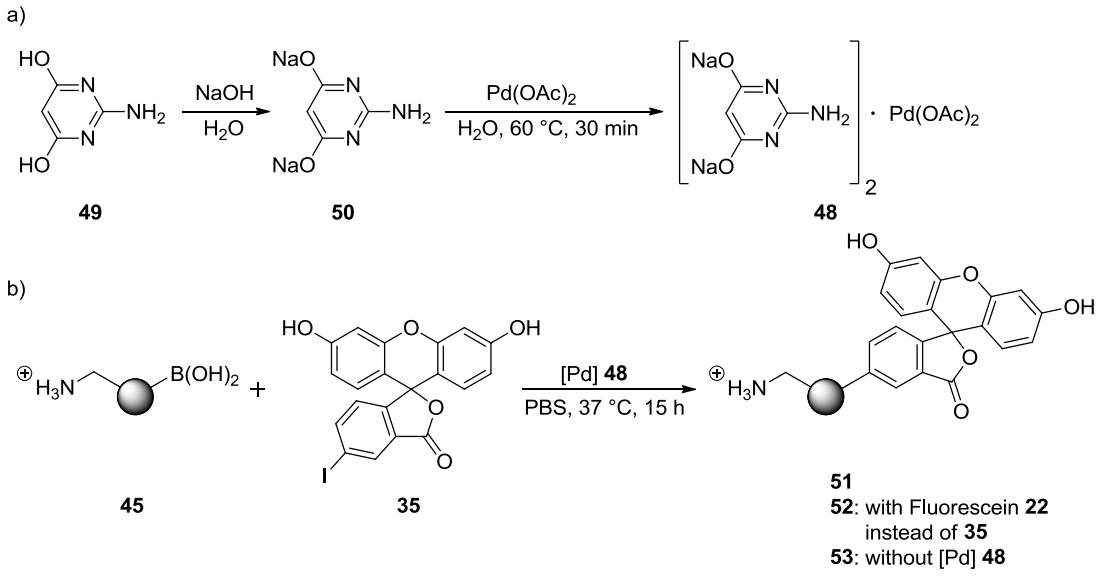

Scheme 4.3. Suzuki-Miyaura cross coupling on polymeric particles: (a) synthesis of palladium catalyst with 2-amino-4,6-dihydroxypyrimidine ligand; and (b) Suzuki-Miyaura cross coupling between 5-iodofluorescein and $(HO)_2B/H_2N$-particles.

An analysis of the boron content of the suspension following the reaction demonstrated that particles **51** containing catalyst and 5-iodofluorescein showed an approximately 40% reduction in boron content (Figure 4.3a). The boron levels in reactions containing non-iodinated fluorescein **52** and lacking catalyst **53** did not change in comparison to starting particles **45**. Additionally, those results were

confirmed by fluorescence intensities of the particles measured via flow cytometry (Figure 4.3b). Unmodified particles **45** had no significant fluorescent properties, but the fluorescence of particles **51** increased approximately 500-fold following 5-iodofluorescein conjugation while the controls had only a slightly increased fluorescence probably due to non-specific adsorption of a small amount of fluorescein. Nevertheless, the loss of boronic acid and increase in fluorescence of the particles demonstrated that the specific Suzuki-Miyaura cross coupling reaction between 5-iodofluorescein and boronic acid had occurred on the particles.

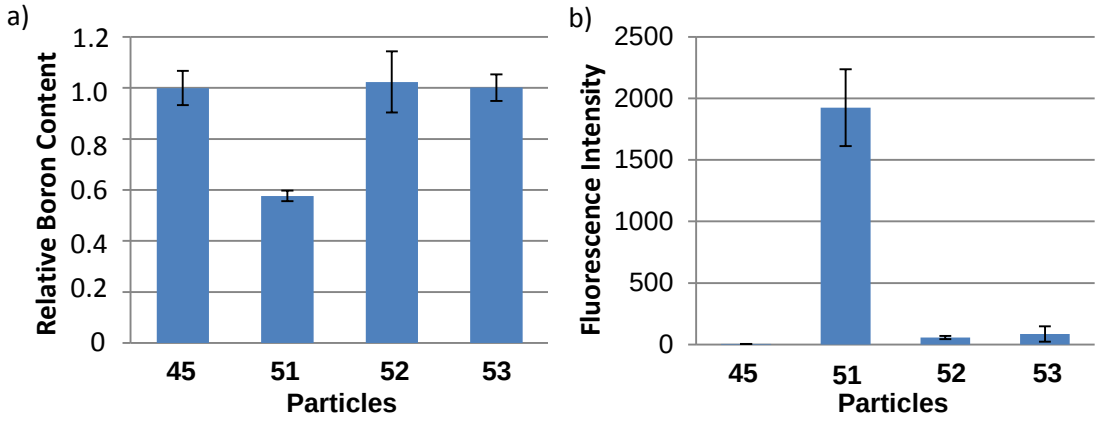

Fig. 4.3. Analysis of $(HO)_2B/H_2N$-particles following Suzuki-Miyaura cross coupling: (a) boron content by ICP-OES; and (b) fluorescence intensity of particles by flow cytometry. (**45**: unmodified $(HO)_2B/H_2N$-particles; **51**: Suzuki-Miyaura cross coupled particles; **52**: with non-iodinated fluorescein; and **53**: without catalyst.)

Further analysis of the reaction was carried out by varying the amount of the aryl halide. It demonstrated that 5 equiv. of the aryl halide were sufficient to conjugate approximately 50% of the boronic acid functionalities as analysed by ICP-OES. However, a further increase in 5-iodofluorescein concentration only slightly increased the coupling efficiency. The fluorescence intensity of the particles peaked

at ~50 equiv. before decreasing, which was probably due to overloading and self-quenching (Figure 4.4).

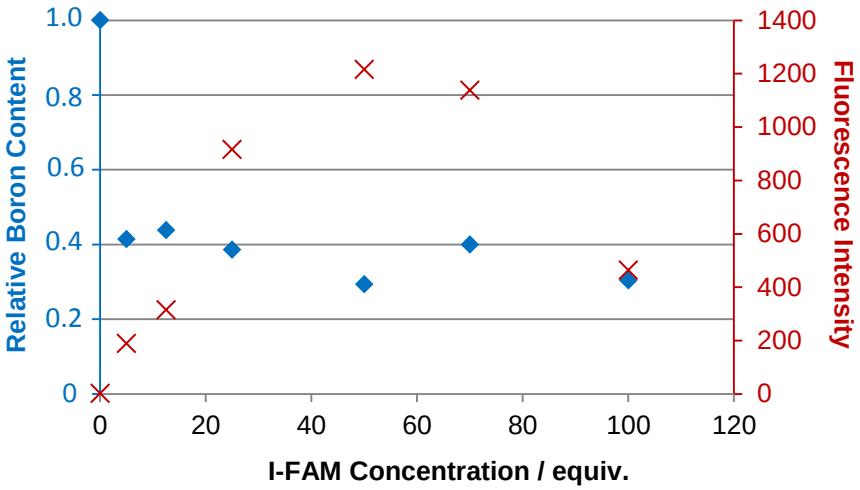

Fig. 4.4. Concentration dependency of Suzuki-Miyaura cross-coupling reaction on solid particles (blue: boron content via ICP-OES; and red: fluorescence via flow cytometry).

4.3 Cellular uptake and viability

CELLUAR UPTAKE. In general, nano and submicron polymer particles are taken up by cells and they are therefore being used extensively as a cellular delivery platform.[53] To investigate if the Suzuki-Miyaura reaction affects cellular uptake and viability following particle exposure, human embryonal kidney 293T cells (HEK293T) and human cervical cancer cells (HeLa) were exposed to 5-iodofluorescein coupled particles **51**. A gradual 14-fold increase in intracellular fluorescence was observed with rising particle concentration. This demonstrated the successful internalisation of the coupled particles (Figure 4.5, external cellular fluorescence was quenched by addition of 2% trypan blue[156]); with a loading of 75 µg/mL sufficient to fluorescently label more than 95% of the cells. These results were verified by fluorescence microscopy images (Figure 4.6).

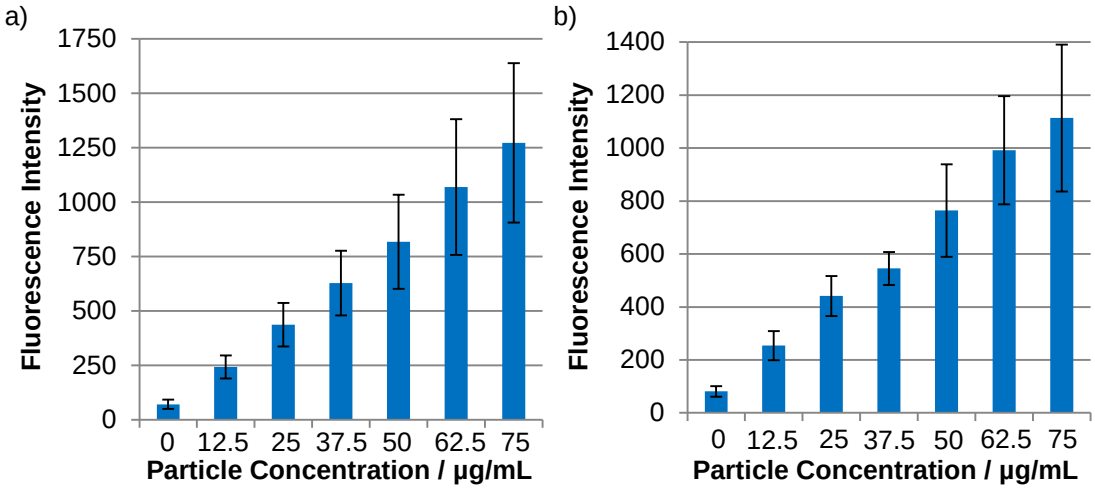

Fig. 4.5. Cellular uptake of fluorescein-functionalised particles **51**: (a) HEK293T cells; and (b) HeLa cells. (24 h uptake followed by 24 h recovery prior analysis by flow cytometry; n = 3).

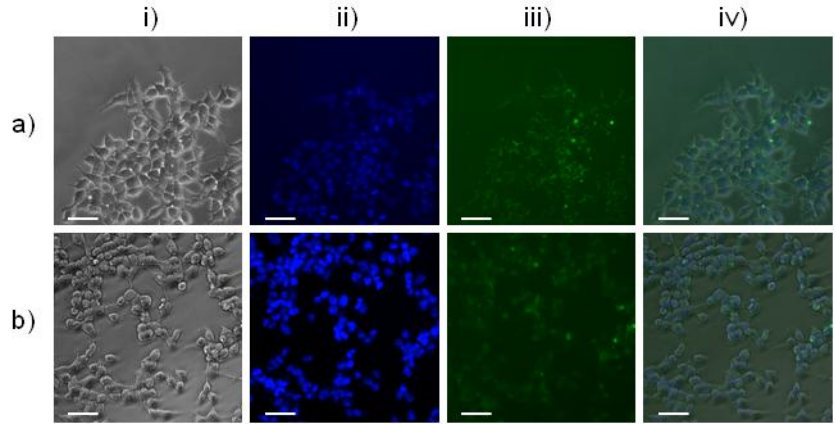

Fig. 4.6. Microscopy images following uptake of fluorescein-functionalised particles (50 µg/mL, 24 h): (a) HEK293T cells; and (b) HeLa cells. (i) bright-field; (ii) green: fluorescent particles **51** (λ_{ex} = 488 nm); (iii) blue: nuclei stain Hoechst 33342 (λ_{ex} = 405 nm) and (iv) overlay. Scale bar = 100 µm.

CELL VIABILITY. The attachment of bioactive compounds by Suzuki-Miyaura cross coupling requires palladium which is known to have adverse side effects on cell viability.[157] However, following 5-iodofluorescein conjugation and washing, a palladium concentration of only 0.04 nM by ICP-OES was detected at a particle concentration of 75 µg/mL. To investigate if palladium treated particles had a toxic side-effect, the number of viable cells were determined following particle uptake.

The assay, which used 3-(4,5-dimethylthiazole-2-yl)-2,5-diphenyltetrazolium bromide (MTT), is based on the conversion of a yellow tetrazolium derivative into a purple formazan dye by reducing enzymes produced only by viable cells.[158]

The assay revealed that the cellular internalisation of the particles (up to 75 µg/mL) had no influence on cell viability (Figure 4.7). These results demonstrated that the Suzuki-Miyaura conjugation enables the attachment of molecules to $(HO)_2B/H_2N$-particles which are taken up by cells without adverse side-effects.

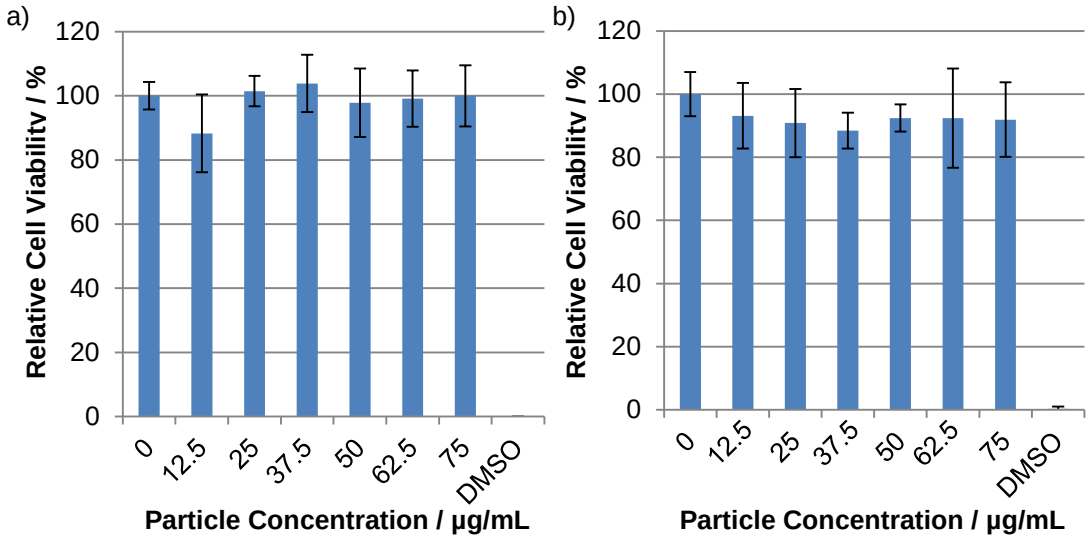

Fig. 4.7. Cell viability following internalisation of fluorescein-functionalised particles **51**: (a) HEK293T cells; and (b) HeLa cells. (24 h uptake followed by 24 h recovery prior analysis by flow cytometry; n = 3).

4.4 Dual-functionalisation of particles

The particles were shown to be able to conjugate molecules by Suzuki-Miyaura cross coupling using the boronic acid functionalities. In addition to this functionality the particles also bear aminomethyl groups which can be used for coupling of molecules via amide bond formation. The two conjugation methods are orthogonal to each other, hence, allowing the controlled attachment of two different molecules on

the same particle. To investigate the potential of the dual-functionalised particles, subsequent conjugation of two different molecules onto the particle surface was investigated.

DUAL-FUNCTIONALISATION. The ability to display two molecules on one particle by subsequent use of amide bond formation and Suzuki-Miyaura cross coupling was investigated by the preparation of a fluorescein-based sensor. The concept was based on a polymeric particle for cellular internalisation and sensing. A stimuli-dependent *turn-on* fluorescent probe (fluorescein-based sensor) and an additional fluorophore to quantify the cellular uptake (cyanine 5) were conjugated onto the particles. The probe would contain fluorescein in close proximity to methyl red separated by a cleavable disulphide linker. If both dyes are in close proximity, the fluorescent output of fluorescein is absorbed by methyl red.[159] However, following cellular uptake the disulphide bond is cleaved and fluorescein is released from the particle, diffuses into the medium and its fluorescent signal can be detected. The disulphide bond is a stable bond in an extracellular environment but is reduced and cleaved in the cytosol due to the presence of reducing agents such as glutathione.[160] Therefore, the release of fluorescein would indicate the successful delivery into the cell, and moreover, demonstrate the reducing environment inside the cell. In addition the particles were labelled with the fluorophore cyanine 5 (Cy5) which is excited in the orange region of the visible light spectrum and emits in the far red region. Hence, the signal is neither influenced by methyl red nor fluorescein and can be used to quantify the internalisation of the particles. Furthermore, the fluorescein part of the construct can be labelled with an additional molecule carrying a targeting sequence or bioactive cargo, whose release can be verified by fluorescein emission. In this proof

of concept study, the cargo was composed of an anionic peptide to avoid membrane leakage of the cleaved fluorescein (Figure 4.9a).

The fluorescein methyl red conjugate was synthesised by standard fluorenylmethoxycarbonyl (Fmoc) solid phase chemistry on Rink amide polystyrene resin prior to attachment to the polymeric particle (Scheme 4.4).[161] The molecule was built up in a *C*- to *N*-direction starting with the conjugation of Fmoc-protected aspartic acid to the Rink amide linker **54**. Following Fmoc-deprotection, another aspartic acid was attached and the cycle repeated with glycine and aspartic acid until attachment of the Fmoc-Lysine(Dde)-OH (**55**). The introduction of 5(6)-carboxyfluorescein on the side-chain was achieved by Dde-deprotection of the ε-amino group of Lysine under orthogonal Fmoc-conditions[162] and subsequent fluorescein coupling (**56**). Following the attachment of 5(6)-carboxyfluorescein, the Fmoc-group of Lysine was deprotected and the synthesis completed with attachment of the disulphide linker, Fmoc-Lysine(Dde)-OH, aminohexanoic acid and *para*-iodobenzoic acid. The Dde-protected ε-amino group of Lysine was deprotected and subsequently coupled to methyl red (**57**). As a control, **58** a molecule containing two non-cleavable aminohexanoic acids instead of the disulphide linker was prepared.

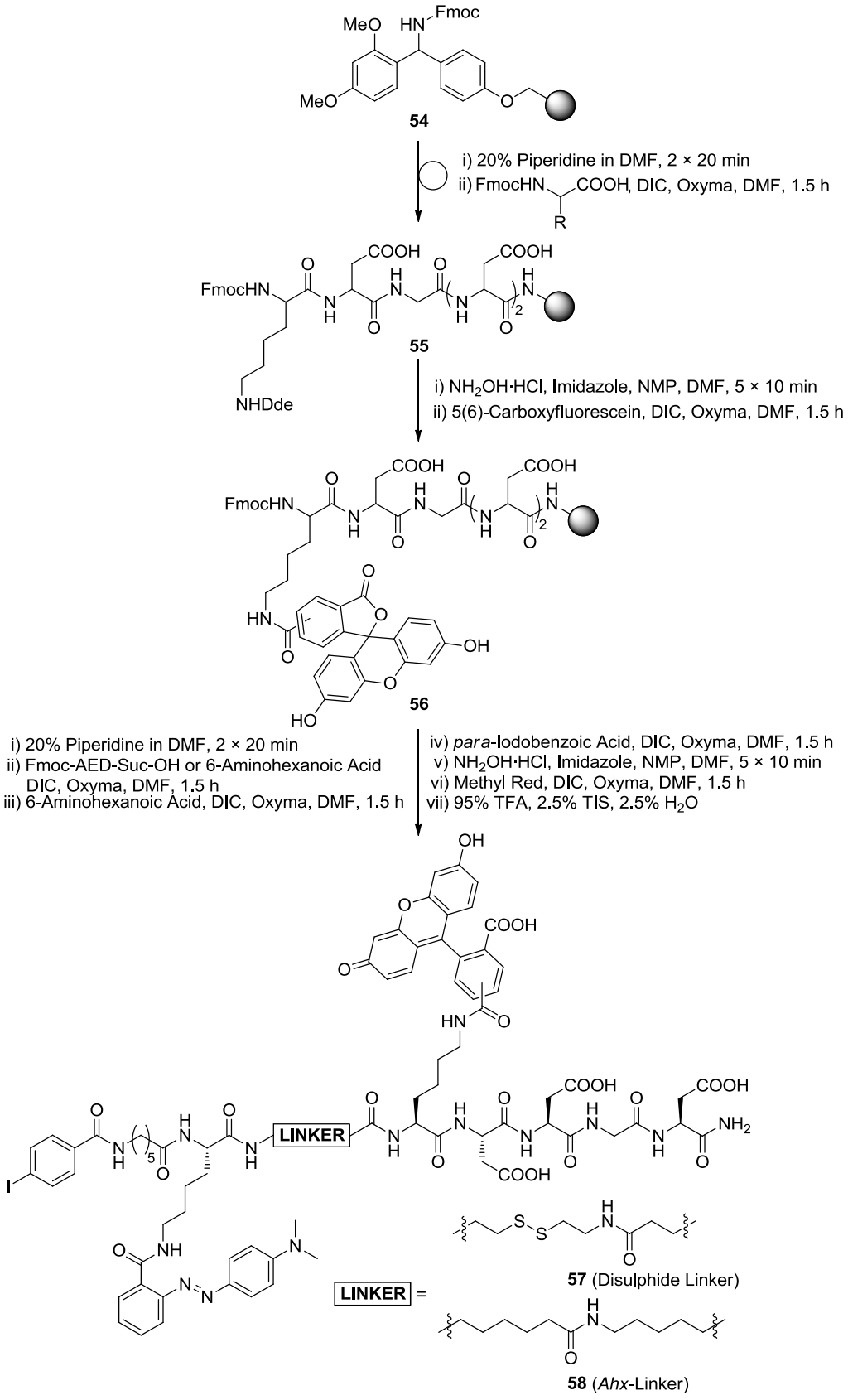

Scheme 4.4. Synthesis of fluorescent *turn-on* probes.

The particle's amino groups were conjugated to carboxylated Cy5 **59** using oxyma/DIC [**60**] followed by Suzuki-Miyaura cross coupling of the fluorescein quencher probe **61** (disulphide-linker) and **62** (*Ahx*-linker) (Scheme 4.5). Successful Cy5-coupling was verified by flow cytometry with a 10,000-fold increasing Cy5-fluorescence while attachment of the fluorescent probe was determined by ICP-OES and showed a reduced boronic acid concentration (disulphide-linker **61**: 77%; *Ahx*-linker **62**: 60%).

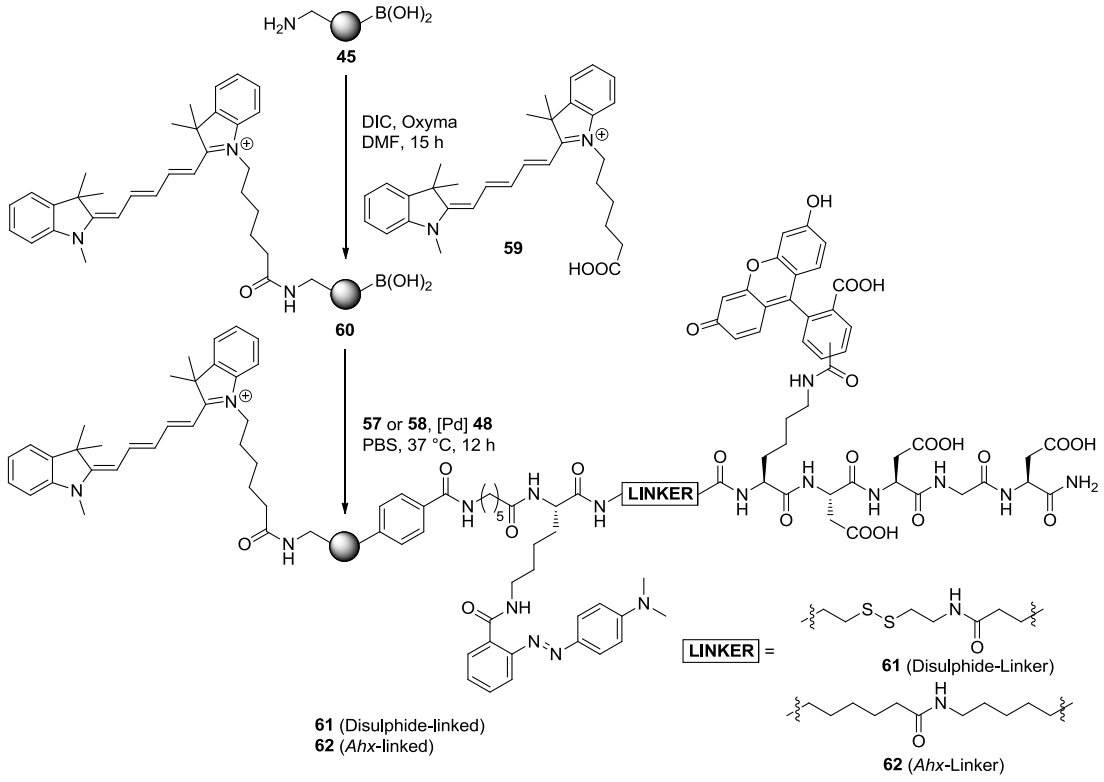

Scheme 4.5. Orthogonal attachment of Cy5 and fluorescein-based probe onto dual-functionalised polymeric particles.

The ability to cleave the disulphide linker and release fluorescein from the particle was investigated by chemically induced cleavage with dithiothreitol (DTT) in PBS buffer (pH 7.4). The fluorescence emission of the supernatant was measured before

and after DTT-treatment, and significant fluorescence intensity was only detected for the disulphide-linked particles **61** after DTT-treatment which verified the cleavage of the disulphide bond and the release of fluorescein (Figure 4.8). In contrast, no fluorescence signal was detected following DTT treatment of aminohexanoic acid linked fluorescein on particles **62**.

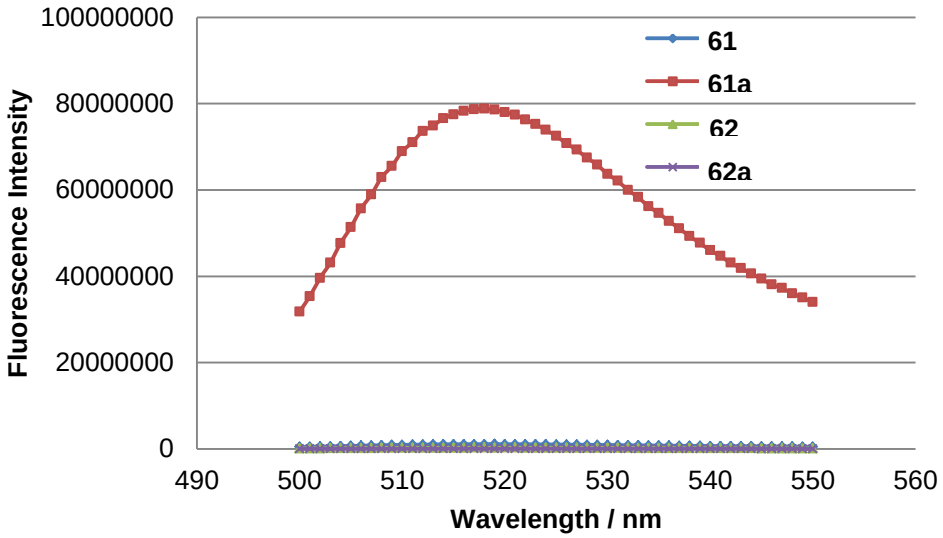

Fig. 4.8. DTT-induced cleavage of the fluorescein quencher probe (fluorescence spectra of supernatant. λ_{ex} = 488 nm in PBS (pH 7.4); blue: disulphide-linker **61** before DTT-treatment; green: *Ahx*-linker **62** before DTT-treatment; red: disulphide-linker **61a** after DTT-treatment; and purple: *Ahx*-linker **62a** after DTT-treatment.).

Following the successful dual conjugation of Cy5 and fluorescein-based probes onto the particles and additional verification of the release of fluorescein following disulphide bond cleavage, an investigation of the intracellular behaviour was carried out. HEK293T and HeLa cells were exposed to varying particle concentrations for 24 h followed by replacement of the medium and 24 h recovery period to allow disulphide bond cleavage to occur (Figure 4.9). Since, the fluorescence of Cy5 is constant and not influenced by fluorescein or methyl red it was used to determine the

intracellular particle concentration (blue). The uptake was identical for disulphide **61** (dark shade) and aminohexanoic acid **62** (light shade) modified particles, however the fluorescein fluorescence (green) changed depending on the linker, with a linear increase observed for the cleavable linker in comparison to the non-cleavable linker.

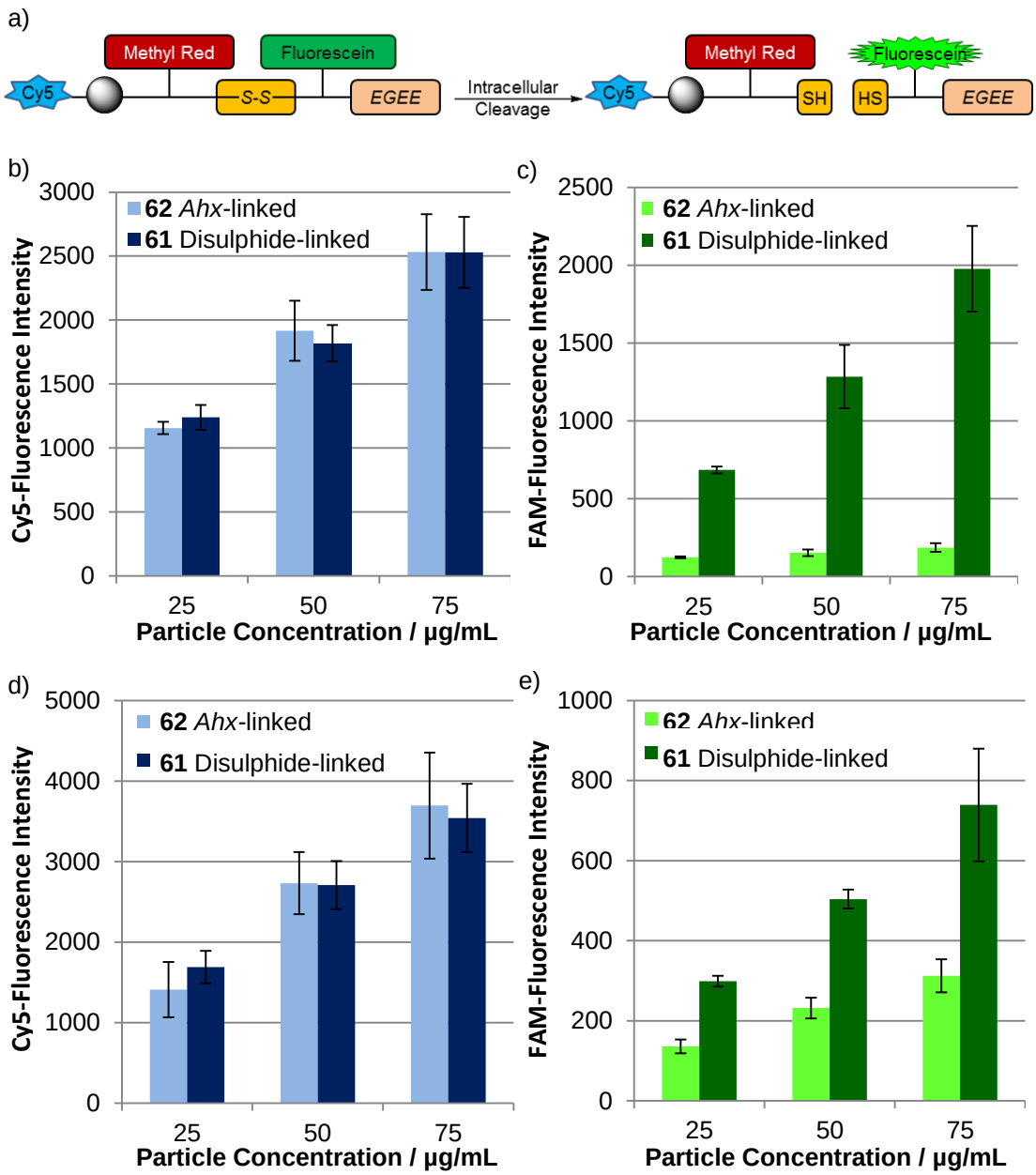

Fig. 4.9. Fluorescent analysis of cells following the internalisation of the fluorescein-based probe containing a cleavable disuphide-linker (**61**) or non-cleavable *Ahx*-linker (**62**): (a) fluorescein release and fluorescence *turn-on* following cellular internalisation; (b) Cy5-fluorescence of HEK293T cells; (c) fluorescein fluorescence of HEK293T cells; (d) Cy5-fluorescence of HeLa cells; (e) fluorescein fluorescence of HeLa cells. (24 h uptake followed by 24 h recovery. Extracellular fluorescence was quenched by addition of 2% trypan blue.[156] Light shade: non-cleavable *Ahx*-linked particles (**62**); dark shade: cleavable disulphide-linked particles (**61**). n = 3.)

Fluorescence microscopy images of the cells were taken to verify the cellular uptake of the particles and subsequent release of fluorescein into the cytosol (Figure

4.10). The nuclei and cytoplasm of HEK293T and HeLa cells were stained with Hoechst 33342 and celltracker red, respectively, to identify the location of the particles and fluorescein. Both disulphide-linked **61** and *Ahx*-linked **62** particles were located in the cytoplasma outside the nucleus in both cell lines. However, a fluorescein signal was detected from the disulphide-linked particles co-localised with the cytosol stain celltracker red verifying the release of fluorescein from the particles into the cytosol. In contrast, no fluorescein signal was detected in cells after exposure to *Ahx*-linked particles demonstrating that fluorescein remained in close proximity to methyl red and attached to the particles.

These results demonstrated the successful preparation of the particle-based probe using amide bond formation and Suzuki-Miyaura cross coupling for orthogonal attachment of two functional molecules and thiol-mediated cleavage of the cargo from the particles.

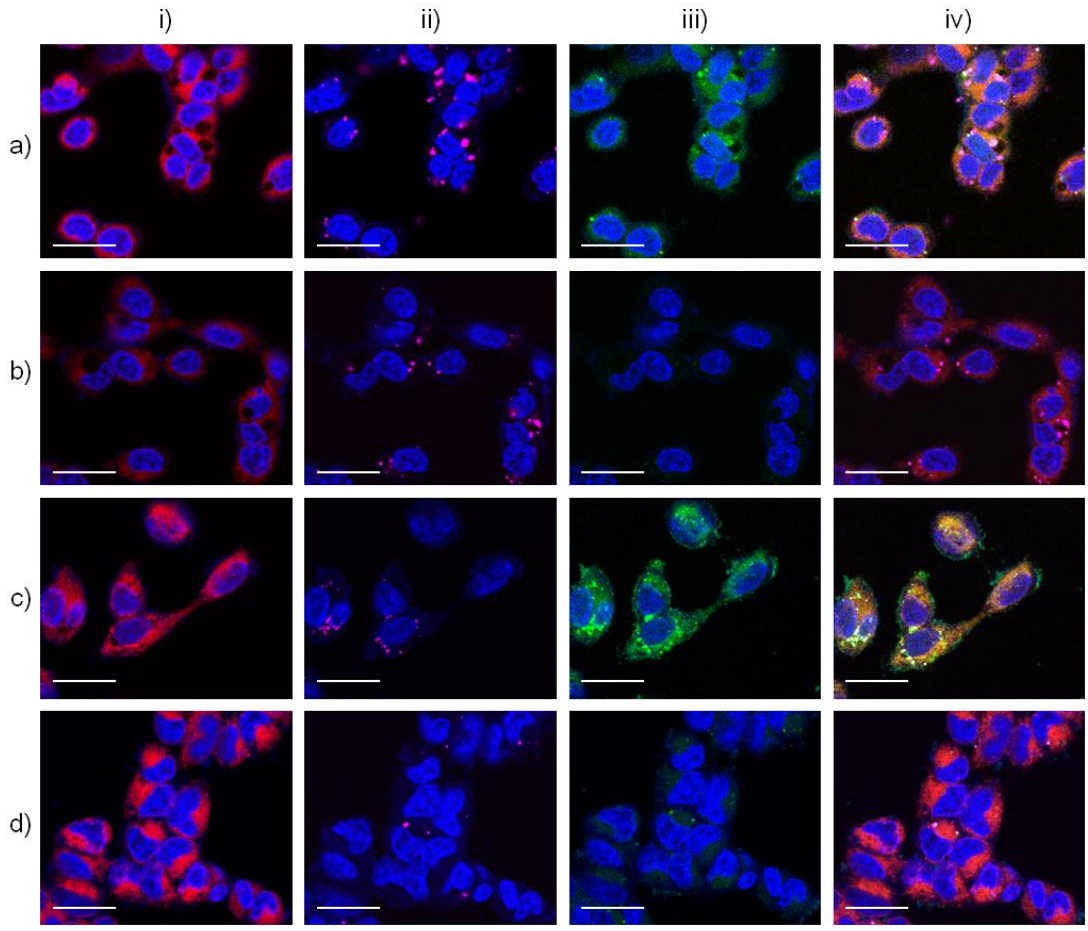

Fig. 4.10. Fluorescence microscopy images of internalised particles and release of fluorescein into the cytosol: (a) disulphide-linked particles **61** in HEK293T cells; (b) *Ahx*-linked particles **62** in HEK293T cells; (c) disulphide-linked particles in HeLa cells; and (d) *Ahx*-linked particles in HeLa cells. (i) Blue: nuclei stain Hoechst 33342 (λ_{ex} = 404 nm, λ_{em} = 414-483 nm), red: cytosol stain celltracker red (λ_{ex} = 594 nm, λ_{em} = 600-628 nm); ii) magenta: Cy5-labelled particles (λ_{ex} = 633 nm, λ_{em} = 642-750 nm); iii) green: released fluorescein (λ_{ex} = 488 nm, λ_{em} = 497-586 nm); and iv) composite image. Bar equals 50 µm.

4.5 Conclusion

The desire to improve conjugation methods in particular by milder and (bio)orthogonal routes compatible with the biological milieu are much sought aften. Herein, novel boronic acid functionalised particles were prepared and their ability to conjugate bioactive cargos in a palladium-mediated Suzuki-Miyaura fashion was demonstrated. The particles were proven to be efficiently taken up by cells without

toxic side-effects, furthermore, the particles contained additional amino groups for the *direct-on-particle* dual-functionalisation via amine-based and Suzuki-Miyaura methodology. As a proof of concept, a fluorophore was attached to the particles by amide bond formation and a cleavable fluorescein-based probe was subsequently attached on the particles by palladium-mediated coupling. The particles were internalised into cells and a fluorescein-based signal was successfully detected in the cytoplasm. This novel route of palladium-mediated particle conjugation increases the number of bioorthogonal methods to functionalise particles. In addition, the availability of the amino group on the particle allows the dual-functionalisation that is required by an increasing number of applications.

The bioconjugation technique might be further improved by identifying conditions to replace palladium, *e.g.* by iron.[163] Moreover, the ability to genetically encode aryl halides into proteins would allow site-specific attachment of proteins onto particles as well as surfaces.[164]

Chapter 5

PARTICLES IN BIOLOGICAL SYSTEMS

Parts of this chapter have been submitted for publication as:

Cho, W.-S., Thielbeer, F., Duffin, R. Johansson, E. M. V., Megson, I. L., MacNee, W., Bradley, M. and Donaldson, K. Functionalization affects the zeta potential, coronal stability and membranolytic activity of polystyrene latex particles. *Submitted* **2012**.

5.1 Particles and their behaviour in biological systems

The technology of engineered nanomaterials is considered to be one of the most promising developments of the near future. It is expected that nanotechnology will have an impact on a variety of fields such as medicine,[8] electronics[165] but also on day-to-day consumer products.[166] Although nanoparticles originate naturally during forest fires and volcanic events, [167] it is thought that human exposure to nanoparticles will dramatically surge over the next decade due to the increased output of novel

anthropogenic nanomaterials. Therefore, a general and thorough understanding of the behaviour of nanoparticles in biological systems is necessary such an understanding includes the characterisation of nanoparticles after they have contacted biological fluids and in particular their interaction with cells and their potential toxic side-effects.[168]

5.2 Adsorption of biomolecules onto particles

BIOMOLECULE ADSORPTION. A biological milieu surrounds most of the cells in an organism and supplys them with nutrients. The concentration and composition of these nutrients is dynamic but it is generally composed of a wide variety of proteins, lipids and sugars. Particles designed to have cell-based applications are initially introduced into this fluid often resulting in the adsorption of the biomolecules present onto the particle's surface. It is this "particle-biomolecule" construct that approaches and contacts a cell prior uptake.[169] The formation and composition of those constructs might influence the particle's cellular uptake and toxicity.[170]

The biomolecule layer or corona on the particle's surface is formed immediately upon dispersion of the particles in the biological fluid (Figure 5.1).[171] At first, highly abundant biomolecules, *e.g.* serum albumin, adsorb quickly onto the particle's surface. However, these are not necessarily the molecules with the highest affinity, and may be displaced over time with stronger binding but less abundant molecules.[172] A distinction can also be made between so-called soft and hard coronas. Molecules in the soft corona are attached with low affinity to the particle surface and have a short residence time with high and dynamic exchange rates in

contrast to biomolecules in the hard corona.[173] Indeed, the corona is by no means a static entity with a dynamic exchange between biomolecules occurring.[174]

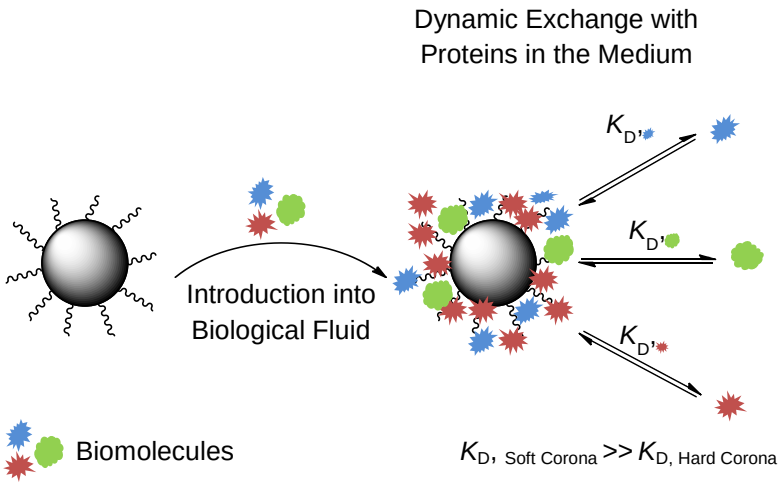

Fig. 5.1. Formation of the biomolecule layer (corona) on the particle surface.

The composition of the particle's corona depends on both the availability of biomolecules, and the particle's properties. It has been shown that the corona is mainly composed of proteins[175] but other molecules bind to particles such as lipids[176] and sugars.[177] In general, proteins present in large quantities in serum or media such as immune and transport proteins are located on particle surfaces.[178] However, even proteins of low abundance, identified in small quantities on particles, can play an important role in cell-particle interactions,[179] and proteins on the corona are internalised when particles are taken up by cells.[180] The adsorption of proteins on the particle surface can induce conformational changes as well as biological activity including the generation of aberrant immuno responses.[181]

The influence of particle properties on the composition of the protein corona is not completely understood. However, surface characteristics such as chemical

functionality, charge, hydrophobicity, heterogeneity, porosity and curvature[182] appear to be more important than particle size and core composition. This effect can be explained by the high surface to volume ratio of nanoparticles which amplifies the characteristics of the surface. In addition, after the formation of the protein corona, the transformed surface can also affect the dispersion stability of the polymeric particles.[183]

In summary, the introduction of particles into biological fluids is followed by an almost immediate formation of a corona surrounding the particles. The composition and structure of the corona is determined by the particle's surface and generates the first point of contact between the particle and the cell. However, so far no clear paradigms have been established to predict the composition of the corona, thus, the effects of variously functionalised particles on the composition of the protein corona was investigated.

PARTICLE'S SURFACE CHEMISTRY AND THE PROTEIN CORONA. Aminomethyl-functionalised polystyrene-based particles **4a** were synthesised and subsequently modified to generate particles with identical cores and sizes but different surface properties (Chapter 2) to investigate its influence on the protein corona. The properties were dependent on the modifications applied and included anionic (sulphonated **10** (SO_3) and carboxylated **9** (COOH)), neutral (hydroxylated **63** (OH), acetylated **16** (NHAc), zwitterionic **12** (ZI), Fmoc-PEGylated **15** (Fmoc-PEG)) and cationic (guanidinium **8** (Gd) and amino **4a** (NH_2)) surface groups (Figure 5.2).

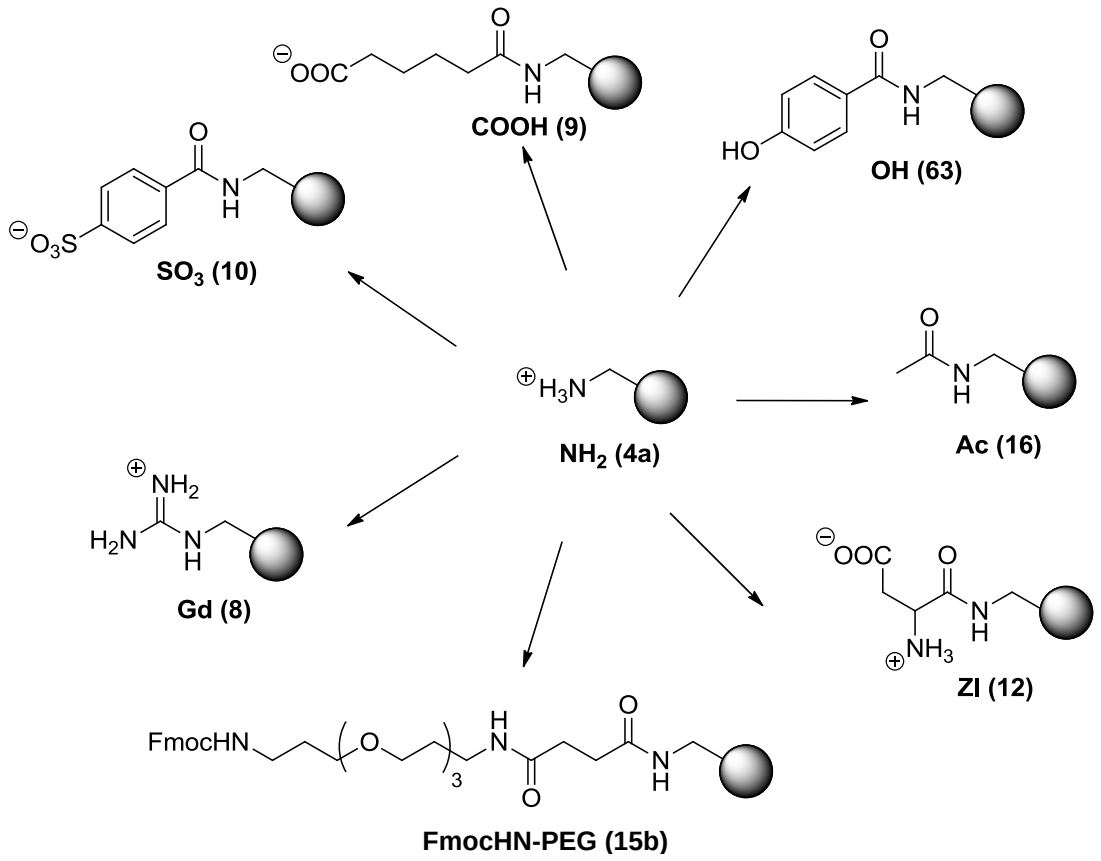

Fig. 5.2. Surface-varying polystyrene-based particles (see also Chapter 2).

The particles were characterised by their zeta potentials in phosphate-buffered saline at pH 7.4 (Figure 5.3a, see also Chapter 2) and also in an acidic environment (saline at pH 5.6) (Figure 5.3b). Zeta potentials for the anionic (**9** and **10**) and cationic particles (**4a** and **8**) were determined to be negative and positive, respectively, in an acidic and basic environment. Neutral particles (**12**, **15b**, **16** and **63**) were measured as having a potential close to zero mV in a basic environment. In an acidic mileu a strong positive zeta potential was determined for PEGylated particles **15** (+20 mV), while zwitterionic particles **12** had a strongly negative zeta potential of -25 mV. Zeta potentials of acetylated **16** and hydroxylated **63** particles were close to zero mV in an acidic environment. To investigate the influence of

biological fluids, particles were dispersed in medium containg 5% serum followed by zeta potential measurements (Figure 5.3c). A zeta potential of -12 mV was determined for all particles independent of surface functionalisation. The collapsed zeta potential indicated the formation of a protein corona. It has been shown previously that particles with different surface functionalities have similar zeta potentials due to formation of a protein corona.[184]

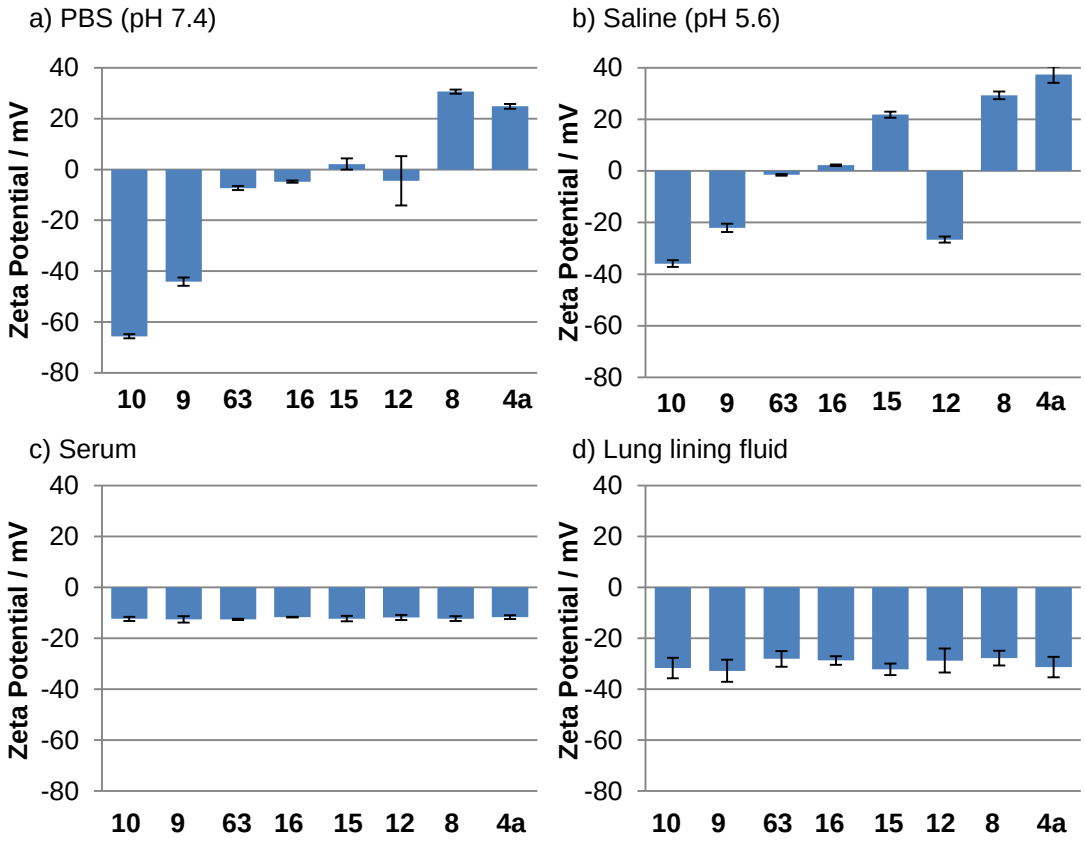

Fig. 5.3. Particle's zeta potential and its dependency on surface chemistry and dispersion medium: (a) PBS (pH 7.4); (b) saline (pH 5.6); (c) cell culture medium supplemented with 5% serum; and (d) artificial lung-lining fluid (LLF). **10** (SO_3); **9** (COOH); **63** (OH); **16** (NHAc); **15** (Fmoc-PEG); **12** (ZI); **8** (Gd); and **4a** (NH_2).

To further investigate the protein corona, a quantitative and qualitative determination of the proteins in the corona was carried out. Thus, particles were incubated in Dulbecco's modified Eagle medium (DMEM) supplemented with 10%

fetal bovine serum (FBS) for 2 h, followed by extensive washing to remove weakly binding proteins. Proteins were detached by boiling the particles in 4% aqueous sodium dodecyl sulphate (SDS) and subsequently analysed via SDS-polyacrylamide gel electrophoresis (SDS-PAGE) and mass spectrometry. Figure 5.4 shows the composition of the protein corona with respect to the particle's surfaces. In general, protein coronas found on different particle surfaces were composed of similar proteins in similar ratios but differed from the protein distribution of the medium. Highly abundant proteins in the media (lane 1) were mainly detected on the particle's surfaces. In particular, bovine serum albumin (BSA) (band e) was the most abundant protein on all particle surfaces independent of their chemical nature.[185] BSA is a highly abundant protein in serum as well as having a high natural affinity to a broad variety of surfaces.[186] However, the abundant serotransferrin was only detected in very low concentrations on the particle surfaces despite having the second highest occurrence in the medium. Further proteins identified in the protein corona belong largely to the groups of transport proteins such as α_2-macroglobulin and apolipoprotein. These results were in accordance with equal zeta potential values determined for particles in protein-containing media. The zeta potential values are mainly influenced by the surface chemistry of the particles, thus the formation of a similar protein corona independent of the particle's surface chemistry masked these and resulted in similar zeta potentials.

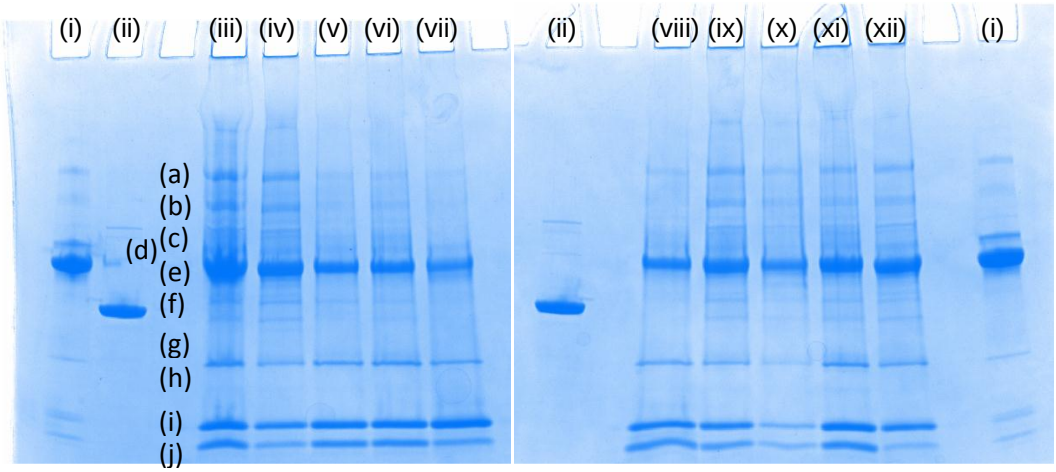

Fig. 5.4. SDS-PAGE analysis of particles following exposure to serum. Lanes: (i) serum; (ii) reference protein serine palmitoyltransferase (*B. fragilis*, 5.4 µg, M = 44 743 g/mol; (iii) **4a** (NH_2); (iv) **8** (Gd); (v) **15** (Fmoc-PEG); (vi) **9** (COOH); (vii) NiO nanoparticles; (viii) **63** (OH); (ix) **16** (NHAc); (x) **10** (SO_3); (xi) **12** (ZI); and Co_3O_4 nanoparticles (xii). Bands: (a) α_2-macroglobulin; (b) inter-α-trypsin inhibitor; (c) complement factor B; (d) serotransferrin; (e) serum albumin; (f) actin; (g) adiponectin; (h) apolipoprotein; (i) haemoglobin; and (j) haemoglobin subunit.

In conclusion, a relationship between surface functionalisation of particles and the composition of the protein corona was not established. The protein corona composition was mainly affected by proteins in the dispersion medium which were adsorbed equally on different particle surfaces.

5.3 Surface-modification and its influence on cellular uptake

CELLULAR UPTAKE OF PARTICLES. The ability of nano and submicron particles to cross the cell membrane has long been established[25] and this phenomenon has been exploited in a variety of biomedical applications such as cellular delivery, intracellular sensing and cellular trafficking.[187] Furthermore, nanoparticles have been shown to be internalised in a wide variety of phagocytotic[188] and non-phagocytotic cell lines.[189] However, a detailed understanding of particle uptake into cells is lacking, in particular the dependency of uptake on the particle's surface properties

and the differences between cell lines. Particle size, surface chemistry and charge seem to be the most important[80,190] although polymeric composition can influence the internalisation process.[191]

It has been shown that the manipulation of a particle's characteristics influence uptake by cells. The presence of surface charge on particles increases the uptake of whether they are positively or negatively charged.[124,189] Presumably, positively charged particles are attracted by the negatively charged cell membrane while the trafficking of negatively charged particles might be governed by the protein corona. In comparison, the positive charge seems to further increase the uptake of particles.[192] Moreover, particle uptake is influenced by particle size with smaller sizes being taken up in larger quantities.[193–195] In addition, particle size also determines the uptake mechanism although surface charge also influences this.[196] In general, a clathrin-dependent endocytotic uptake has been implicated for particles below a diameter of 200 nm while bigger particles are predominantly taken up by caveolae-dependent endocytosis.[196,197] However, it has been shown that non-phagocytotic cells can also internalise particles via a passive mechanism, with anchoring to the extracellular membrane followed by the particle "puncturing" through into the cytosol.[193,198]

Moreoever, it is clear that formation of a protein corona "masks the particle's surface" in solution, but the "pristine surface's properties" are presumably exposed following the contact with the cell membrane and influence the uptake into cells. Furthermore, the composition of the protein corona could additionally influence particle uptake.[199,200]

The recently investigated effects of particle properties on cellular uptake demonstrate that a simple prediction of uptake efficiency is difficult. In addition, uptake data vary between cell lines. However, particular particle characteristics such as surface chemistry, charge and size all seem to influence the uptake despite the formation of the corona. To maximise the potential of intracellular particle-based applications, the ability to design particles for efficient cellular uptake is neccessary and key to this is an understanding of surface group influences.

CELLULAR UPTAKE. To investigate the influence of the particle surface and its protein corona on cellular uptake, fluorescent aminomethyl-functionalised polystyrene particles **40b** were synthesised via co-polymerisation of styryl fluorescein[126] (Chapter 3) and subsequently modified to give various surface groups; anionic (sulphonated **64** (SO_3) and carboxylated **65** (COOH)), neutral (hydroxylated **66** (OH), acetylated **67** (NHAc), zwitterionic **68** (ZI)) and cationic (guanidinium **69** (Gd), PEGylated **70** (H_2N-PEG) and amino **40b** (NH_2)). The modifications of the particle's surfaces were carried out using identical conditions as described for non-fluorescent particles (Chapter 2). As shown above, the composition of the protein corona was not affected by the particle's surface chemistry and seemed to mask the surface.

To investigate if the surface chemistry influences even when masked by a corona, particle uptake, the particles were incubated with human cervical cancer cells (HeLa). The uptake was carried out in cell culture media containing DMEM supplemented with 10% FBS for 24 h. The particle uptake was quantified by determination of the fluorescence of the cells correlating with the level of internalised fluorescently labelled particles (Figure 5.5). Positively charged particles

were taken up by cells in higher quantities in comparison to neutrally or negatively charged particles. These results suggested that the surface charge of the particles dominates the ability to be internalised rather than the protein corona composition which was independent of surface functionalisation. Similar results have been established previously.[201,202] However, surprisingly particles functionalised with a PEG-spacer linked amino group **70** were taken up much more rapidly than amino-functionalised particles **40b** lacking a spacer.

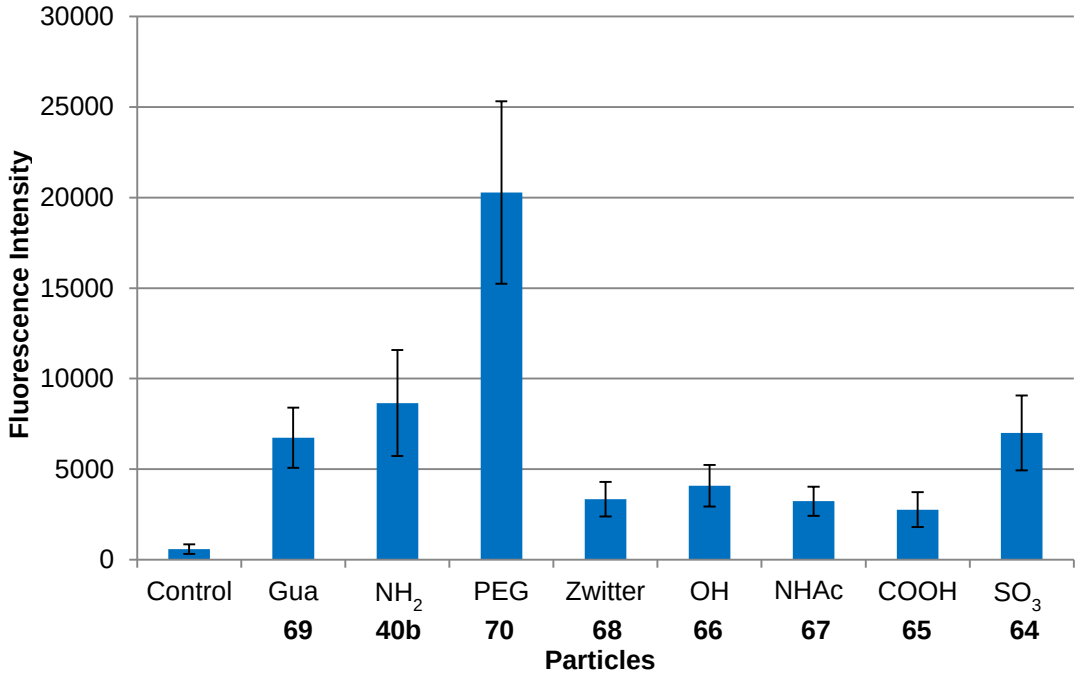

Fig. 5.5. The influence of surface functionalisation on the cellular uptake of fluorescent particles in HeLa cells (24 h; n = 3).

Further analysis of cellular uptake and particle surface chemistry was carried out by studying the influence of the attached spacer while maintaining the terminal amino group. This was achieved by using combinations of aminohexanoic acid and H_2N-PEG_3-OH as spacers (Figure 5.6). The particles were prepared following standard oxyma/DIC methodology followed by Fmoc-deprotecion of the attached

spacer and all had a positively charged surface determined by zeta potential analysis (Table 5.1). The effect of adsorbed proteins onto the particle's zeta potential was investigated; incubation with medium supplemented with 10% serum resulted in zeta potentials of approximately -20 mV which was independent of spacer length, thus demonstrating the formation of protein coronae.

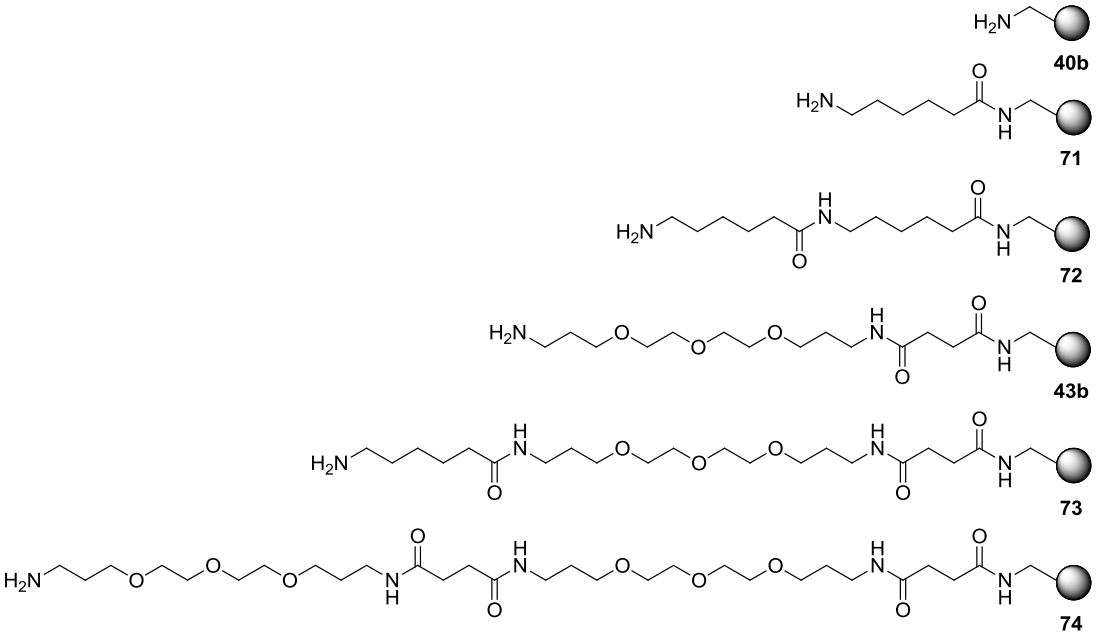

Fig. 5.6. Amino-functionalised fluorescent particles with varying spacer length.

Table 5.1. Particle's zeta potential and its dependency on dispersion medium.

Particle	Zeta Potential Saline (pH 5.6)	Zeta Potential 10% Serum	Zeta Potential Reduced-Serum
40b	(+46.0 ± 0.1) mV	(-23.7 ± 1.7) mV	(-3.5 ± 2.1) mV
71	(+46.3 ± 2.5) mV	(-22.6 ± 1.6) mV	(-6.5 ± 1.2) mV
72	(+23.2 ± 1.1) mV	(-21.2 ± 1.3) mV	(-7.6 ± 0.2) mV
43b	(+27.5 ± 1.1) mV	(-17.6 ± 1.3) mV	(-5.4 ± 1.0) mV
73	(+36.2 ± 1.9) mV	(-18.5 ± 0.7) mV	(-4.1 ± 0.9) mV
74	(+13.1 ± 2.8) mV	(-18.8 ± 1.9) mV	(-7.0 ± 0.1) mV

The cellular uptake of the particles was investigated in HeLa cells in 10% serum supplemented medium. To emphasise the differences between the particles, the uptake time was reduced to 2 h (Figure 5.7, red columns). As can be seen the attachment position of the amino group significantly influenced particle internalisation. A small distance to the particle surface (one atom **40b** and eight atoms **71**) resulted in good uptake, however, the particle uptake increased 5-fold if a 15-atom spacer (**72**) was used instead. If the spacer was further extended (20-atoms (**43b**), 27-atoms (**73**) and 39-atoms (**74**)), particle uptake dropped back down to the level of the short spacers (**40b**). These results verified that the surface characteristics penetrate through the formed corona which was identical for all particles.

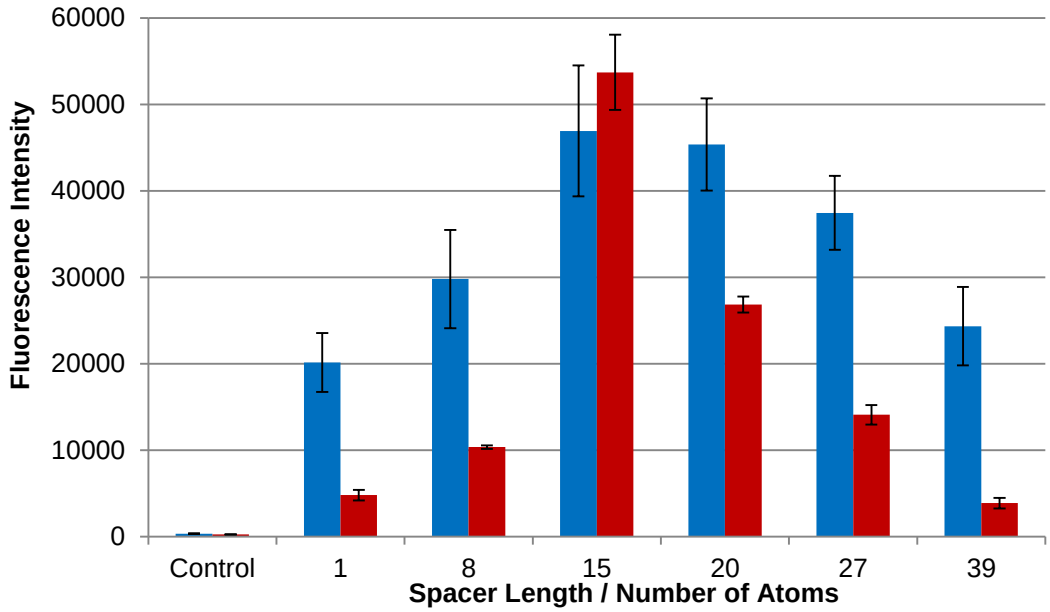

Fig. 5.7. Cellular uptake in HeLa cells of amino group functionalised particles with varying spacer length. Cellular uptake in serum/DMEM (red) and cellular uptake in low-protein medium (blue). (Uptake 2 h; n = 3).

As demonstrated, varying spacer length influenced cellular internalisation of the particles, although the protein corona was composed of similar proteins in similar

ratios. Thus it appears that the spacer influences particle uptake while the influence of the adsorbed proteins is marginal. To further investigate this theory, the various amino-functionalised particles were analysed in reduced-serum medium. This decreases the amount of adsorbed proteins, hence, amplifying the spacer characteristics. Reduction of the protein content resulted in zeta potentials of -5 mV for all particle surfaces although functionalised with different length spacers (Table 5.1). A SDS-PAGE revealed that the composition of the corona was identical for different spacer functionalised particles and mainly consisted of serum albumin (Figure 5.8). However, in comparison to medium supplemented with 10% serum, particles had less protein bound.

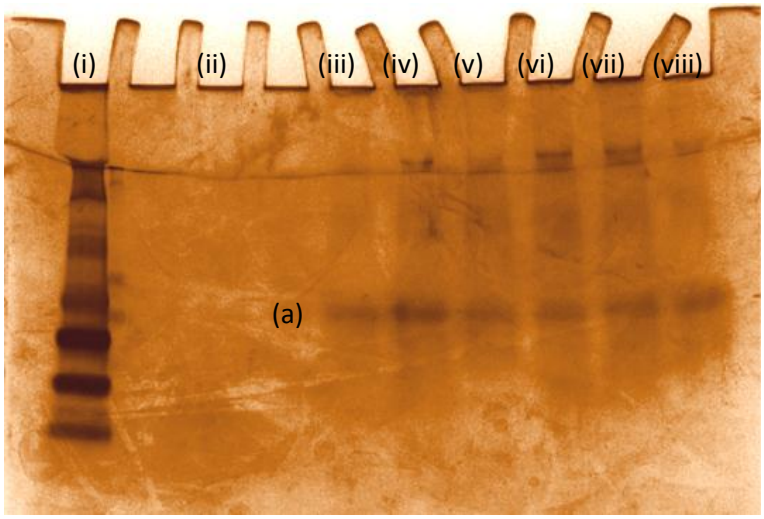

Fig. 5.8. Composition of the protein corona on particles with varying spacer length in low-protein medium. Lanes: (i) protein-ladder; (ii) reduced-serum medium; (iii) 1-atom (**40b**); (iv) 8-atoms (**71**); (v) 15-atoms (**72**); (vi) 20-atoms (**43b**); (vii) 27-atoms (**73**); (viii) 39-atoms (**74**). Bands: (a) serum albumin.

The cellular uptake pattern of the particles under these conditions was identical in comparison to the 10% serum incubated particles; the most efficient uptake was observed for particles carrying a “15-atom” and “20-atom” spacer while it decreased

for shorter or longer spacer lengths. Achieving the same results in low-protein medium, suggests that the spacer influences cellular uptake rather than the protein corona.

These studies demonstrate that the spacer length can be used to tune cellular uptake. The spacer on the particles probably influences this by acting as an anchor group which improves binding. Herein, the anchor supports an interaction between the particle and the biological surface, with protein coatings on the particle surface supporting attachment onto the cell membrane. A membrane-attached particle will then gain entry into the cell.[193] The length of the spacer needs to be long enough to possess the flexibility to interact with the cellular membrane but also close enough to the particle's surface that stable adsorbtion to the membrane surface is achieved (Figure 5.9). In fact, it has been shown previously that rougher surfaces promote protein binding,[203,204] hence, explaining the advantages of a defined spacer length for efficient interaction. A spacer length of circa 15-20 atoms was most efficiently taken up.

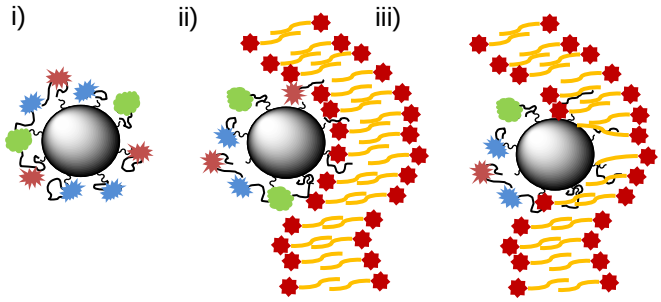

Fig. 5.9. Proposed spacer-dependent interaction with the cell membrane: (i) particle with adsorbed proteins approaches cell membrane; (ii) spacer groups on the particle interact with cell membrane; and (iii) particle diffuses through the cellular membrane.

5.4 Surface-modification and its influence on cellular toxicity

TOXICITY OF PARTICLES. In developing particle-based applications, the effects on human health have to be taken into consideration. In fact, a number of different particles have been shown to have adverse side-effects.[205] However, not all nano and submicron-sized particles are toxic and so far extensive *in vitro* and *in vivo* studies have yet to be carried out to identify the risk of different types of particles.[206]

A general source of potential hazardousness is based on the behaviour of such material towards cells which can be summarised by three principles.[167] Firstly, the *transport principle* defines the ability of nanoparticles to uncontrollably enter cells and to dissolve or degrade releasing further possible harmful fragments. Secondly, the *surface principle* describes the large surface area to volume ratio of the particles generating high reactivity which is potentially harmful and thirdly, the *material principle* states that particles of the same composition can behave differently depending on their size.[167]

The liberation of nanoparticles into the environment and their exposure to humans is not new. Nanoparticles originate from natural process such as forest fires, volcanoes and nature, including pollens and viruses; however the number and variety of particles has increased dramatically over the last decades. To date the main route of nanoparticle uptake into humans is via the lung, while oral and dermal uptake is considered to be low due to the protection offered by the gastrointestinal tract and skin, respectively. In future, the uptake by direct injection into the blood stream might grow due to the field of nanomedicine.[167] Moreover, administered nanoparticles might be distributed throughout the body by the bloodstream[207,208] or even cross the brain blood barrier.[209]

On a cellular and molecular level, particles have been shown to induce oxidative stress by forming reactive oxygen species (ROS). ROS formation results from the high surface area and associated high reactivity of the particles. This reactivity can lead to potential interference with the redox system of cells as well as activation of neutrophils and macrophages leading to the production of an organism's own ROS.[210] For example, following the inhalation of combustion-derived particles into the lung, uptake by epithelia cells occurs with a potential interaction with cellular organelles (Figure 5.10). Once inside the cell, the particles are able to produce independent of their chemical composition or physical appearance, reactive oxygen species in a variety of ways. For example structural defects and metal impurities on the surface can chemically (*e.g.* redox chemistry) or physically (*e.g.* light) induce the formation of superoxide radicals which can lead to the oxidation of molecular components such as proteins, lipids and nucleic acids. This oxidative stress also initiates signal cascades which can lead to inflammation and eventually diseases such as asthma or lung cancer.[13,168,211]

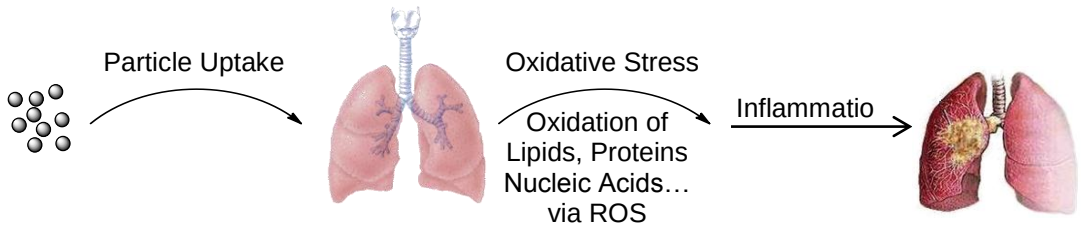

Fig. 5.10. Oxidative stress paradigm.

Another route to the introduction of oxidative stress has been identified via membrane rupture. The damage of the membrane, in particular the lysosomal membrane,[212] has been shown to release various cytotoxic and inflammogenic

enzymes[213–216] and has been used to detect the inflammogenic potential of particles.[217,218] Although a positive surface charge could be the driving force leading to rupture,[182,219–222] the relationship between surface charge and membrane rupture is not fully understood.

The current major challenge of assessing nanoparticle risk is the development of assays to validate the toxicity of particles, preferably by *in vitro* means to reduce ethical and financial burdens.[223] The design of those tests is closely linked to the identification of key physical and chemical parameters that result in adverse health effects. In addition, the above mentioned practical aims are extended by an understanding of toxicological mechanisms and their relation to particle properties such as composition, surface chemistry and size to name but a few. In accordance with the surface characteristics and its influence on cellular uptake, it was likely that these properties would also affect the toxicity of particles. Due to the ever increasing importance of nanotechnology, it was desirable to identify key parameters to predict the toxic potential of particles. Furthermore, the knowledge of those parameters could allow specific modifications to reduce particle toxicity.

SURFACE-FUNCTIONALISED PARTICLES. To further investigate the relationship between surface charge and the toxicity of particles, 200 nm aminomethyl-functionalised polystyrene-based particles were synthesised and subsequently modified into anionic (sulphonated **10** (SO_3) and carboxylated **9** (COOH)), neutral (hydroxylated **63** (OH), acetylated **16** (NHAc), zwitterionic **12** (ZI), Fmoc-PEGylated **15** (Fmoc-PEG)) and cationic (guanidinium **8** (Gd) and amino **4a** (NH_2)) surface groups (Figure 5.2 and Chapter 2). The different behaviour of the particles towards cells is based on a different surface chemistry as all the particles were based

on amino-functionalised precursor particles **4a**. To evaluate the toxic potential of the particles these were also compared to metal oxide nanoparticles NiO ((92 ± 2) nm, zeta potential pH 7.4: -18.7 mV) and Co_3O_4 (185 ± 12) nm, zeta potential pH 7.4: -30.1 mV).[218] The determination of the zeta potential of the polymeric and metal oxide particles in medium supplemented with 5% serum revealed the formation of a protein corona (Figure 5.3c) of similar composition (Figure 5.4).

STABILITY OF THE CORONA. To further investigate the effects of various surface groups and their protein corona, the particle's behaviour with macrophages was studied. It has been shown previously that the corona is digested by lysosomal enzymes.[224] The removal of the protein corona directly affects the zeta potential of the particles (Figure 5.3) and can lead to restoration of the primary charges. The behaviour of the protein corona in macrophages was modelled by incubation of the particles with lung lavage fluid and subsequent treatment with phospholipase A2 (PLA_2) (Figure 5.11a-b).[†] To compare differently sized polymer and metal oxide particles, solutions were standardised by surface area and the phospholipids contained in the protein corona were quantified. Initially, all polymeric particles bound comparable amounts of phospholipids independent of surface functionalisation. However, significantly increased binding was observed on theses particles than on metal oxide particles (Figure 5.11a). Following exposure of the particles to enzymatic digestion, the amount of non-digested, attached phospholipids was determined (Figure 5.11b). The total amount of phospholipids adsorbed onto the polymeric particle surface exceeded the amount on metal oxide particles while sulphonated **10**, hydroxylated **63** and Fmoc-PEGylated **15** particles had considerably

[†] Digestion assays were carried out by Dr Wan-Seob Cho at the Centre for Inflammation Research, University of Edinburgh.

larger amounts of phospholipids bound to the surface than the other particles of the panel. Analysis also revealed that spacer length correlated with the amount of undigested phospholipids (Figure 5.11c). Interestingly, sulphonated **10** and hydroxylated **63** particles which contained aryl spacers were outside the linear correlation of alkyl-spacer functionalised particles. Presumably a strong hydrophobic and/or π-π interactions promoted phospholipid binding.

These data suggest that the surface chemistry supports the retention of the corona by hindering access to the adsorbed biomolecules. In comparison to metal oxide particles, polymeric particles have a comparably rough surface with improved protection of the corona. Furthermore, the correlation between spacer length and retained phospholipids supports this hypothesis.

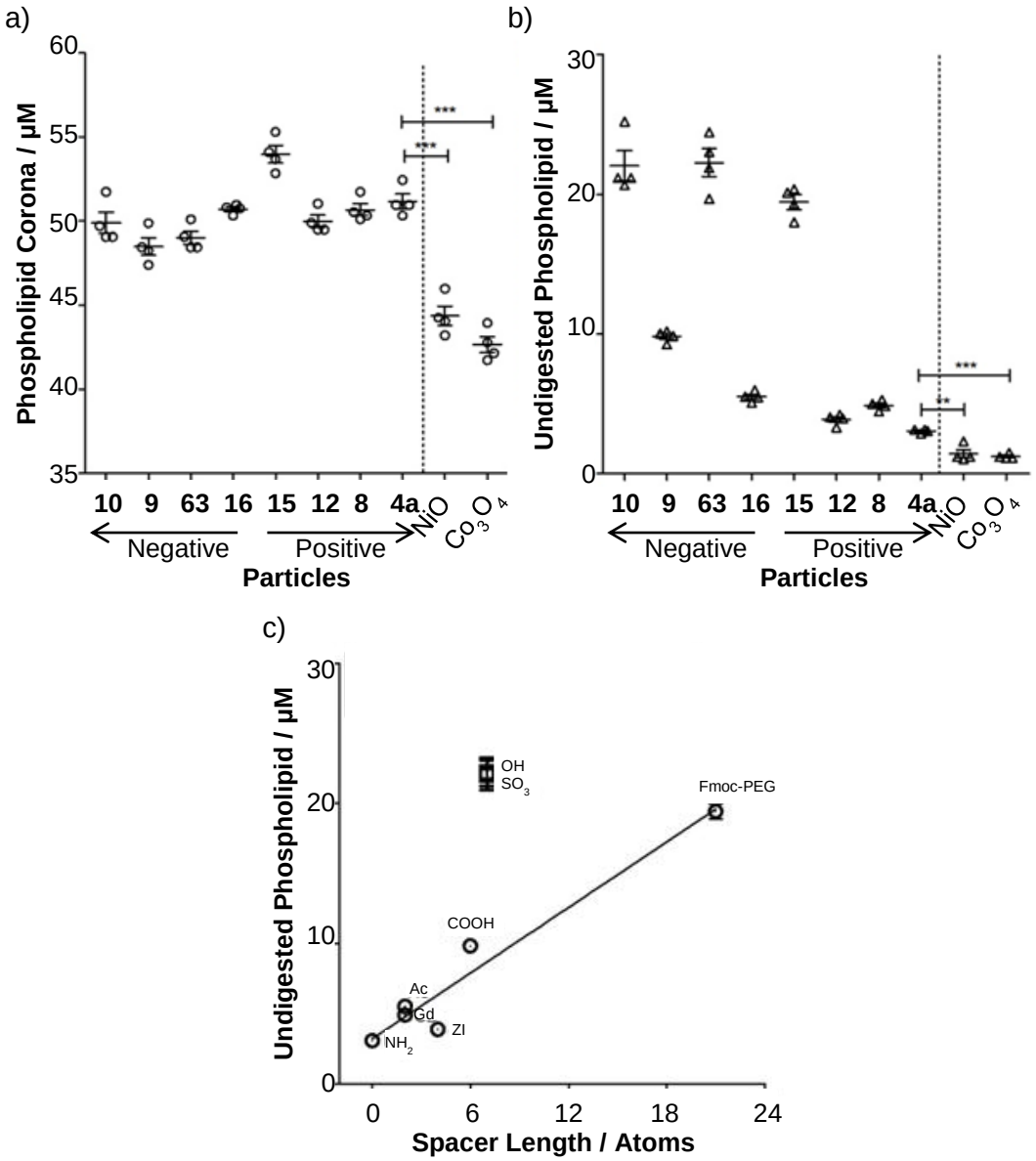

Fig. 5.11. Influence of enzymes on the phospholipid corona: (a) quantification of phospholipids on particles; (b) quantification of phospholipids on particles following PLA_2 digestion; and (c) correlation between amount of phospholipid and spacer length (n = 4 and significance versus vehicle control: $^{**}p < 0.01$, $^{***}p < 0.001$. **10**: SO_3; **9**: COOH; **63**: OH; **16**: Ac; **15**: FmocHN-PEG; **12**: ZI; **8**: Gd; and **4a**: NH_2.

HAEMOLYTIC ACTIVITY. To further study the impact of the surface functionalisation on the formation of a protein corona, particles were analysed for their ability to cause membrane rupture. A simple model to determine the ability to cause membrane rupture is the haemolysis assay. It has been shown that the zeta

potential of metal oxide particles correlates with haemolytic activity and lung inflammogenicity.[218] If the particle's zeta potential (as determined in saline at pH 5.6) was less than +14 mV, no haemolytic potential was detected. However, it was demonstrated that an intact protein corona reduced the zeta potential and prevented haemolysis of the metal oxide particles. The stability of the corona on polymeric particles towards the digestion enzymes that influence the haemolytic activity of the particles was investigated.‡

The haemolytic activity was determined with respect to triton X-100 (TX-100) in protein-free physiological saline.[225] Negatively charged particles (SO_3 **10** and COOH **9**) and neutral particles (Ac **16** and FmocHN-PEG **15**) did not induce haemolysis at 30, 100 and 300 cm^2/mL (Figure 5.12a). In contrast, positively charged (NH_2 **4a** and Gd **8**) ruptured the membrane at 100 cm^2/mL or more. Haemolytic potential was also found for zwitterionic **12** and hydroxylated **63** particles at more than 100 cm^2/mL. The haemolytic activity was found to be induced by particles with a zeta potential higher than +14 mV and correlated with increasing zeta potentials.

‡ Haemolysis assays were carried out by Dr Wan-Seob Cho at the Centre for Inflammation Research, University of Edinburgh.

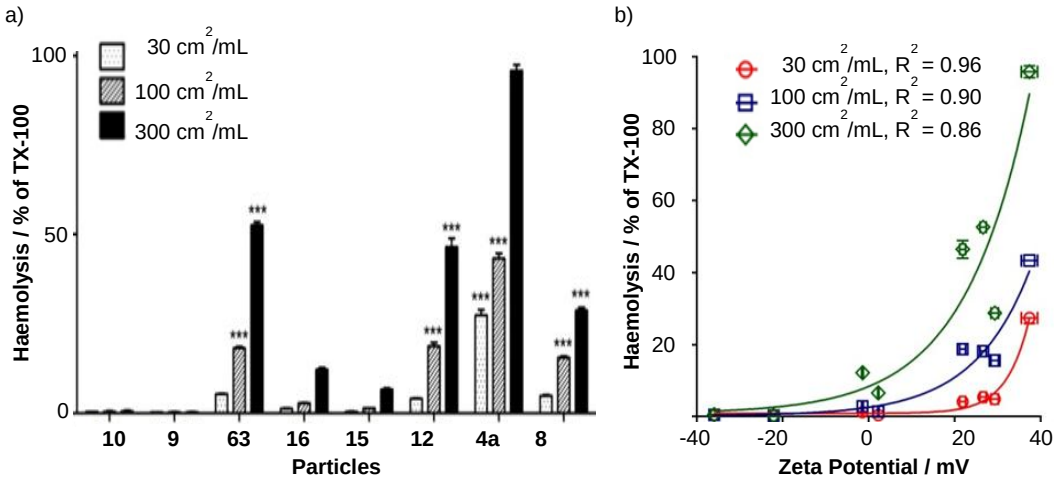

Fig. 5.12. Relationship of haemolytic activity and zeta potential: (a) haemolytic activity of particles at different surface area doses (significance versus vehicle control: *** $p < 0.001$. n = 4); and (b) correlation of haemolysis and zeta potential (particles were dispersed in saline, pH 5.6. Non-linear regression was applied. $n = 4$). **10**: SO_3; **9**: COOH; **63**: OH; **16**: Ac; **15**: FmocHN-PEG; **12**: ZI; **8**: Gd; and **4a**: NH_2.

However, the uptake of particles leads to formation of a protein corona prior cellular membrane contact. For example, particle inhalation by the lung exposes particles to lung lining fluid (LLF). This fluid contains a wide-variety of biomolecules which adsorb onto the particle's surface and form a corona. To model pulmonic ingestion, polymeric particles (**10**: SO_3; **9**: COOH; **63**: OH; **16**: Ac; **15**: FmocHN-PEG; **12**: ZI; **8**: Gd; and **4a**: NH_2) were incubated in artificial LLF and a surface independent zeta potential of -35 mV was determined for all particles (Figure 5.3d).

The protein corona and its effective reduction of the zeta potential has previously been shown to prevent haemolysis by metal/metal oxide particles.[218] In fact, preincubation of particles with serum proteins or LLF medium prevented haemolysis of polymeric particles (Figure 5.13a). To evaluate the polymeric particles, NiO and Co_3O_4 particles were also included and identical effects were observed; the formation of a protein corona prevented haemolysis.

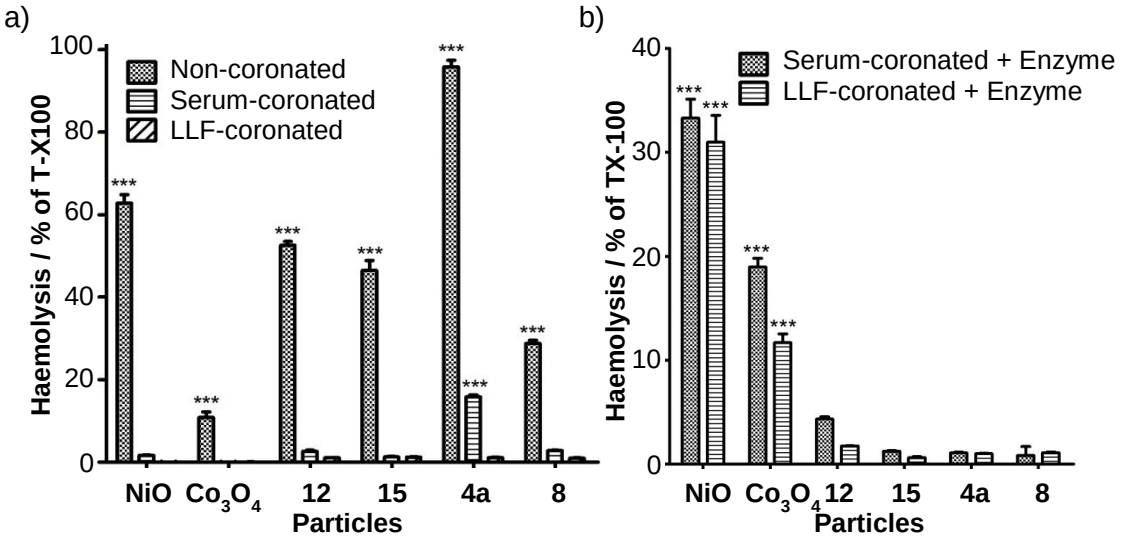

Fig. 5.13. Haemolytic activity of particles: (a) non-coronated and serum or LLF coronated particles; and (b) following incubation with the enzymes PLA_2 and proteinase K and dispersion in saline. Significance versus vehicle control: *** $p < 0.001$; n = 4.

To analyse the effects of the intracellular presence of enzymes on haemolytic activity, preincubated particles were exposed to digestion enzymes PLA_2 and proteinase K (Figure 5.13b). Metal oxide particles showed a restored haemolytic activity, in contrast, polymeric particles (ZI **12**, FmocHN-PEG **15**, NH_2 **4a**, Gd **8**) did not induce haemolysis. This implied that the corona was not completely removed from the polymeric material and the particle charges were still sheltered by the retained protein corona.

In conclusion, under protein-free conditions, the zeta potential of polymeric particles (saline, pH 5.6) showed an excellent correlation with the lysis of human erythrocytes; higher zeta potentials lead to increased rupture of red blood cells.[214,215] However, in the presence of biomolecules a corona is formed that alters the zeta potential and the particles are non-lytic. Under the conditions found inside phagolysosomes a restoration of the prisitine particle surface can take place restoring the membranolytic activity correlating with the zeta potential in saline. However,

functional groups can promote protein stability hindering access to the proteins adsorbed on the particle surface. This protein corona shields the membranolytic potential of the particles (Figure 5.14).

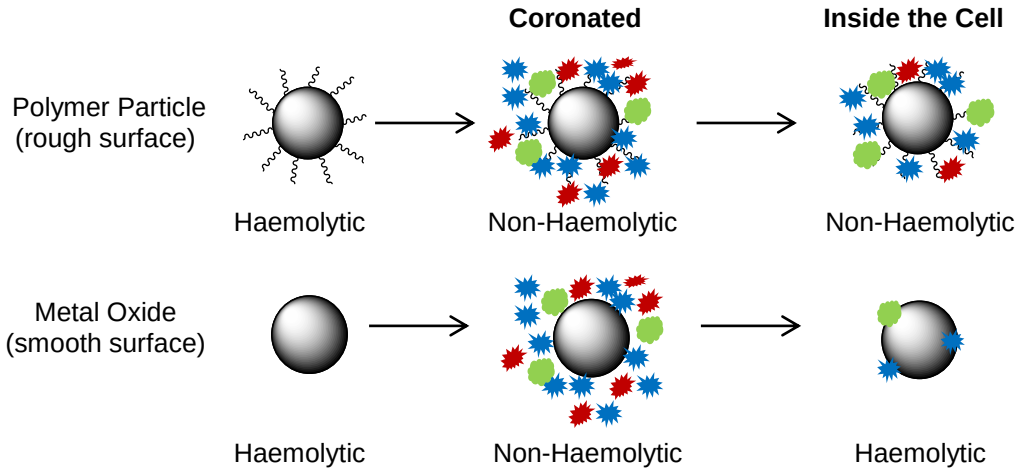

Fig. 5.14. Model of influence of protein corona on toxicity of particles.

5.5 Conclusion

In contrast to the fast and extensive developments in the application-driven nanotechnology, the understanding of the behaviour of nanoparticles in biological systems is lacking. Herein, the contribution of the surface chemistry on the interactions with biological fluids and their implications for cellular uptake and toxicity were studied. Although, surface chemistry does not appear to significantly contribute to the composition of a protein corona, a positive surface charge facilitates the cellular uptake while uptake can be tuned by functionalisation with spacer molecules. These results imply that functionalisation could improve the internalisation of particles that would otherwise be poorly taken up.

However, the formation of a protein corona masked the surface charge of particles which is associated with the inflammogenic properties of particles. In fact, the formation of a protein corona suppressed their haemolytic activity. The haemolytic potential could also not be restored by enzymatic digestion of the corona. The retained corona reduced the immediate surface-charge, thus shielding the membranolytic properties of the surface. Presumably, the surface roughness increased by attachment of a spacer hindering the enzymatic digestion of the corona on the particle's surfaces. In contrast, comparable smooth metal oxide particles were unable to retain the protein corona and, thus, were found to be haemolytic following enzymatic digestion.

Broadly based studies that investigate the influence of cellular uptake and toxicity are needed to improve the understanding of particle surface-cell-interaction. These studies should include various sized and functionalised particles as well as different cell types. The results could support the development of nanotechnology with particles fine-tuned to reduce toxicity, while promoting cellular internalisation.

Chapter 6

EXPERIMENTAL SECTION

Parts of this chapter were previously published or have been submitted as:

Thielbeer, F., Donaldson, K. and Bradley, M. Zeta Potential Mediated Reaction Monitoring on Nano and Microparticles. *Bioconjugate Chemistry* **2011**, *22,* 144-150.

Thielbeer, F., Chankeshwara, S. V. and Bradley, M. Polymerizable Fluorescein Derivatives: Synthesis of Fluorescent Particles and Their Cellular Uptake. *Biomacromolecules* **2011**, *12,* 4386–4391.

Thielbeer, F., Chankeshwara, S. V., Johansson, E. M. V. and Bradley M. Pd-mediated bio-orthogonal conjugation of nanoparticles for intracellular delivery and targeting. *Submitted* **2012**.

Cho, W.-S., Thielbeer, F., Duffin, R. Johansson, E. M. V., Megson, I. L., MacNee, W., Bradley, M. and Donaldson, K. Functionalization affects the zeta potential,

coronal stability and membranolytic activity of polystyrene latex particles. *Submitted* **2012**.

6.1 General methods

All chemicals were purchased from Aldrich, Acros or Fluka and used as received. Reactions involving moisture sensitive reagents were performed under positive pressure of dry nitrogen. The glassware used for these reactions was oven dried and cooled under dry nitrogen. Evaporation of solvents was performed at reduced pressure, using a Büchi rotary evaporator. Microwave-assisted heating was carried out by irradiating the mixture in a Biotage Initiator at 2.45 GHz.

^{1}H and ^{13}C nuclear magnetic resonance spectra were recorded on a Bruker DPX-500 spectrometer (500 and 126 MHz respectively) at 298 K in deutered solvents. Residual protic solvents $CHCl_3$ (δH= 7.26 ppm, δC= 77.0), CD_2HOH (δH= 3.30 ppm, δC= 49.0) and DMSO-d_5 (δH= 2.50 ppm, δC= 39.5) were used as internal reference and peak position are reported as downfield shifts in parts per million (δ) from TMS. Coupling constants were measured in Hertz (Hz). Resonances were characterised as singlet (s), doublet (d), doublet of doublet (dd), triplet (t), multiplet (m), or a broad singlet (bs).

Chromatographic purification was performed on columns prepared with silica gel 60-120 mesh. Analytical thin layer chromatography was performed using commercially available Silica gel F254 (Merck). The plates were visualized at 254 nm and 344 nm wavelength or stained with ninhydrin (0.3% ninhydrin in *n*-butanol

and 3% acetic acid) or permanganate solutions [($KMnO_4$ (3 g), K_2CO_3 (20 g), 5% aqueous NaOH solution (5 mL) and water (300 mL)].

Low Resolution Mass Spectra (LRMS) were obtained using Hewlett Packard LCMS 1100 ChemStation with a G1946B mass detector. Reverse phase analytical HPLC (RP HPLC) was performed using an Agilent 1100 Chemstation on Supelco's Discovery C18 (50 mm × 2.1 mm × 5 µm), and compounds were detected using an evaporative light scattering detector (ELSD) (Polymer Lab PL-ELS 1000 with detection at 220, 254, 260, 282, and 495 nm). All solvents used were HPLC grade.

96 well plates were analysed on a Benchmark Bio-Rad microplate reader at 570 nm using the Microplate manager 4.0 software.

SEM images were obtained on a Philips XL30CP SEM with PGT spirit X-ray analysis and a HKL channel Electron Backscatter Diffraction (EBSD) system on samples coated with a thin layer of gold, to a depth of approximately 20 nm, under vacuum. ICP-OES was performed on a Perkin Elmer Optima 5300 DV ICP-OES (detection limits: 0.0002-1000 ppm). Surface area measurements were carried out on a Micromeritics Gemini 2370 BET device. Centrifugation was performed on Eppendorf 5430R equipped with a fixed-angle rotor (Eppendorf, 45-24-11-HS). Fluorescence spectra were recorded on a SPEX Fluoromax, using a 1 cm path length with fused silica cuvettes. UV/Visible spectra were recorded on an Agilent 8453 spectrophotometer using a 1 cm path length with fused silica cuvettes. Flow cytometry analysis was carried out on a Becton Dickinson (BD) FACSAriaTM using the FlowJo software for data analysis. Protein gels were imaged on a BioRad Laboratories Molecular Imager and processed with BioRad Laboratories Image Lab Software 3.0.

Cell culture experiments were carried out in a HERAsafe KS 18 class II negative-flow cabinet from Heraeus and in a HERAcell 150 incubator from Heraeus. Live HeLa cells were monitored using an x20 objective (Leica fluorescence microscope) under bright light and 488 nm (fluorescein) and 254 nm (Hoechst 33342) excitation, respectively. Fluorescence microscopy was performed on a Leica SP5 Confocal and Zeiss 510 Meta software was used for digital acquisition.

Carboxylated cyanine 5 (Cy5) dye and 1-(9H-fluoren-9-yl)-3,12-dioxo-2-oxa-7,8-dithia-4,11-diazapentadecan-15-oic acid (Fmoc-AED-Suc-OH) were from N. Nourozi and S.V. Chankeshwara, respectively.

6.2 Functional molecules

6.2.1 *para*-Vinylbenzylamine hydrochloride

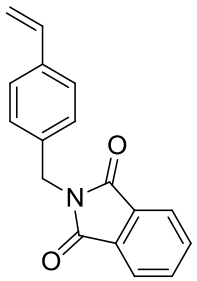

6

***PARA*-VINYLBENZYLPHTHALIMIDE.** *para*-Vinylbenzylphthalimide was prepared following a procedure of Delair.[52] *para*-Vinylbenzylchloride (15.3 g, 100 mmol) and potassium phthalimide (18.5 g, 100 mmol, 1 equiv.) were added to DMF (50 mL) and stirred to give an orange suspension. The reaction mixture was stirred for 17 h. The solution was added to 1.7 M NaOH (1000 mL) and the precipitate was collected via filteration under vacuum. The residue was dissolved in EtOAc (100 mL) to give a cloudy white solution. The solvent was removed under reduced pressure and the

product was purified by recrystallisation from MeOH (2 ×) to give *para*-vinylbenzylphthalimide as a white solid (17.0 g, 64.6 mmol, 65%). ^{1}H NMR (250 MHz, $CDCl_3$) δ 7.79 (m, 4 H), 7.38 (m, 4 H), 6.67 (dd, J = 17.5 Hz, J = 10.9 Hz, 1 H), 5.71 (d, J = 17.5, 1 H), 5.22 (d, J = 10.9, 1 H), 4.83 (s, 2 H). ^{13}C NMR (62.5 MHz, $CDCl_3$) δ 168.3, 137.5, 136.6, 136.2, 134.3, 132.4, 129.2, 126.8, 123.7, 114.5, 41.7. MS (ESI^+, MeOH : H_2O) *m/z* 286.0 $[M + Na]^+$.

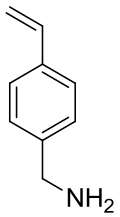

7

***PARA*-VINYLBENZYLAMINE.** *para*-Vinylbenzylamine was prepared following a procedure of Delair.[52] *para*-Vinylbenzylphthalimide **6** (7.3 g, 27 mmol) was dissolved in nitrogen-flushed ethanol (75 mL) and heated under reflux until dissolution of the starting material. Hydrazine hydrate (2.6 g, 53 mmol, 1.9 equiv.) was added and the reaction mixture was stirred for 3 h. The solution was filtered and washed twice with EtOH (10 mL). The filtrate was concentrated *in vacuo* to give a white solid, which was treated with 1.5 M KOH (200 mL) and extracted with Et_2O (3 × 150 mL). The combined organic phases were washed with 2% K_2CO_3 (150 mL), dried over $MgSO_4$, and concentrated under reduced pressure to give the product as a white solid (2.3 g, 17.0 mmol, 64%). ^{1}H NMR (250 MHz, $CDCl_3$): δ 7.32 (m, 4 H), 6.71 (dd, J = 17.6 Hz, J = 10.9 Hz, 1 H), 5.73 (d, J = 17.6, 1 H), 5.22 (d, J = 10.9, 1 H), 3.84 (s, 2 H), 1.61 (s, 2 H). ^{13}C NMR (62.5 MHz, $CDCl_3$): δ 140.3, 138.7, 137.8,

129.8, 128.2, 114.7, 45.2. MS (ESI^+, MeOH : H_2O) *m/z* 134.0 $[M + H]^+$ ($C_9H_{11}N$); *m/z* 117.0 $[M - NH_2]^+$.

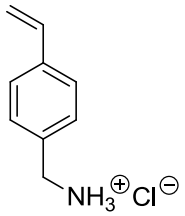

1

PARA*-VINYLBENZYLAMINE HYDROCHLORIDE *(VBAH). *para*-Vinylbenzylamine hydrochloride was prepared following a procedure of Delair.[52] *para*-Vinylbenzylamine (0.8 g, 6.3 mmol) was dissolved in MeOH (30 mL) and cooled to 0 °C before 6 M aqueous HCl (9 mmol) in *iso*-propanol (1.5 mL) was slowly added over 1.5 h. Et_2O (150 mL), was added slowly and the precipitate was recovered by filtration to give a white solid which was dried *in vacuo* to give VBAH (0.5 g, 2.8 mmol, 45 %). ^1H NMR (250 MHz, CD_3OD): δ 7.44 (m, 4 H), 6.74 (dd, J = 17.7 Hz, J = 11.1 Hz, 1 H), 5.82 (d, J = 17.7, 1 H), 5.27 (d, J = 11.1, 1 H), 4.07 (s, 2 H). ^{13}C NMR (62.5 MHz, CD_3OD): δ 140.8, 138.2, 134.6, 131.1, 128.7, 116.2, 44.9. MS (ESI^+, MeOH : H_2O) *m/z* 134.0 $[M - Cl]^+$ ($C_9H_{12}N$), *m/z* 117.0 $[M - Cl - NH_3]^+$.

6.2.2 Fmoc-4,7,10-trioxa-1,13-tridecaneediamine succinamic acid

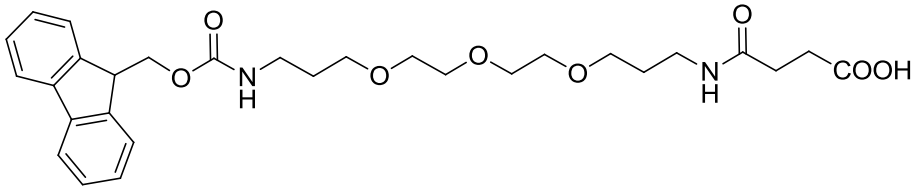

14

FmocHN-PEG_3-OH was prepared following a procedure of Zhao.[87] A solution of succinic anhydride (1.0 g, 10 mmol, 1 equiv.) in MeCN (25 mL) was added drop wise, over 1 h, to 4,7,10-trioxa-1,13-tridecanediamine (2.2 g, 10 mmol) in MeCN (50 mL) and stirred for a further 3 h until formation of a liquid and gel phase. The liquid phase was decanted and discarded. The gel phase was redissolved in MeCN : water (1 : 1, 50 mL) and the solution was cooled to 0 °C prior to the drop wise addition of Fmoc-*O*-succinimide (4.4 g, 13 mmol, 1.3 equiv.) in MeCN (25 mL), with the solution kept at approximately 'pH 8' by the addition of DIPEA.

After 12 h the solvents were removed *in vacuo* and the residue dissolved in 5% aqueous $NaHCO_3$ (100 mL) which was washed with EtOAc (3 × 50 mL). The aqueous phase was acidified to pH 2 with aqueous 1 M HCl, extracted with EtOAc (3 × 50 mL) and the organic phases were combined, washed with brine (50 mL) and dried over $MgSO_4$ and concentrated *in vacuo* to give FmocHN-PEG_3-COOH as a yellow oil (2.4 g, 4.4 mmol, 44%). ^{13}C NMR (62.5 MHz, $CDCl_3$): δ 175.3, 172.5, 156.6, 143.9, 141.2, 127.5, 126.9, 124.9, 119.8, 70.2, 69.8, 69.1, 66.3, 47.1, 38.7, 38.1, 30.7, 29.9, 29.2, 28.4. MS (ESI^+, MeOH : H_2O): *m/z* 543.2 $[M + H]^+$, $(C_{29}H_{39}N_2O_8)^+$; *m/z* 565.1 $[M + Na]^+$.

6.2.3 Fluorescein-based monomers[§]

6.2.3.1 Xanthine-styryl fluorescein

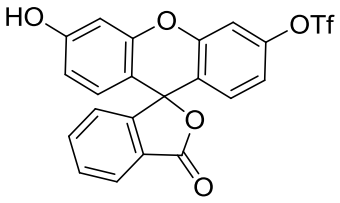

31

3'-HYDROXY-3-OXO-3*H*-SPIRO[ISOBENZOFURAN-1,9'-XANTHENE]-6'-YL TRIFLUOROMETHANESULFONATE. A mixture of fluorescein (1.1 g, 3.2 mmol), *N*-phenyl-bis(trifluoromethanesulfonimide) (1.3 g, 3.6 mmol) and potassium carbonate (0.65 g, 4.8 mmol) were stirred in DMF (10 mL) and microwave-irradiated at 80 °C for 30 min. The reaction mixture was evaporated to dryness and the crude residue was partitioned between EtOAc (150 mL) and 1 M HCl (50 mL). The aqueous layer was extracted with EtOAc (2 × 50 mL), and the combined organic layers dried ($MgSO_4$) and concentrated *in vacuo*. Purification of the residue *via* flash chromatography on silica gel (4 : 1 hexane : EtOAc) afforded the title product as an off-white solid (0.82 g, 1. 8 mmol, 56%). ^{1}H NMR (500 MHz, DMSO-d_6): δ 10.29 (brs, 1H), 8.05 (d, J = 7.6 Hz, 1H), 7.83 (t, J = 7.5 Hz, 1H), 7.77 (t, J = 7.5 Hz, 1H), 7.71 (d, J = 2.6 Hz, 1H), 7.38 (d, J = 7.6 Hz, 1H), 7.25 (dd, J = 2.6 Hz, J = 8.8 Hz, 1H), 7.03 (d, J = 8.8 Hz, 1H), 6.76 (d, J = 2.6 Hz, 1H), 6.64 (d, J = 2.6 Hz, 2H) ppm. ^{13}C NMR (125 MHz, DMSO-d_6): δ 168.9, 160.3, 152.6, 151.9, 151.7, 150.1, 136.4, 131.0, 129.7, 126.1, 125.4, 124.6, 120.4, 117.7, 113.9, 111.2, 109.3, 102.8, 81.8 ppm. MS (ESI) *m/z* 465.5 $[M + H]^+$.

[§] Fluorescein derivatives were jointly synthesised with Dr S. V. Chankeshwara.

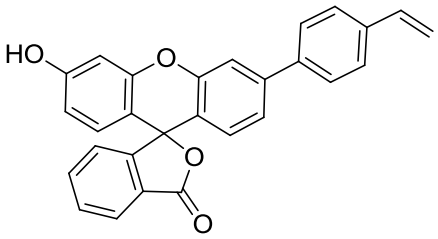

32

3'-HYDROXY-6'-(4-VINYLPHENYL)-3*H*-SPIRO[ISOBENZOFURAN-1,9'-XANTHEN]-3-ONE (XANTHINE-STYRYL). A mixture of compound **31** (0.26 g, 0.5 mmol), 4-vinylphenylboronic acid (90 mg, 0.6 mmol), palladium acetate (4.5 mg, 0.02 mmol) and triphenylphosphine (21 mg, 0.08 mmol) was stirred in dioxane (4.5 mL). Potassium carbonate (0.14 g, 1 mmol) in water (0.5 mL) was added and the resulting mixture was microwave irradiated at 120 °C for 30 min. The reaction mixture was partitioned between EtOAc (40 mL) and 1 M HCl (10 mL), the aqueous layer was extracted with EtOAc (2 × 25 mL) and the combined organic phases dried ($MgSO_4$) and filtered through celite. The filtrate was further treated with SiliaMetS® Thiol resin (2.5 g, 2 equiv, loading 1.41 mmol/g) overnight filtered and the organic layer concentrated *in vacuo*. Purification of the residue via flash chromatography on silica gel (4 : 1 Hexane : EtOAc) afforded the title compound as an orange solid (0.17 g, 0.41 mmol, 82%). ^{1}H NMR (500 MHz, $CDCl_3$): δ 8.08 (d, J = 7.5 Hz, 1H), 7.68-6.72 (m, 3H), 7.60 (d, J = 8.3 Hz, 1H), 7.52-7.54 (m, 3H), 7.30 (d, J = 7.2 Hz, 1H), 7.23 (d, J = 7.5 Hz, 1H), 6.88 (d, J = 8.3 Hz, 1H), 6.81 (d, J = 2.5 Hz, 1H), 6.77 (dd, J = 10.9 Hz, J = 17.6 Hz, 1H), 6.71 (d, J = 8.6 Hz, 1H), 6.58 (dd, J = 2.5 Hz, J = 8.6 Hz, 1H), 5.84 (d, J = 17.6 Hz, 1H), 5.39 (s, 1H) 5.33 (d, J = 10.9 Hz, 1H) ppm. ^{13}C NMR (125 MHz, $CDCl_3$): δ 169.7, 157.6, 153.3, 152.5, 151.6, 143.3, 138.9, 137.5,

136.2, 135.2, 135.1, 129.8, 129.5, 128.5, 128.1, 127.3, 126.8, 126.6, 125.2, 123.9, 122.4, 117.8, 115.2, 114.5, 112.3, 111.4, 103.2. MS (ESI) *m/z* 419.0 $[M + H]^+$.

6.2.3.2 *O*-Xanthine-styryl fluorescein

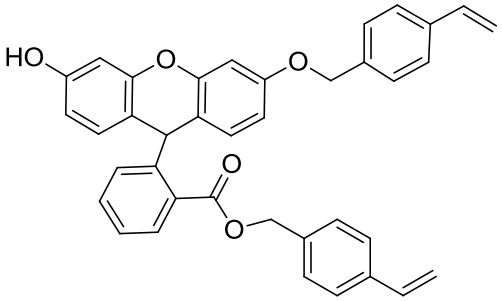

33

4-VINYLBENZYL 2-(3-OXO-6-(4-VINYLBENZYLOXY)-3*H*-XANTHEN-9-YL)BENZOATE. A mixture of fluorescein (1.0 g, 3.0 mmol), 4-vinylbenzyl chloride (1.1 g, 7.0 mmol) and potassium carbonate (0.56 g, 4.0 mmol) was stirred in DMF (10 mL) at 60 °C for 12 h. The reaction mixture was evaporated to dryness, the crude residue was added to water to precipitate the product. The precipitate was collected by filtration and dried under vacuum at 40 °C. The crude residue was purified by triturating with EtOAc and hexane to afford the title product as a yellow solid (1.51 g, 2.7 mmol, 90%). ^{1}H NMR (500 MHz, $CDCl_3$): δ 8.30 (dd, J = 1.3 Hz, J = 7.8 Hz, 1H) 7.73 (t, J = 7.5 Hz, 1H) 7.69 (t, J = 7.8 Hz, 1H) 7.49 (d, J = 8.2 Hz, 2H) 7.43 (d, J = 8.2 Hz, 2H) 7.27 (d, J = 7.5 Hz, 1H) 7.20 (d, J = 8.2 Hz, 1H) 6.80-6.86 (m, 4H) 6.80 (d, J = 2.4 Hz, 1H) 6.75-6.79 (m, 2H) 6.68-6.71 (m, 2H) 6.54 (dd, J = 1.9 Hz, J = 9.7 Hz, 1H) 6.33 (d, J = 1.9 Hz, 1H) 5.80 (dd, J = 6.9 Hz, J = 17.6 Hz, 2H) 5.30-5.34 (m, 2H) 5.15 (s, 2H) 4.93 (d, J = 2.1 Hz, 2H) ppm. ^{13}C NMR (125 MHz, $CDCl_3$): δ 185.6, 171.2, 165.4, 162.8, 158.6, 136.3, 136.2, 135.0, 135.6, 133.6,

132.7, 131.5, 130.4, 130.2, 130.0, 128.9, 127.7, 126.6, 126.4, 114.7, 114.6, 113.8, 105.7, 101.2, 70.4, 67.3 ppm. MS (ESI) *m/z* 565.2 $[M + H]^+$.

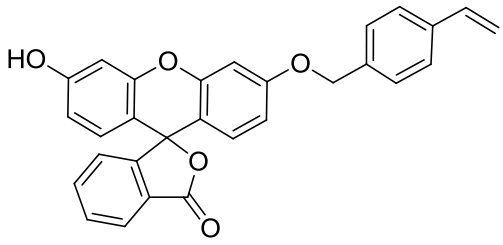

34

3'-HYDROXY-6'-(4-VINYLBENZYLOXY)-3*H*-SPIRO[ISOBENZOFURAN-1,9'-XANTHEN]-3-ONE (*O*-XANTHINE STYRYL). Compound **33** (1.31 g, 2.0 mmol) was dissolved in THF (5 mL) and lithium hydroxide (0.14 g, 6.0 mmol) dissolved in water (5 mL) was added and the resultant mixture was heated at 50 °C for 6 h. After completion of reaction (tlc), the reaction mixture was evaporated to dryness. The crude residue obtained was added to water and acidified to pH ~3 by the addition of concentrated HCl (3 mL) to precipitate the product from the aqueous layer. The precipitate was collected by filtration, washed with water (3 × 10 mL) and dried overnight under vacuum at 40 °C to afford the title product as a yellow solid (0.72 g, 1.6 mmol, 80%). ^{1}H NMR (500 MHz, $CDCl_3$): δ 8.05 (d, J = 7.6Hz, 1H), 7.69 (t, J = 7.5 Hz, 1H), 7.64 (t, J = 7.5 Hz, 1H), 7.46 (d, J = 8.2 Hz, 2H), 7.40 (d, J = 8.2 Hz, 2H), 7.19 (d, J = 7.6 Hz, 1H), 6.84 (dd, J = 10.4 Hz, J = 17.0 Hz, 1H), 5.29 (d, 1H), 6.70-6.79 (m, 4H), 6.62 (d, J = 8.6 Hz, 1H), 6.52 (d, J = 8.6 Hz, 1H), 5.93 (br s, 1H), 5.79 (d, J = 17.0 Hz, 1H), 5.29 (d, J = 10.4 Hz, 1H), 5.10 (s, 2H) ppm. ^{13}C NMR (125 MHz, $CDCl_3$): δ 169.9, 160.5, 157.8, 153.2, 152.5, 152.4, 137.6, 136.4, 135.8, 135.2, 129.8, 129.4, 129.2, 127.2, 126.8, 126.5, 125.1, 124.0, 114.3, 112.3, 111.3, 111.2, 103.2, 101.9, 70.1 ppm. MS (ESI) *m/z* 448.9 $[M + H]^+$.

6.2.3.3 Phthalic-styryl fluorescein

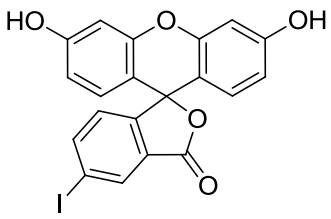

35

3',6'-DIHYDROXY-5-IODO-3*H*-SPIRO[ISOBENZOFURAN-1,9'-XANTHEN]-3-ONE.

The titled compound was prepared following the originally reported procedure.[226] 5-Aminofluorescein (0.46 g, 1.32 mmol) was suspended in 12 N (4 mL) HCl and 3 g of ice was added. The mixture was cooled and stirred in an ice / water bath. Sodium nitrite (0.13 g, 1.9 mmol) in water (3 mL) was added dropwise over 2 min. The mixture was stirred for 30 min at 0 °C, then potassium iodide (2.9 g, 14.5 mmol) in water (4 mL) was added dropwise over 2 min with vigorous stirring at 0 °C. The cooling bath was removed and stirring was continued for a further 1 h. The reaction mixture was extracted with 25% *i*PrOH/$CHCl_3$ (3 × 40 mL). The combined organic extracts were washed with saturated aqueous $Na_2S_2O_3$ (40 mL), then dried over Na_2SO_4 and concentrated *in vacuo*. The resulting residue was adsorbed onto silica and purified by flash chromatography eluting with 10% MeOH/CH_2Cl_2 to afford a yellow solid (0.25 g, 0.86 mmol, 65%) of 5-iodofluorescein. ^{1}H NMR (500 MHz, DMSO-d_6): δ 10.16 (brs, 2H), 8.31 (d, J = 1.5 Hz, 1H), 8.11 (dd, J = 1.5 Hz, J = 8.1 Hz, 1H), 7.10 (d, J = 8.1 Hz, 1H), 6.68 (d, J = 2.4 Hz, 2H), 6.63 (d, J = 8.7 Hz, 2H), 6.57 (d, J = 2.4 Hz, 1H), 6.55 (d, J = 2.4 Hz, 1H) ppm. ^{13}C NMR (125 MHz, DMSO-d_6): δ 167.6, 160.1, 152.3, 152.2, 144.4, 133.5, 129.7, 128.9, 126.6, 113.2, 113.1, 109.5, 102.8, 102.7, 96.7, 84.0 ppm. MS (ESI) *m/z* 458.8 $[M + H]^+$.

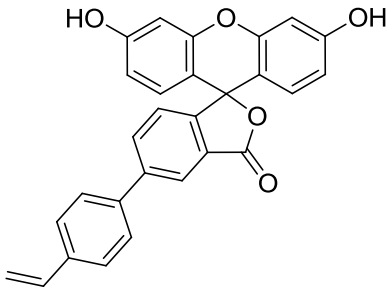

37

3',6'-DIHYDROXY-5-(4-VINYLPHENYL)-3*H*-SPIRO[ISOBENZOFURAN-1,9'-XANTHEN]-3-ONE (PHTHALIC-STYRYL). A mixture of compound **35** (0.23 g, 0.5 mmol), 4-vinylphenylboronic acid (90 mg, 0.6 mmol), palladium acetate (4.5 mg, 0.02 mmol) and triphenylphosphine (21 mg, 0.08 mmol) were stirred in dioxane (4.5 mL). Potassium carbonate (0.14 g, 1 mmol) in water (0.5 mL) was added and the resulting mixture was microwave irradiated at 120 °C for 30 min. The reaction mixture was partitioned between 25% *i*PrOH/$CHCl_3$ (50 mL) and 1 M HCl (10 mL), the aqueous layer was extracted with 25% *i*PrOH/$CHCl_3$ (2 × 25 mL) and the combined organic phases were dried over $MgSO_4$ and filtered through celite. The filtrate was further treated with SiliaMetS® Thiol resin (2.5 g, 2 equiv., loading 1.41 mmol/g) overnight filtered and the filtrate concentrated *in vacuo*. Purification of the residue via flash chromatography on silica gel (4 : 1, hexane : EtOAc) afforded the title compound as a yellow solid (0.15 g, 0.35 mmol, 70%). ^{1}H NMR (500 MHz, DMSO-d_6): δ 10.15 (brs, 2H), 8.23 (d, J = 1.2 Hz, 1H), 8.12 (dd, J = 1.7 Hz, J = 8.0 Hz, 1H), 7.84 (d, J = 8.4 Hz, 2H), 7.64 (d, J = 8.4 Hz, 2H), 7.36 (d, J = 8.0 Hz, 1H), 6.83 (dd, J = 11.5 Hz, J = 17.7 Hz, 1H,), 6.70 (d, J = 2.4 Hz, 2H), 6.67 (s, 1H), 6.65 (m, 1H), 6.59 (d, J = 2.4 Hz, 1H), 6.57 (d, J = 2.4 Hz, 1H), 5.96 (d, J = 17.7 Hz, 1H), 5.35 (d, J = 11.5 Hz, 1H) ppm. ^{13}C NMR (125 MHz, DMSO-d_6): δ

169.0, 160.0, 152.3, 151.9, 142.1, 138.3, 137.6, 136.5, 134.5, 129.6, 127.8, 127.6, 127.4, 125.1, 122.5, 115.5, 113.1, 110.0, 102.3 ppm. MS (ESI) *m/z* 435.2 $[M + H]^+$.

6.2.4 Fmoc-Lysine(Dde)-OH

6.2.4.1 2-Acetyldimedone

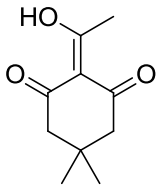

2-acetyldimedone was synthesised according to a procedure by Bycroft.[227] DCC (7.4 g, 35.7 mmol, 1 eq.) was added to a solution of dimedone (5.0 g, 35.7 mmol) and DMAP (0.4 g, 3.6 mmol, 0.1 equiv.) in 75 mL DMF. Subsequently, acetic acid was added to the solution and the reaction mixture was stirred for 60 h. The solvent was removed under reduced pressure, the solid compound re-dissolved in EtOAc (50 mL) and the organic layer washed with 1 M HCl (50 mL). The organic layer was dried over Na_2SO_4 and the solvent evaporated under reduced pressure. The compound was purified via flash chromatography (SiO_2, EtOAc : hexane, 2 : 1) to yield 3.7 g (20.0 mmol, 56%) of the title compound as a yellow oil. ^{1}H-NMR (200 MHz, $CDCl_3$) δ 2.65 (s, 3 H), 2.59 (s, 2 H), 2.41 (s, 2 H), 1.13 (s, 6 H). ^{13}C-NMR (60 MHz, $CDCl_3$) δ 202.1, 197.6, 194.8, 112.1, 52.2, 46.6, 30.4, 28.3, 28.0. MS (ESI) *m/z* 183.1 $[M + H]^+$.

6.2.4.2 N^{ε}-1-(4,4-dimethyl-2,6-dioxocyclohexylidene)ethyl

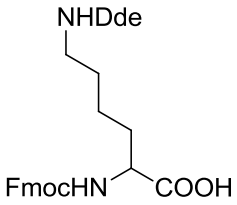

Fmoc-Lys(Dde)-OH was synthesised according to a procedure by Bycroft.[227] Trifluoroacetic acid (45 µL, 0.6 mmol, 0.1 eq.) was added to a suspension of Dde-OH (2.14 g, 11.8 mmol, 2 equiv.) and Fmoc-Lys-OH (2.17 g, 5.9 mmol) in ethanol (60 mL) and refluxed at room temperature for 60 h. The reaction mixture was monitored by analytical tlc (95 : 5, EtOAc : hexane). The reaction mixture was concentrated under reduced pressure and the residue re-suspended in EtOAc (100 mL), washed with 1 M aqueous $KHSO_4$ (2 x 150 mL) and dried over $MgSO_4$. The product was purified by flash chromatography (SiO_2, DCM : MeOH, 8 : 1) to afford a white solid (1.6 g, 50%). ^{1}H-NMR (200 MHz, $CDCl_3$) δ 1.02 (s, 6H), 1.24-1.28 (m, 2H), 1.46-1.61 (m, 2H), 1.67-1.80 (m, 2H), 2.17 (s, 3H), 2.53-2.55 (m, 4H), 3.42 (s, 2H), 4.21 (t, 1H), 4.47 (dd, J = 7.1 Hz, J = 12.6 Hz, 1H), 5.66 (d, J = 7.9 Hz, 2H), 7.30 (ddt, J = 1.1 Hz, J = 2.2 Hz, J = 7.5 Hz, 2H), 7.39 (t, J = 7.4 Hz, 2H), 7.59 (t, J = 7.7 Hz, 2H), 7.75 (d, J = 7.6 Hz, 2H), 13.32 (s, 1H). ^{13}C-NMR (60 MHz, $CDCl_3$) δ 18.5, 23.0, 28.6, 30.5, 43.7, 52.8, 67.4, 108.1, 120.4, 125.5, 127.5, 128.1, 141.6, 144.1, 144.3, 156.8, 174.4, 175.7, 198.7. MS (ESI) *m/z* 533.2 $[M + H]^+$.

6.2.5 Fluorescein quencher probe

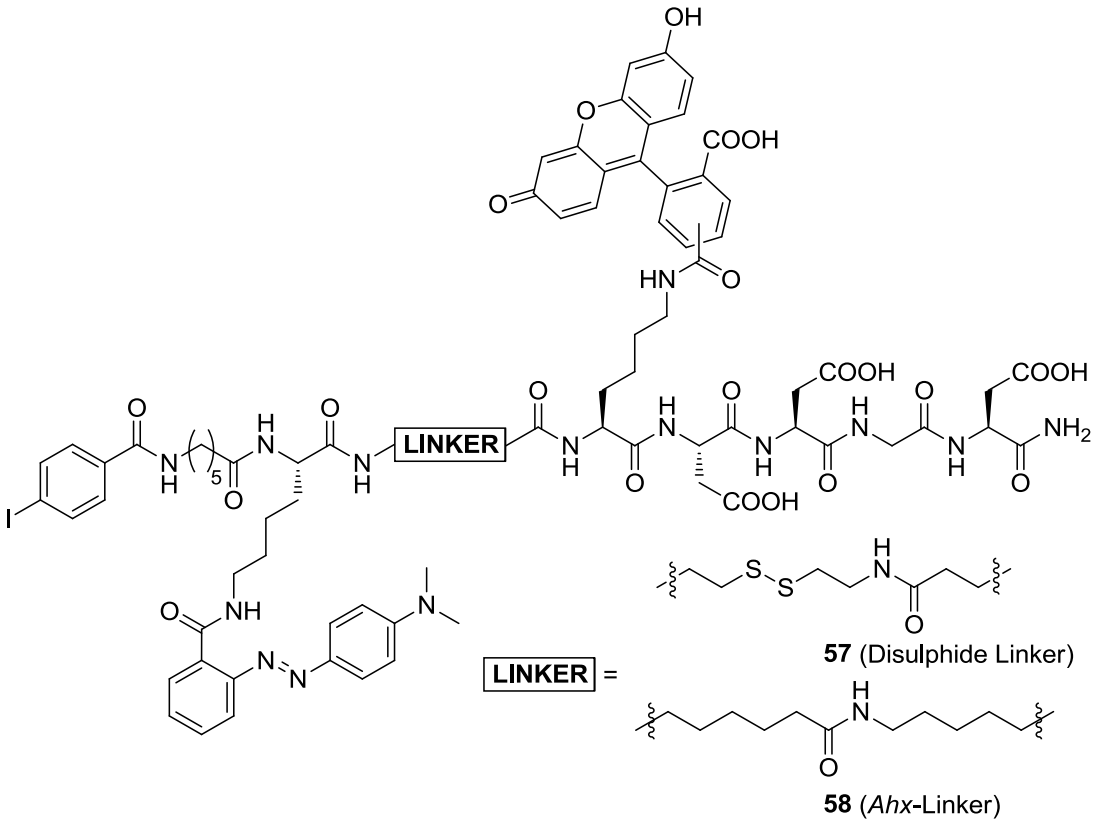

The fluorescein-based quencher probes were synthesised by Fmoc-solid phase chemistry on PS Rink-amide resin (loading: 1.23 mmol/g, size: 30 – 40 µm, cross-linking: 1% DVB). Amide bond couplings were carried out under identical conditions until full length of the molecule had been prepared (Table 6.1 and 6.2). Following coupling of Lysine(Dde), the ε-amino group was deprotected and subsequently coupled with fluorescein (Lys-5) and methyl red (Lys-8), respectively, prior Fmoc-deprotection of the α-amino group..

Coupling procedure. The Fmoc-amino acid residue (3 equiv.) was shaken with oxyma (3 equiv.) and DIC (3 equiv.) in DMF (0.5 mL) for 10 min prior to addition to the resin in (pre-swollen in) DMF (0.5 mL) and shaking for 1.5 h. The resin was washed with DMF (5 ×1 mL) and MeOH (5 × 1 mL). Fmoc-deprotection was

carried out with 20% piperidine in DMF (2 × 1 mL) for 10 min, followed by washing with DMF (5 × 1 mL) and MeOH (5 × 1 mL).

DDE-DEPROTECTION. The resin was treated with DMF : cleaving solution (1 : 5) for 1 × 1 mL (2 min) and 5 × 1 mL (10 min) and shaken, followed by washing with DMF (5 × 1 mL) and MeOH (5 × 1 mL). The cleaving solution consisted of hydroxylamine hydrochloride (1.25 g, 1.8 mmol) and imidazole (0.92 g, 1.35 mmol) in *N*-methylpyrrolidone (5 mL).[162]

PROBE CLEAVAGE. Resin was suspended in a cleavage solution (1 mL) consisting of 95% TFA, 2.5% water and 2.5% triisopropylsilane and shaken for 3 h. The resin was removed by filtration, the cleavage solution was evaporated by a flow of air and the peptide re-dissolved in water and lyophilised.

57: (MALDI-ToF) found: *m/z* 1863.6 $[M + H]^+$; calcd. 1862.8; HPLC (λ = 495 nm eluent A: water and formic acid (0.1 %); eluent B: acetonitrile, formic acid (0.1%) (A = 95% 5 min, 95% to 5% over 20 min) Retention time: 14.5 min (purity: 99%).

58: (MALDI-ToF) found: *m/z* 1855.9 $[M + Na]^+$; calcd. 1854.8; HPLC (λ = 495 nm eluent A: water and formic acid (0.1 %); eluent B: acetonitrile, formic acid (0.1%) (A = 95% 5 min, 95% to 5% over 20 min) Retention time: 15.5 min (purity: 99%).

Table 6.1. Reaction conditions for the synthesis of disulphide-linked probe **57**.

Residue	n / mmol	equiv.	m / mg	V / µL
Aminomethyl PS resin	0.1	1	80	-
Rink amide linker	0.3	3	162	-
Oxyma	0.3	3	43	-
DIC	0.3	3	-	47
Fmoc-Asp(O^{t}Bu)-OH	0.3	3	123	-
Fmoc-Gly-OH	0.3	3	89	-
Fmoc-Lys(Dde)-OH	0.3	3	160	-
Fmoc-Ahx-OH	0.3	3	106	-
Fmoc-ADE-OH	0.3	3	163	-
p-Iodobenzoic acid	0.3	3	74	-
Methyl red	0.3	3	79	-
5(6)-Carboxyfluorescein	0.3	3	113	-

Table 6.2. Reaction conditions for the synthesis of *Ahx*-linked probe **58**.

Residue	**n / mmol**	**equiv.**	**m / mg**	**V / µL**
Aminomethyl PS resin	0.1	1	80	-
Rink amide linker	0.3	3	162	-
Oxyma	0.3	3	43	-
DIC	0.3	3	-	47
Fmoc-Asp(O^{t}Bu)-OH	0.3	3	123	-
Fmoc-Gly-OH	0.3	3	89	-
Fmoc-Lys(Dde)-OH	0.3	3	160	-
Fmoc-Ahx-OH	0.3	3	106	-
p-Iodobenzoic acid	0.3	3	74	-
Methyl red	0.3	3	79	-
5(6)-Carboxyfluorescein	0.3	3	113	-

6.3 Particle synthesis

6.3.1 Aminomethyl-functionalised polystyrene-based particles

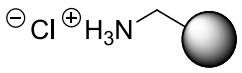

4

Aminomethyl-functionalised polystyrene-based particles were prepared following a procedure by Sanchez-Martin.[41] Styrene (122 µL, 1 mmol, freshly washed with 4 × 25% NaOH and 4 × brine), divinylbenzene (DVB) (3.1 µL, 22 µmol, 2 mol% with regards to styrene, freshly washed with 4 × 25% NaOH and 4 × brine), VBAH **4** (5.9 mg, 35 µmol, 3 mol%), 2,2-azobis (2-methylpropionamidine) dihydrochloride (V-50) (1.6 mg, 6 µmol) and $MgSO_4$ (0.4 mg, 3 µmol) were added to nitrogen-purged water (2 mL) and stirred for 15 min under a nitrogen atmosphere. The reaction mixture was stirred at 80 ºC for 15 h. The particles were collected by centrifugation (15 min at 30,000 *g*) and washed with DMF (3 × 2 mL), MeOH (3 × 2 mL) and water (3 × 2 mL). The particles were stored in water at a solid content of 2%.

Table 6.3. Properties of aminomethyl-functionalised polystyrene-based particles.

Particle	Size / nm	PDI	Amine-loading	Yield
4a	232	0.027	135 µmol/g	43%
4b	240	0.037	70 µmol/g	27%
4c	224	0.014	78 µmol/g	23%
4d	229	0.060	82 µmol/g	34%

6.3.2 Fluorescent aminomethyl-functionalised polystyrene-based particles

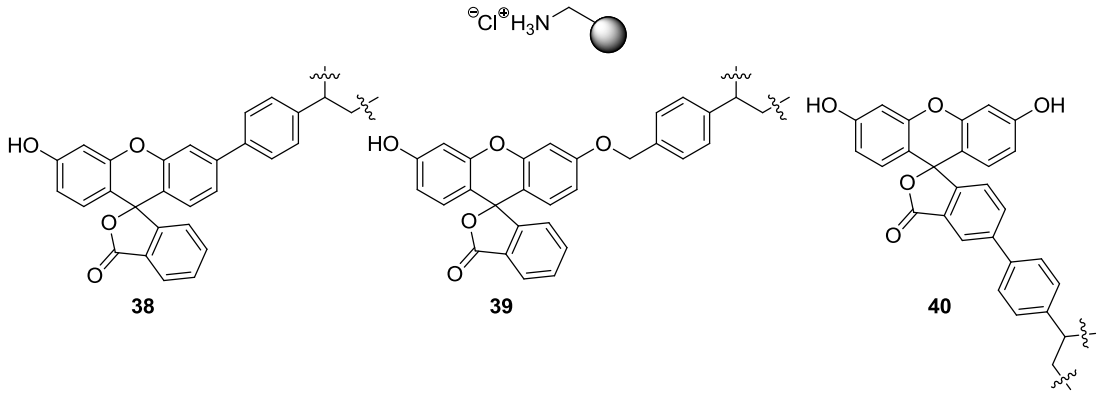

Styrene (122 µL, 1 mmol, freshly washed with 4 × 25% NaOH and 4 × brine), divinylbenzene (DVB) (3.1 µL, 22 µmol, 2 mol% with regards to styrene, freshly washed with 4 × 25% NaOH and 4 × brine), VBAH **4** (5.9 mg, 35 µmol, 3 mol%) fluorescein derivatives (35 µmol, 3 mol%, Table 6.4), V-50 (1.6 mg, 6 µmol) and $MgSO_4$ (0.4 mg, 3 µmol) were added to nitrogen-purged water (2 mL) and stirred for 15 min under a nitrogen atmosphere. The reaction mixture was stirred at 80 ºC for 15 h. The particles were collected by centrifugation (15 min at 30,000 *g*) and washed with DMF (3 × 2 mL), MeOH (3 × 2 mL) and water (3 × 2 mL). The particles were stored in water at a solid content of 2%.

Table 6.4. Fluorescein monomer contents and particle properties.

Particle	Monomer	m / mg	n / µmol	Size / nm (PDI)	Amine-loading µmol/g
38	**32**	14.6	35 (3 mol%)	189 (0.099)	121
39	**34**	15.7	35 (3 mol%)	217 (0.043)	114
40a	**37**	15.3	35 (3 mol%)	187 (0.041)	105
40b	**37**	15.3	35 (3 mol%)	248 (0.093)	119

6.3.3 Boronic acid and aminomethyl-functionalised particles

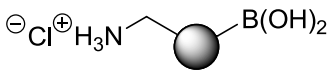

45

Styrene (122 µL, 1 mmol, freshly washed with 4 × 25% NaOH and 4 × brine), *p*-divinylbenzene (3.1 µL, 22 µmol, 2 mol% with regards to styrene, freshly washed with 4 × 25% NaOH and 4 × brine), VBAH **1** (5.9 mg, 35 µmol, 3 mol%), *p*-vinylbenzylboronic acid (see Table 6.5), V-50 (1.6 mg, 6 µmol) and $MgSO_4$ (0.4 mg, 3 µmol) were added to nitrogen-purged water (2 mL) and stirred for 15 min under a nitrogen atmosphere. The reaction mixture was stirred at 80 ºC for 15 h. The particles were collected by centrifugation (15 min at 30,000 *g*) and washed with DMF (3 × 2 mL), MeOH (3 × 2 mL) and water (3 × 2 mL). The particles were stored in water at a solid content of 2%.

Table 6.5. *para*-Vinylbenzylboronic acid contents and particle properties.

Particle	m / mg	n / µmol	Size / nm (PDI)	H_2N-loading µmol/g	B-loading µmol/g
45	5.2	35 (3 mol%)	240 (0.071)	129	62
46	10.4	70 (6 mol%)	260 (0.190)	163	116
47	15.5	105 (9 mol%)	211 (0.313)	76	204

6.3.5 Characterisation of particles

SOLID CONTENT. Solid contents of particles were determined by drying the particle suspension (100 µL) under vacuum (< 20 bar) at 40 °C overnight and weighing. The solid content was calculated from the dry mass using equation 6.1.

Equation 6.1. Determination of the solid content.

$$\text{sc}\,[\%] = \frac{\text{m}}{\text{V}} \cdot 0.1$$

sc Solid content in %

m Mass in mg

V Volume in µL

AMINE LOADING – QUALITATIVE AND QUANTITATIVE KAISER TEST. Quantitative and qualitative contents of free aminomethyl groups were determined *via* the Kaiser test as reported previously.[54,55] The analytical sample was prepared by washing a dispersion of particles (3 mg) with MeOH (2 × 500 µL) and removing the supernatant. The Kaiser test was carried out by the addition of Kaiser test solutions

(90 µL solution A and 30 µL solution B) to the particles followed by heating to 110 ºC for 3 min. Kaiser test solutions: solution A (1.3 mg KCN in water (2 mL), phenol : EtOH (8 : 2; 50 mL), freshly distilled pyridine (100 mL)) and solution B (2.5 g ninhydrin in EtOH (50 mL)).

Afterwards 60% aqueous EtOH (0.5 mL) was added and the reaction mixture was centrifuged. The particles were twice washed with 60% EtOH and the absorbance of the combined supernatant was measured at 570 nm. The amine content was determined from the Beer-Lambert law (Equation 6.2).

Equation 6.2. Amine-loading determination via the Beer-Lambert law.

$$\Lambda\,[\frac{mmol}{g}] = \frac{A \cdot V \cdot 1000}{\varepsilon \cdot m \cdot l}$$

Λ	Loading
A	Absorbance
V	Volume in mL
ε	Extinction coefficient ($\varepsilon_{570,\ \text{Ruheman's Purple}}$ = 15,000 L · (cm · mol)$^{-1}$)
m	Mass in mg
l	Path length in cm

ELLMAN'S TEST. Free thiol groups were detected using the Ellman test.[57] A particle suspension (50 µL, 1 mg) was added to 5,5´-dithiobis-(2-nitrobenzoic acid (DTNB) (50 µL) solution (50 mM sodium acetate and 2 mM DTNB in water), 100 µL Tris-buffer (1 M, pH 8) and 800 µL water and incubated for 5 min at room temperature. Formation of a yellow colour indicated the presence of free thiols.

FMOC-QUANTIFICATION. Fmoc-content was determined as reported previously.[228] The sample was prepared by washing a dispersion of particles (3 mg) in DMF (3 × 500 µL). Afterwards, 20% piperidine in DMF (500 µL) were added and the mixture shaken for 20 min and the supernatant removed (2 ×). The absorbance of the combined supernatant was determined at 301 nm in a quartz cuvette and the Fmoc content calculated by the Beer-Lambert law (Equation 6.2, $\varepsilon_{301,\ Fmoc}$ = 4,800 L · (cm · mol)$^{-1}$).

PARTICLE SIZE – DYNAMIC LIGHT SCATTERING. The hydrodynamic diameter was determined with a Malvern Zetasizer Nano-ZS. A suspension of particles 1 µL was diluted in 10% PBS (pH = 7.4, 8 g/L NaCl, 0.2 g/L KCl, 1.15 g/L Na_2HPO_4, 0.2 g/L KH_2PO_4) in water (1 mL), vortexed and transferred into a 4 mL polystyrene cuvette (FB55143, Fisher Scientific). This solution was measured and resulted in a light scattering intensity which was converted into the hydrodynamic diameter. The data were collected and analysed with the Dispersion Technology Software 4.20 (Malvern) giving histograms for the particles size as a number distribution.

PARTICLE SIZE AND SHAPE – SCANNING ELECTRON MICROSCOPY. A solution of 10 µL particle suspension was dried onto carbon-coated stubs under vacuum (40 ˚C, 12 h) and gold coated by sputtering (approximately a 20 nm layer) before analysis on a Phillips XL30CP Scanning Electron Microscope.

SURFACE AREA MEASUREMENT – BET. Surface areas of particles **4a** were determined on a Micromeritics Gemini 2370. An aqueous dispersion containing 150 mg of sample was dried under vacuum overnight in a glass vial. The dry sample was attached to the BET-device and a fully automatic program was started. Briefly, the sample was cooled in liquid nitrogen and evacuated until generation of a stable

vacuum, followed by pressurisation with different nitrogen pressures and measurement of the resulting nitrogen pressure. The measurement was repeated thrice to give an average value. The pressure data were internally transformed by use of the Brunauer-Emmett-Teller equation to give a surface area of (29.6 ± 0.5) m^2/g.

ZETA POTENTIAL – LASER DOPPLER VELOCIMETRY. The zeta potential was determined with the Zetasizer Nano-ZS equipped with an MPT-2 autotitrator from Malvern Instruments. A suspension of 1 µL particles was diluted in 10% PBS (pH = 7.4, 8 g/L NaCl, 0.2 g/L KCl, 1.15 g/L Na_2HPO_4, 0.2 g/L KH_2PO_4) in water (1 mL), vortexed and transferred into a 1 mL clear zeta potential cuvette (DTS1060, Malvern). The solution was measured and resulted in a electrophoretic mobility which was converted into the hydrodynamic diameter. Titration experiments were carried out using the fully automated MPT-2 autotitrator. Particles were suspended in pure water and titrated against NaOH (0.1 M). Zeta potential measurements were determined at ΔpH 0.5 intervals. The data were collected and analysed with the Dispersion Technology Software 4.20 (Malvern) giving zeta potential distributions.

FLUORESCENT MEASUREMENT – FLOW CYTOMETRIC ANALYSIS. A suspension of particles (1 µL, 20 µg, solid content 20 mg/mL) was diluted in 350 µL of water, vortexed and measured (Table 6.6, Fluorescein: λ_{ex} = 488 nm, λ_{em} = 515-545 nm filter; Cy5: λ_{ex} = 633 nm, λ_{em} = 720-840 nm filter).

Table 6.6. Particle fluorescence measurement.

Fluorophore	Particle	Intensity	Particle	Intensity
Fluorescein	**4c**	139	**41**	9220
	38	8210	**45**	4
	39	24460	**51**	1923
	40a	51010	**52**	248
	40b	72000	**53**	229
Cy5	**45**	6	**59**	12100

METAL AND METALLOID CONTENT – ICP-OES. Boron and palladium content of the particle suspensions were determined as reported previously.[155] A suspension of the particles (3 mL, 1 mg/mL) in 0.5 wt% SDS in water was prepared and analysed by ICP-OES using a Perkin Elmer Optima 5300 DV, employing an RF forward power of 1400 W, with argon gas flows of 15, 0.2 and 0.75 L/min for plasma, auxiliary, and nebuliser flows, respectively (Table 6.7). Using a peristaltic pump, sample solutions were taken up into a Gem Tip cross-Flow nebuliser and Scotts spray chamber at a rate of 1.5 mL/min. The instrument was operated in axial mode for B and Pd. A range of calibration standards were prepared using single element 1000 mg l^{-1} stock solutions (boron: Fisher Scientific UK LTD; palladium: Merck certipur), diluted with 0.5 wt%/v SDS dissolved in deionised water (18Ω, Elga USF). A Merck multi element standard (ICP Multi element standard solution VI CertiPUR®) was employed as a reference standard for boron. The selected wavelengths for each element and were analysed in fully quantitative mode (three points per unit wavelength). Five replicate runs per sample were employed to ensure

that the suspension remained stable throughout each analysis. In addition each sample was sonicated for 3 minutes prior to analysis. The boron concentration was determined using the emission line at 249.677 nm while the concentration of palladium was determined at 248.892 nm. Standards: 0, 0.1, 1, 2, 10, and 20 mg/l were prepared for each element. The majority of the samples fell below 10 mg/l, and were therefore re-calculated against a calibration up to 10 mg/l. With all of the calibration lines the correlation coefficients for the linear regression were 0.9997 or better.

Table 6.7. Boron and palladium measurement of particles.

Fluorophore	Particle	c / µmol/g	Particle	c / µmol/g
Boron	**4d**	(2 ± 1)	**52**	(61 ± 1)
	45	(62 ± 1)	**53**	(60 ± 1)
	46	(116 ± 2)	**60**	(48 ± 2)
	47	(204 ± 1)	**61**	(37 ± 2)
	51	(36 ± 1)		
Palladium	**51**	< 0.01		

6.4 Particle modification

6.4.1 General amide bond formation procedure

Ethyl-2-cyano-2-(hydroxyimino) acetate (oxyma)/diisopropylcarbodiimide (DIC) couplings were carried out.[86] Particle dispersion (75 mg, 1 mL, 10 µmol, 1 equiv.) were washed with DMF (3 × 1 mL) with centrifugation (30,000 *g*) and re-dispersed

in DMF (500 µL). Oxyma (7 mg, 50 µmol, 5 equiv.) and DIC (8 µL, 50 µmol, 5 equiv.) were added to the acid (Table 6.8) in DMF (200 µL) and shaken for 10 min prior addition to the particle dispersion. The reaction mixture was heated to 60 °C using microwave irradiation for 20 min. Afterwards, the particles were washed in DMF (3 × 1 mL), MeOH (2 × 1 mL) and water (2 × 1 mL) and successful conjugation verified with the Kaiser test.

Table 6.8. Oxyma/DIC mediated conjugation onto polymeric particles.

Particle	Acid	n_{Acid}	m
10, 72	*p*-Sulfobenzoic acid	50 µmol	9 mg
11	Hydroxycaproic acid	50 µmol	7 mg
12, **68**	Fmoc-Glu(O*t*Bu)-OH	50 µmol	22 mg
15, **42**, **70**, **73**, **74**	Fmoc-HN-PEG_3-OH	50 µmol	27 mg
41	5(6)-Carboxyfluorescein	50 µmol	19 mg
60	Cyanine 5 (3 equiv.)	30 µmol	14 mg
71 – 73	Fmoc-Aminohexanoic acid	50 µmol	18 mg
63, **66**	*p*-Hydroxybenzoic acid	50 µmol	7 mg

6.4.2 Guanidinium-conjugated particles

A solution of *N´*,*N*-bis-(*tert*-butoxycarbonyl)-*S*-methylurea (15 mg, 50 µmol, 5 equiv.) in DMF (0.2 mL) and TEA (4 µL, 50 µmol, 5 equiv.) was added to prewashed (DMF, 3 × 1 mL) particles **4a** (1 mL, 75 mg, 10 µmol, 1 equiv) in DMF (2 mL) and heated to 60 °C under microwave irradiation for 30 min. The particles (**8**, **69**) were washed with DMF (3 × 1 mL) with centrifugation (30,000 g for 15 min).

6.4.3 Carboxylated particles

A solution of DIC (8 µL, 50 µmol, 5 equiv.) in DMF (100 µL) was added to adipic acid (7 mg, 50 µmol, 5 equiv.) or 3,3-dithiopropionic acid (11 mg, 50 µmol, 5 equiv) in DMF (1 mL), and the mixture was shaken for 10 min and subsequently added to prewashed (DMF, 3 × 1 mL) particles **4a** (**9**, **18**, **19**) or **40b** (**65**) (75 mg, 10 µmol, 1 equiv.) and *N*,*N*´-diisopropylethylamine (DIPEA) (2 µL, 10 µmol, 1 equiv.) in DMF (2 mL). The reaction mixture was heated to 60 °C using microwave irradiation for 20 min. Finally, particles were washed with DMF (3 × 2 mL) with centrifugation (30,000 g for 15 min).

6.4.4 NTA-conjugation

Attachment of 5-amino-3-(bis-(carboxymethyl)amino)pentanoic acid (NTA) was carried out by preactivation with oxyma (0.3 mg, 2 µmol, 1 equiv.) and DIC (0.3 µL, 2 µmol, 1 equiv) in DMF (0.2 mL) of acid-functionalised particles (15 mg, 2 µmol, 1 equiv.) followed by addition of NTA (2 mg, 6 µmol, 3 equiv.) and heating to 60 °C under microwave irradiation for 20 min. Afterward, the particles **21** were washed, with centrifugation (30,000 g for 15 min) with DMF (3 × 2 mL).

6.4.5 *N*-Acetylated particles

Particles **4a** (**16**) or **40c** (**67**) (1 mL, 75 mg, 10 µmol, 1 equiv.) were washed with DMF (3 × 2 mL), and the supernatant was removed. A solution of acetic anhydride, pyridine, and DMF (2:3:15 (v/v/v), 1 mL) was added and the reaction mixture shaken for 10 min. The particles were centrifuged, the supernatant was removed, and the *N*-

acetylation reaction was repeated. The reaction mixture was removed and washed with DMF (3 × 2 mL) with centrifugation (30,000 g for 15 min).

6.4.5 Disulphide-reduction

TCEP-MEDIATED DISULPHIDE BOND CLEAVAGE. Particles **19** (7.5 mg, 1 μmol), previously coupled to 3,3´-dithiopropionic acid, were washed with PBS (3 × 2 mL, pH 7.4) and suspended in a solution of 50 mM tris(2-carboxyethyl)phosphine (TCEP) in PBS (pH 7.4, 1 mL). The reaction mixture was shaken for 3 h at 30 °C. Finally, the particles were washed with PBS (3 × 1 mL, pH 7.4) with centrifugation (30,000 *g* for 15 min).

DTT-MEDIATED DISULPHIDE BOND CLEAVAGE. Particles (**61**, **62**) (1 mg) were suspended in a solution of 10 mM dithiothreitol (DTT) in PBS (100 μL, pH 7.4) and shaken at 37 °C for 1 h. Afterwards, the particle suspension (**61a**, **62a**) was centrifuged and the fluorescence of the supernatant measured (in PBS at pH 7.4; λ_{ex} = 488 nm; $\lambda_{em, max}$ = 518 nm).

6.4.8 Suzuki-Miyaura cross coupling

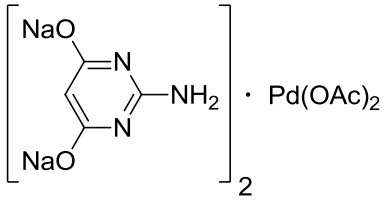

48

CATALYST (48**) PREPARATION.** A solution of the catalyst was prepared as reported previously.[145] 2-Amino-4,6-dihydroxypyrimidine (13 mg, 10 mmol) was dissolved in NaOH (0.1 M, 2 mL) at 65 °C. $Pd(OAc)_2$ (11 mg, 50 mmol) was added, the solution

stirred at 65 °C for 30 min and 3 mL of water added to give a stock solution of 10 mM catalyst which was stored in the fridge.

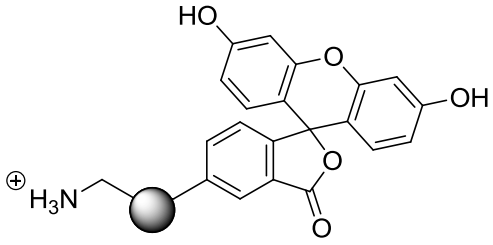

51

5-IODOFLUORESCEIN CONJUGATION. Conjugation of 5-iodofluorescein **35** onto $(HO)_2B/H_2N$-particles **45** was carried out by Suzuki-Miyaura cross coupling. A stock solution of 5-iodofluorescein (25 mg, 55 µmol) in DMSO (550 µL) was prepared and reactions carried out as indicated in Table 6.9. Catalyst levels, as given in Table 6.9, were added to a suspension of $(HO)_2B/H_2N$-particles (10 mg, 0.11 µmol) in PBS (400 µL, pH 7.4) with sonication for 1 min. The reaction mixture was shaken at 1,400 rpm at 37 °C for 15 h. Control reactions were carried out with fluorescein [**52**] (1.8 mg, 5.5 µmol, 50 equiv.) or without catalyst [**53**] (2.5 mg, 5.5 µmol, 50 equiv. 5-iodofluorescein).

Table 6.9. Suzuki-Miyaura cross coupling of 5-iodofluorescein **35.**

5-Iodofluorescein	5-Iodofluorescein	Catalyst (5 %)
6.25 equiv.	0.3 mg, 0.7 µmol	7 µL, 0.03 µmol
12.5 equiv.	0.6 mg, 1.4 µmol	14 µL, 0.07 µmol
25 equiv.	1.3 mg, 2.7 µmol	27 µL, 0.14 µmol
50 equiv.	2.5 mg, 5.5 µmol	55 µL, 0.28 µmol
75 equiv.	3.8 mg, 8.2 µmol	82 µL, 0.42 µmol
100 equiv.	5.0 mg, 11 µmol	110 µL, 0.56 µmol

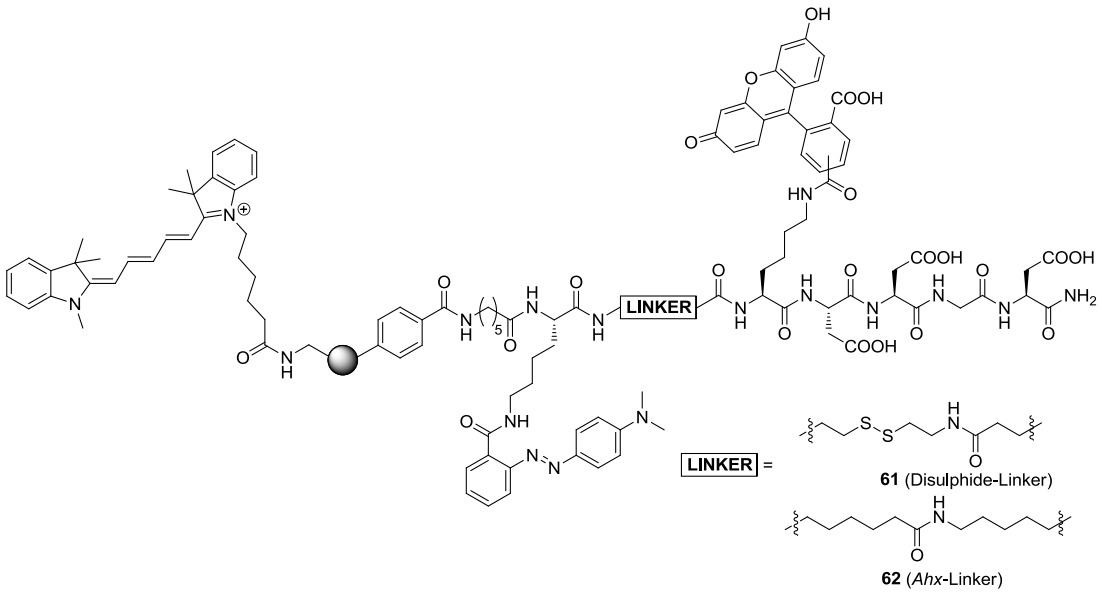

Probe conjugation. Conjugation of fluorescein quencher probes (disulphide-linked **57**, *Ahx*-linked **58**) were carried out by Suzuki-Miyaura cross coupling. A solution of the respective probe (13 mg, 7 µmol) in DMSO (50 µL) was prepared and added to a suspension of Cy5-labelled $(HO)_2B$-particles **59** (13 mg, 0.14 µmol (-$B(OH)_2$)) in PBS (300 µL, pH 7.4) and sonicated for 1 min. The catalyst stock solution (5%, 0.35 µmol) was added and the reaction mixture shaken at 1,400 rpm at

37 °C for 15 h followed by washing the particles with PBS (1 × 500 µL), DMF (3 × 500 µL), MeOH (3 × 500 µL) and water (3 × 500 µL). The reaction was verified by ICP-OES measurement via relative boron concentration measurements with respect to the concentration prior to coupling (77% ± 1% (disulphide-linker) and 60% ± 1% (Ahx-linker)) and DTT-induced induced fluorescein release (see 6.4.5).

6.4.9 Protecting group removal

FMOC-DEPROTECTION. Particles were washed in DMF (3 × 2 mL) and the supernatant removed. A solution of 20% piperidine in DMF (2 mL) was added to the particles and the reaction mixture was shaken for 20 min. The particles were centrifuged (30,000 g for 15 min), the supernatant was removed, and the procedure repeated. The particles were washed in DMF (3 × 1 mL), MeOH (3 × 1 mL) and water (3 × 1 mL).

***t*BUTYLESTER AND *t*BUTYLOXYCARBONYL CARBAMATE DEPROTECTION.** Functionalised particles with ^{t}Bu **12** and Boc **8** protecting groups on side chains of amino acids were washed in DMF (3 × 2 mL) and re-suspended in a solution of 20% TFA in DMF (2 mL). The reaction mixture was shaken for 4 h followed by centrifugation of the particles, removal of the supernatant, and washing with DMF (3 × 2 mL) with centrifugation (30,000 *g* for 15 min).

6.5 Protein adsorption

6.5.1 Serum binding assay

Polymeric particles (**4a**, **8** – **10**, **12**, **15**, **16**, **63** and (**40b**, **43b**, **71** – **74**) and metal oxide nanoparticles (NiO and Co_3O_4, Nanostructural and Amorphous Materials)

from a aqueous solution in water (particle amount: surface area 29.6 mm^2) were incubated with Dubelcco's modified Eagle medium (DMEM) supplemented with 10% fetal bovine serum (FBS), glutamine (4 mM) and antibiotics (penicillin and streptomycin, 100 units/mL) or in reduced-serum medium (Opti-minimal essential medium; Opti-MEM™) and gently shaken (800 rpm) for 24 h. The samples were centrifuged to pellet the particles with protein attached to the surface and the supernatant was removed. The pellets were re-suspended and washed trice in sterile PBS to remove any non-binding proteins. The proteins were removed from the particles by re-suspension of the particles in SDS-sample buffer (0.5M Tris-HCl (pH 8.8), SDS 4% (w/v), glycerol 20% (v/v), 2-mercaptoethanol 2% (v/v), and bromophenol blue 0.0025% in distilled/deionized water) and subsequent boiling of the sample for 5 min. The proteins were separated on a mini-PROTEAN TGX 4-20% SDS/PAGE 1D gel in TGS buffer (Tris 0.025M, Glycine 0.192M, w/v SDS 0.1%, 200 V, 180 mA, 35 min) stained with Coomassie Blue or ProteoSilver™ silver stain and imaged and processed.

6.5.2 Protein identification

Detected protein bands were reduced with 10 mM DTT, 0.2% EDTA in 100 mM ammonium bicarbonate in acetonitrile (AbC) at 56 °C for 30 min followed by alkalation with 50 mM iodoacetamide in 100 mM AbC in the dark at room temperature for 30 min. After washing the mixture was digested in trypsin buffer (13 ng/µL trypsin in 50 mM AbC) at 37 °C for 12 h. The digested mixture was analyzed by LC-MS/MS (Dionic Ultimate 3000; Solvent A: 98% H_2O, 2% acetonitrile (ACN), 0.1% formic acid (FA); Solvent B: 80% ACN, 20% H_2O, 0.1% FA; 100 % A to

100% B in 1 h; MS/MS: Bruker HCT Ultra PTM). The data were analyzed with DataAnalysis v.4.0 SP4, BioTools 3.2 SR1 and compared with a protein database (Mascot version 2.2.07).

6.5.3 Surfactant binding assay[**]

To mimic the surfactant binding to inhaled particles and digestion of any attached protein corona (while inside the phagolysosome) a surfactant binding/digestion assay was performed. Briefly, polymeric particles at 100 cm^2/mL were suspended in non-diluted lung lining fluid (LLF). After 1 min of incubation, the supernatant from particle suspensions were collected by three rounds of centrifugation at 15000 × *g* for 20 min. As benchmark particles, NiO and Co_3O_4 nanoparticles were tested at the same surface area dose. The concentrations of phospholipids were measured using a phospholipid assay kit (Bioassay systems). The adsorbed phospholipid levels were calculated by subtracting the levels of LLF from those of particle supernatants. After washing the unbound LLF from the particle suspensions, particles were re-suspended with the same volume of saline and phospholipase A_2 (PLA_2) was applied overnight. The undigested phospholipid levels were measured in the particle suspensions using the phospholipids assay kit (Bioassay systems, CA, USA). After colour development, the optical density at 570 nm of the particle-free supernatant was measured.

[**] Digestion assays were carried out by Dr Wan-Seob Cho at the Centre for Inflammation Research, University of Edinburgh, Edinburgh.

6.6 Cell culture

6.6.1 General cell culture

Human embryonic kidney cells (HEK293T) and human cervical cancer cells (HeLa) were cultured in Dulbecco's modified eagle medium (DMEM) supplemented with 10% (v/v) heat inactivated fetal bovine serum, *L*-glutamine (4 mM) and antibiotics (100 units/mL penicillin and 100 units/L streptomycin) at 37 °C and 5% CO_2. Cells were cultured in T-75 flasks (Nunc) until 80% confluency followed by removal of growth medium, washing with PBS (10 mL) and harvesting by trypsination (trypsin/EDTA, Gibco) (1 mL) at 37 ºC. Detached cells were collected in fresh growth media and an aliquot was reseeded to a flask for re-growth. Cell densities were determined with a Neubauer chamber. An aliquot (10 µL) of cells was pipetted into the Neubauer chamber and the number of cells counted. Cell experiments were carried out with cells passaged between 4- and 20-times.

6.6.2 Particle incubation and subsequent cell analysis

HEK293T and HeLa were plated in DMEM, supplemented with 10% (v / v) heat inactivated fetal bovine serum, *L*-glutamine (4 mM) and antibiotics (100 units/mL penicillin and 100 units/L streptomycin) in a 24-well plate at a density of 20,000 cells per well and grown for 24 h at 37 °C and 5% CO_2. Thereafter, particles (12.5 µg/mL – 75 µg/mL, Table 6.10) were added and incubated with the cells for 24 h. Cells were washed with PBS (2 × 350 µL) and incubated for a further 12 h in DMEM (350 µL). After incubation, cells were washed with PBS, harvested with trypsin/EDTA and analyzed by flow cytometry or imaged under a Leica DM IRB fluorescence microscope (**40a**, **41**, **51** concentrations: Table 6.10). Quantitative flow

cytometric analysis was carried out in triplicate and by addition of 2% trypan blue to quench extracellular fluorescence.[156]

To perform cellular uptake of particles **40b**, **43b** and **71** – **74**, HEK293T and HeLa were plated in DMEM, supplemented with 10% (v / v) heat inactivated fetal bovine serum, *L*-glutamine (4 mM) and antibiotics (100 units/mL penicillin and 100 units/L streptomycin) in a 24-well plate at a density of 20,000 cells per well and grown for 24 h at 37 °C and 5% CO_2. Thereafter, particles (12.5 µg/mL – 75 µg/mL, Table 6.10) were added and incubated with the cells for 2 h. Cells were washed with PBS (2 × 350 µL) and analyzed by flow cytometry. Quantitative flow cytometric analysis was carried out in triplicate and by addition of 2% trypan blue to quench extracellular fluorescence.[156]

Table 6.10. Particle incubation in HEK293T and HeLa cells.

Particles	Studied concentrations
40a and **41**	12.5, 25, 50 µg/mL
51	12.5, 25, 37.5, 50, 62.5, 75 µg/mL
61 and **62**	12.5, 25, 50 µg/mL
40b and **64** – **70**	50 µg/mL
40b, **43b** and **71** – **74**	50 µg/mL

6.6.3 Cell viability

HEK293T and HeLa were plated in DMEM, supplemented with 10% (v/v) heat inactivated fetal bovine serum, *L*-glutamine (4 mM) and antibiotics (100 units/mL penicillin and 100 units/mL streptomycin) in a 96-well plate at a density of 5,000 cells per well and grown for 24 h at 37 °C and 5% CO_2. Thereafter, particles (12.5 µg/mL – 75 µg/mL) were added and incubated with the cells for 24 h. Cells were

washed with PBS (2 × 350 µL) and incubated for a further 24 h in DMEM (350 µL). After incubation, cells were washed with PBS and incubated in 3-(4,5-dimethylthiazol-2-yl)-2,5-diphenyltetrazolium bromide (MTT) solution (7 mg MTT in 7 mL PBS and 3 mL phenol red free DMEM) for 3 h at 37 °C. Afterwards, 100 µL solubilisation solution (10% triton-X 100 in acidic isopropanol (0.1 M HCl)) was added and the absorbance at 570 nm measured (Benchmark Biorad microplate reader) and results compared to untreated cells.

6.6.4 Cell staining

Sterilised cover slips (24 mm) were coated with 0.01% poly-lysine in water for 10 minutes at room temperature then washed with PBS (6 ×). The cover slips were placed in 6-well plates and seeded with 90,000 treated cells/well in 1.6 mL Dulbecco's modified eagle medium (DMEM) and incubated overnight. The media was removed and replaced with particles **61** or **62** (12.5, 25 and 50 µg/mL) in DMEM for 24 h. Cells were washed with PBS (2 × 350 µL) and incubated for a further 12 h in DMEM (350 µL). The media was removed and the nuclei were stained by incubation of the cells with a 10 µM solution of Hoechst 33342 in media (DMEM) for 5 minutes at 37 °C and 5% CO_2. The cells were washed with PBS (2 ×) and the cytosol was subsequently stained with a 6 µM solution of CellTracker™ Red CMTPX in serum free media (Opti-MEM^{TM}) for 50 min at 37 °C and 5% CO_2. The cells were washed with PBS (2 ×) fixed with 4% formaldehyde in PBS for 30 min at room temperature, washed again with PBS (2 ×). Cells were imaged using a Leica SP5 Confocal. Microscope lasers setting were: excitation laser lines at 404 nm, 488 nm, 595 and 633 nm with emission filters of 414-483 nm for Hoechst 33342 (nuclei

stain), 497-586 nm for released fluorescein, 600-628 nm for CellTracker™ Red (cytosol stain), 642-750 nm for Cy5 (particles).

6.6.5 Haemolysis assay[††]

Hemolysis Assy. Erythrocytes were obtained from fresh human venous blood, drawn from healthy volunteer donors with informed oral consent, under the full institutional ethical approval of the University of Edinburgh. The preparation of erythrocytes and hemolysis assay was conducted according to the previously described method.[229] Surface functionalised polymeric particles (**4a**, **8** – **10**, **12**, **15**, **16** and **63**) were tested at a surface area dose of 30, 100, and 300 cm^2/mL and saline and 0.1% Triton X-100 was used as negative and positive controls, respectively. The percentage of hemolysis was calculated compared to complete hemolysis (Triton X-100).

Influence of the protein corona on hemolytic activity. To evaluate the impact of the protein corona following the particle's residence in phagolysosomes, particles (**4a**, **8** – **10**, **12**, **15**, **16** and **63**) were incubated with 5% FBS or 10% LLF for 1 min and washed with saline (3 ×) by the method described above. Afterwards, the particles were incubated with phospholipase A_2 (1 U/mL) at 37 °C for 24 h followed by a saline wash (3 ×) and incubation with proteinase K (30 mAU/mL) at 37 °C for 24 h. The enzymatic digestion was stopped by addition of EDTA (2 mM) followed by a saline wash (3 ×) and resuspension in saline and determining the hemolytic activity of the particles.

[††] Haemolysis assays were carried out by Dr Wan-Seob Cho at the Centre for Inflammation Research, University of Edinburgh, Edinburgh.

References

(1) Comission of the European Communities. *Communication from the Comission: Towards a European Strategy for Nanotechnology* **2004**.

(2) UK Government. *UK Nanotechnologies Strategy: Small Technologies, Great Opportunities* **2010**.

(3) Gould, P. *Nano Today* **2006**, *1*, 34-39.

(4) Organisation for Economic Co-operation and Development - Directorate for Science, Technology and Industry. *Nanotechnology: An Overview based on Indicators and Statistics* **2009**.

(5) Goesmann, H.; Feldmann, C. *Angew. Chem. Int. Ed.* **2010**, *49*, 1362-1395.

(6) Medintz, I. L.; Uyeda, H. T.; Goldman, E. R.; Mattoussi, H. *Nat. Mater.* **2005**, *4*, 435-446.

(7) Althues, H.; Henle, J.; Kaskel, S. *Chem. Soc. Rev.* **2007**, *36*, 1454-1465.

(8) Wagner, V.; Dullaart, A.; Bock, A.-K.; Zweck, A. *Nat. Biotechnol.* **2006**, *24*, 1211-1217.

(9) Rao, C. N. R.; Kulkarni, G. U.; Thomas, P. J.; Edwards, P. P. *Chemistry* **2002**, *8*, 28-35.

(10) Bell, A. T. *Science* **2003**, *299*, 1688-1691.

(11) Turner, M.; Golovko, V. B.; Vaughan, O. P. H.; Abdulkin, P.; Berenguer-Murcia, A.; Tikhov, M. S.; Johnson, B. F. G.; Lambert, R. M. *Nature* **2008**, *454*, 981-983.

(12) Nozaki, C.; Lugmair, C. G.; Bell, A. T.; Tilley, T. D. *J. Am. Chem. Soc.* **2002**, *124*, 13194-13203.

(13) Stone, V.; Donaldson, K. *Nat. Nanotechnol.* **2006**, *1*, 23-24.

(14) Irifune, T.; Kurio, A.; Sakamoto, S.; Inoue, T.; Sumiya, H. *Nature* **2003**, *421*, 599-600.

(15) Sun, Y.-P.; Zhou, B.; Lin, Y.; Wang, W.; Fernando, K. A. S.; Pathak, P.; Meziani, M. J.; Harruff, B. A.; Wang, X.; Wang, H.; Luo, P. G.; Yang, H.; Kose, M. E.; Chen, B.; Veca, L. M.; Xie, S.-Y. *J. Am. Chem. Soc.* **2006**, *128*, 7756-7757.

(16) Letchford, K.; Burt, H. *Eur. J. Pharm. Biopharm.* **2007**, *65*, 259-269.

(17) Mora-Huertas, C. E.; Fessi, H.; Elaissari, A. *Int. J. Pharm.* **2010**, *385*, 113-142.

(18) Tanner, P.; Baumann, P.; Enea, R.; Onaca, O.; Palivan, C.; Meier, W. *Acc. Chem. Res.* **2011**, *44*, 1039-1049.

(19) Na, H. B.; Song, I. C.; Hyeon, T. *Adv. Mater.* **2009**, *21*, 2133-2148.

(20) van Vlerken, L. E.; Amiji, M. M. *Expert Opin. Drug Delivery* **2006**, *3*, 205-216.

(21) Gokmen, M. T.; Du Prez, F. E. *Prog. Polym. Sci.* **2012**, *37*, 365-405.

(22) Lee, D. I. *Prog. Org. Coat.* **2002**, *45*, 341-358.

(23) Kumari, A.; Yadav, S. K.; Yadav, S. C. *Colloids Surf., B* **2010**, *75*, 1-18.

(24) Algar, W. R.; Prasuhn, D. E.; Stewart, M. H.; Jennings, T. L.; Blanco-Canosa, J. B.; Dawson, P. E.; Medintz, I. L. *Bioconjugate Chem.* **2011**, *22*, 825-858.

(25) Couvreur, P.; Tulkenst, P.; Roland, M.; Trouet, A.; Speiser, P. *FEBS Lett.* **1977**, *84*, 323-326.

(26) Lee, Y.-E. K.; Kopelman, R. *Wiley Interdiscip. Rev. Nanomed. Nanobiotechnol.* **2009**, *1*, 98-110.

(27) Sánchez-Martín, R. M.; Cuttle, M.; Mittoo, S.; Bradley, M. *Angew. Chem. Int. Ed.* **2006**, *45*, 5472-5474.

(28) Meallet-Renault, R.; Pansu, R.; Amigoni-Gerbier, S.; Larpent, C. *Chem. Commun.* **2004**, 2344-2345.

(29) Bradley, M.; Alexander, L.; Duncan, K.; Chennaoui, M.; Jones, A. C.; Sánchez-Martín, R. M. *Bioorg. Med. Chem. Lett.* **2008**, *18*, 313-317.

(30) Kuang, Y.; Walt, D. R. *Biotechnol. Bioeng.* **2007**, *96*, 318-325.

(31) Xu, H.; Aylottb, J. W.; Kopelman, R. *Analyst* **2002**, *127*, 1471-1477.

(32) Kim, K.; Lee, M.; Park, H.; Kim, J.-H.; Kim, S.; Chung, H.; Choi, K.; Kim, I.-S.; Seong, B. L.; Kwon, I. C. *J. Am. Chem. Soc.* **2006**, *128*, 3490-3491.

(33) Kim, J.-H.; Lee, S.; Park, K.; Nam, H. Y.; Jang, S. Y.; Youn, I.; Kim, K.; Jeon, H.; Park, R.-W.; Kim, I.-S.; Choi, K.; Kwon, I. C. *Angew. Chem. Int. Ed.* **2007**, *46*, 5779-82.

(34) Leader, B.; Baca, Q. J.; Golan, D. E. *Nat. Rev. Drug Discovery* **2008**, *7*, 21-39.

(35) Basarkar, A.; Singh, J. *Int. J. Nanomed.* **2007**, *2*, 353-360.

(36) Sanchez-Martin, R. M.; Alexander, L.; Muzerelle, M.; Cardenas-Maestre, J. M.; Tsakiridis, A.; Brickman, J. M.; Bradley, M. *Chembiochem* **2009**, *10*, 1453-1456.

(37) Sy, J. C.; Phelps, E. A.; García, A. J.; Murthy, N.; Davis, M. E. *Biomaterials* **2010**, *31*, 4987-4994.

(38) Alexander, L. M.; Sánchez-Martín, R. M.; Bradley, M. *Bioconjugate Chem.* **2009**, *20*, 422-426.

(39) Bradley, M.; Alexander, L.; Sanchez-Martin, R. M. *J. Fluoresc.* **2008**, *18*, 733-739.

(40) Cohen, H.; Levy, R. J.; Gao, J.; Fishbein, I.; Kousaev, V.; Sosnowski, S.; Slomkowski, S.; Golomb, G. *Gene Therapy* **2000**, *7*, 1896-1905.

(41) Sanchez-Martin, R. M.; Muzerelle, M.; Chitkul, N.; How, S. E.; Mittoo, S.; Bradley, M. *Chembiochem* **2005**, *6*, 1341-1345.

(42) Holzapfel, V.; Musyanovych, A.; Landfester, K.; Lorenz, M. R.; Mailänder, V. *Macromol. Chem. Phys.* **2005**, *206*, 2440-2449.

(43) Palma, A.; Alvarez, L. A.; Scholz, D.; Frimannsson, D. O.; Grossi, M.; Quinn, S. J.; O'Shea, D. F. *J. Am. Chem. Soc.* **2011**, *133*, 19618-19621.

(44) Baumes, J. M.; Gassensmith, J. J.; Giblin, J.; Lee, J.-J.; White, A. G.; Culligan, W. J.; Leevy, W. M.; Kuno, M.; Smith, B. D. *Nat. Chem.* **2010**, *2*, 1025-1030.

(45) Arshady, R. *Colloid Polym. Sci.* **1992**, *270*, 717-732.

(46) Bamnolker, H.; Margel, S. *J. Polym. Sci. A: Polym. Chem.* **1996**, *34*, 1857-1871.

(47) Landfester, K. *Top. Curr. Chem.* **2003**, *227*, 75-123.

(48) Harkins, W. D. *J. Am. Chem. Soc.* **1947**, *69*, 1428-1444.

(49) Smith, W. V.; Ewart, R. H. *J. Chem. Phys.* **1948**, *16*, 592.

(50) Chern, C. S. *Prog. Polym. Sci.* **2006**, *31*, 443-486.

(51) Yan, C.; Cheng, S.; Feng, L. *J. Polym. Sci. A: Polym. Chem.* **1999**, *37*, 2649-2656.

(52) Delair, T.; Marguet, V.; Pichot, C.; Mandrand, B. *Colloid Polym. Sci.* **1994**, *272*, 962-970.

(53) Sánchez-Martín, R. M.; Alexander, L.; Bradley, M. *Ann. N. Y. Acad. Sci.* **2008**, *1130*, 207-217.

(54) Kaiser, E.; Colescott, R.; Bossinger, C.; Cook, P. *Anal. Biochem.* **1970**, *34*, 595-598.

(55) Sarin, V.; Kent, S.; Tam, J.; Merrifield, R. *Anal. Biochem.* **1981**, *117*, 147-157.

(56) Kay, C.; Lorthioir, O. E.; Parr, N. J.; Congreve, M.; McKeown, S. C.; Scicinski, J. J.; Ley, S. V. *Biotechnol. Bioeng.* **2001**, *71*, 110-118.

(57) Ellman, G. *Arch. Biochem. Biophys.* **1959**, *82*, 70-77.

(58) Pomonis, G. J.; Severson, R.; Freeman, P. *J. Chromatogr. A* **1969**, *40*, 78-84.

(59) Kawaguchi, S. *J. Colloid Interface Sci.* **1995**, *176*, 362-369.

(60) Uchida, E.; Uyama, Y.; Ikada, Y. *Langmuir* **1993**, *9*, 1121-1124.

(61) Kang, E. T.; Tan, K. L.; Kato, K.; Uyama, Y.; Ikada, Y. *Macromolecules* **1996**, *29*, 6872-6879.

(62) Hennig, A.; Hoffmann, A.; Borcherding, H.; Thiele, T.; Schedler, U.; Resch-Genger, U. *Anal. Chem.* **2011**, *83*, 4970-4974.

(63) Hennig, A.; Hoffmann, A.; Borcherding, H.; Thiele, T.; Schedler, U.; Resch-Genger, U. *Chem. Commun.* **2011**, *47*, 7842-7844.

(64) Slater, M.; Snauko, M.; Svec, F.; Fréchet, J. M. J. *Anal. Chem.* **2006**, *78*, 4969-4975.

(65) Wang, R.; Zhang, Y.; Ma, G.; Su, Z. *Colloids Surf., B* **2006**, *51*, 93-99.

(66) Mirica, K. A.; Phillips, S. T.; Shevkoplyas, S. S.; Whitesides, G. M. *J. Am. Chem. Soc.* **2008**, *130*, 17678-17680.

(67) Kanemitsu, T.; Wong, C.-H.; Kanie, O. *J. Am. Chem. Soc.* **2002**, *124*, 3591-3599.

(68) Salvino, J. M.; Patel, S.; Drew, M.; Krowlikowski, P.; Orton, E.; Kumar, N. V.; Caulfield, T.; Labaudiniere, R. *J. Comb. Chem.* **2001**, *3*, 177-180.

(69) Furrer, J.; Piotto, M.; Bourdonneau, M.; Limal, D.; Guichard, G.; Elbayed, K.; Raya, J.; Briand, J.-P.; Bianco, A. *J. Am. Chem. Soc.* **2001**, *123*, 4130-4138.

(70) Gaborieau, M.; Nebhani, L.; Graf, R.; Barner, L.; Barner-Kowollik, C. *Macromolecules* **2010**, *43*, 3868-3875.

(71) Yan, B.; Gremlich, H.-U.; Moss, S.; Coppola, G. M.; Sun, Q.; Liu, L. *J. Comb. Chem.* **1999**, *1*, 46-54.

(72) Semmler, A.; Weber, R.; Przybylski, M.; Wittmann, V. *J. Am. Soc. Mass Spectrom.* **2010**, *21*, 215-219.

(73) Marani, M. M.; Oliveira, E.; Côte, S.; Camperi, S. A.; Albericio, F.; Cascone, O. *Anal. Biochem.* **2007**, *370*, 215-222.

(74) Egner, B. J.; Langley, G. J.; Bradley, M. *J. Org. Chem.* **1995**, *60*, 2652-2653.

(75) Han, Y.; Shi, Q.; Hu, J.; Du, Q.; Chen, X.; Jing, X. *Macromol. Biosci.* **2008**, *8*, 638-644.

(76) Goddard, J. M.; Hotchkiss, J. H. *Prog. Polym. Sci.* **2007**, *32*, 698-725.

(77) Kuzmin, A.; Poloukhtine, A.; Wolfert, M. A.; Popik, V. V. *Bioconjugate Chem.* **2010**, *21*, 2076-2085.

(78) Goldmann, A. S.; Walther, A.; Nebhani, L.; Joso, R.; Ernst, D.; Loos, K.; Barner-Kowollik, C.; Barner, L.; Müller, A. H. E. *Macromolecules* **2009**, *42*, 3707-3714.

(79) Stevens, M. P. *Polymer Chemistry: An Introduction*; 3rd Ed.; Oxford University Press: New York, **1999**.

(80) Mailänder, V.; Landfester, K. *Biomacromolecules* **2009**, *10*, 2379-2400.

(81) Malvern Instruments *Dynamic Light Scattering: Technical Note (MRK656-01)*; **2011**.

(82) Delgado, A. V.; González-Caballero, F.; Hunter, R. J.; Koopal, L. K.; Lyklema, J. *Pure Appl. Chem.* **2005**, *77*, 1753-1805.

(83) Hall Jr., H. K. *J. Am. Chem. Soc.* **1957**, *79*, 5441-5444.

(84) Weiner, B. B.; Tscharnuter, W. W.; Fairhurst, D. *Can. Mineral Anal.*, **1993**.

(85) Hunter, R. J. *Zeta Potential in Colloid Science: Principles and Applications*; Academic Press, New York, **1988**.

(86) Subirós-Funosas, R.; Prohens, R.; Barbas, R.; El-Faham, A.; Albericio, F. *Chemistry* **2009**, *15*, 9394-9403.

(87) Zhao, Z. G.; Im, J. S.; Lam, K. S.; Lake, D. F. *Bioconjugate Chem.* **1999,** *10*, 424-430.

(88) Derfus, A. M.; Chen, A. A.; Min, D.-H.; Ruoslahti, E.; Bhatia, S. N. *Bioconjugate Chem.* **2007**, *18*, 1391-1396.

(89) Ackerson, C. J.; Jadzinsky, P. D.; Jensen, G. J.; Kornberg, R. D. *J. Am. Chem. Soc.* **2006**, *128*, 2635-2640.

(90) Lauer, S. A.; Nolan, J. P. *Cytometry* **2002**, *48*, 136-145.

(91) Kreevoy, M. M.; Harper, E. T.; Duvall, R. E.; Wilgus III, H. S.; Ditsch, L. T. *J. Am. Chem. Soc.* **1960**, *82*, 4899-4902.

(92) Thielbeer, F.; Donaldson, K.; Bradley, M. *Bioconjugate Chem.* **2011**, *22*, 144-150.

(93) Ranu, B. C.; Dey, R.; Chatterjee, T.; Ahammed, S. *ChemSusChem* **2011**, *5*, 22-44.

(94) Reynolds, C. H.; Annan, N.; Beshah, K.; Huber, J. H.; Shaber, S. H.; Lenkinski, R. E.; Wortman, J. A. *J. Am. Chem. Soc.* **2000**, *122*, 8940-8945.

(95) Pressly, E. D.; Rossin, R.; Hagooly, A.; Fukukawa, K.-I.; Messmore, B. W.; Welch, M. J.; Wooley, K. L.; Lamm, M. S.; Hule, R. A.; Pochan, D. J.; Hawker, C. J. *Biomacromolecules* **2007**, *8*, 3126-3134.

(96) Engel, T.; Drobny, G.; Reid, P. *Physical Chemistry for the Life Science*; Pearson Education: London, **2008**.

(97) Sjöback, R.; Nygren, J.; Kubista, M. *Spectrochim. Acta, Part A* **1995**, *51*, L7-L21.

(98) Urano, Y.; Kamiya, M.; Kanda, K.; Ueno, T.; Hirose, K.; Nagano, T. *J. Am. Chem. Soc.* **2005**, *127*, 4888-4894.

(99) Charreyre, M. *J. Colloid Interface Sci.* **1995**, *170*, 374-382.

(100) Zhang, Q.; Han, Y.; Wang, W.; Zhang, L.; Chang, J. *Eur. Polym. J.* **2009**, *45*, 550-556.

(101) Han, M.; Gao, X.; Su, J. Z.; Nie, S. *Nat. Biotechnol.* **2001**, *19*, 631-635.

(102) Taniguchi, T.; Takeuchi, N.; Kobaru, S.; Nakahira, T. *J. Colloid Interface Sci.* **2008**, *327*, 58-62.

(103) Zhang, Z.; Long, Y.; Pan, J.; Yan, X. *J. Mater. Chem.* **2010**, *20*, 1179-1185.

(104) Nanthakumar, A.; Pon, R. T.; Mazumder, A.; Yu, S.; Watson, A. *Bioconjugate Chem.* **2000**, *11*, 282-288.

(105) Cardenas-Maestre, J. M.; Panadero-Fajardo, S.; Perez-Lopez, A. M.; Sanchez-Martin, R. M. *J. Mater. Chem.* **2011**, *21*, 12735-12743.

(106) Portal, C.; Launay, D.; Merritt, A.; Bradley, M. *J. Comb. Chem.* **2005**, *7*, 554-560.

(107) Ando, K.; Kawaguchi, H. *J. Colloid Interface Sci.* **2005**, *285*, 619-626.

(108) Chen, J.; Zeng, F.; Wu, S.; Su, J.; Tong, Z. *Small* **2009**, *5*, 970-897.

(109) Szymanski, C.; Wu, C.; Hooper, J.; Salazar, M. A.; Perdomo, A.; Dukes, A.; McNeill, J. *J. Phys. Chem. B* **2005**, *109*, 8543-8546.

(110) Wu, C.; Bull, B.; Szymanski, C.; Christensen, K.; McNeill, J. *ACS Nano* **2008**, *2*, 2415-2423.

(111) Laurenti, M.; López-Cabarcos, E.; García-Blanco, F.; Frick, B.; Rubio-Retama, J. *Langmuir* **2009**, *25*, 9579-9584.

(112) Tronc, F.; Li, M.; Lu, J.; Winnik, M. A.; Kaul, B. L.; Graciet, J.-C. *J. Polym. Sci., Part A: Polym. Chem.* **2003**, *41*, 766-778.

(113) Sun, H.; Scharff-Poulsen, A. M.; Gu, H.; Almdal, K. *Chem. Mater.* **2006**, *18*, 3381-3384.

(114) Grazon, C.; Rieger, J.; Méallet-Renault, R.; Clavier, G.; Charleux, B. *Macromol. Rapid Commun.* **2011**, *32*, 699-705.

(115) Kalinina, O.; Kumacheva, E. *Macromolecules* **1999**, *32*, 4122-4129.

(116) Grabchev, I.; Petkov, C.; Bojinov, V. *Macromol. Mater. Eng.* **2002**, *287*, 904-908.

(117) Fujikawa, Y.; Urano, Y.; Komatsu, T.; Hanaoka, K.; Kojima, H.; Terai, T.; Inoue, H.; Nagano, T. *J. Am. Chem. Soc.* **2008**, *130*, 14533-14543.

(118) Ueno, T.; Urano, Y.; Setsukinai, K.-I.; Takakusa, H.; Kojima, H.; Kikuchi, K.; Ohkubo, K.; Fukuzumi, S.; Nagano, T. *J. Am. Chem. Soc.* **2004**, *126*, 14079-14085.

(119) Miura, T.; Urano, Y.; Tanaka, K.; Nagano, T.; Ohkubo, K.; Fukuzumi, S. *J. Am. Chem. Soc.* **2003**, *125*, 8666-8671.

(120) Egner, B. J.; Rana, S.; Smith, H.; Bouloc, N.; Frey, J. G.; Brocklesby, W. S.; Bradley, M. *Chem. Commun.* **1997**, 735-736.

(121) Kress, J.; Rose, A.; Frey, J. G.; Brocklesby, W. S.; Ladlow, M.; Mellor, G. W.; Bradley, M. *Chemistry* **2001**, *7*, 3880-3883.

(122) Mineno, T.; Ueno, T.; Urano, Y.; Kojima, H.; Nagano, T. *Org. Lett.* **2006**, *8*, 5963-5966.

(123) Lin, H.-C.; Lin, H.-H.; Kao, C.-Y.; Yu, A. L.; Peng, W.-P.; Chen, C.-H. *Angew. Chem. Int. Ed.* **2010**, *49*, 3460-3464.

(124) Lorenz, M. R.; Holzapfel, V.; Musyanovych, A.; Nothelfer, K.; Walther, P.; Frank, H.; Landfester, K.; Schrezenmeier, H.; Mailänder, V. *Biomaterials* **2006**, *27*, 2820-2828.

(125) Stringer, B.; Imrich, A.; Kobzik, L. *Cytometry* **1995**, *20*, 23-32.

(126) Thielbeer, F.; Chankeshwara, S. V.; Bradley, M. *Biomacromolecules* **2011**, *12*, 4386-4391.

(127) He, X.; Wang, K.; Cheng, Z. *Wiley Interdiscip. Rev. Nanomed. Nanobiotechnol.* **2010**, *2*, 349-66.

(128) Kim, H. N.; Guo, Z.; Zhu, W.; Yoon, J.; Tian, H. *Chem. Soc. Rev.* **2011**, *40*, 79-93.

(129) Shen, L.; Zhu, W.; Meng, X.; Guo, Z.; Tian, H. *Sci. China, Ser. B. Chem.* **2009**, *52*, 821-826.

(130) Tanaka, K.; Kitamura, N.; Chujo, Y. *Macromolecules* **2010**, *43*, 6180-6184.

(131) Hu, L.; Mao, Z.; Gao, C. *J. Mater. Chem.* **2009**, *19*, 3108-3115.

(132) Sletten, E. M.; Bertozzi, C. R. *Angew. Chem. Int. Ed.* **2009**, *48*, 6974-6998.

(133) Abdelrahman, A. I.; Thickett, S. C.; Liang, Y.; Ornatsky, O.; Baranov, V.; Winnik, M. A. *Macromolecules* **2011**, *44*, 4801-4813.

(134) Valeur, E.; Bradley, M. *Chem. Soc. Rev.* **2009**, *38*, 606-631.

(135) Aryal, S.; Hu, C.-M. J.; Zhang, L. *ACS Nano* **2010**, *4*, 251-8.

(136) Ji, S.; Zhu, Z.; Hoye, T. R.; Macosko, C. W. *Macromol. Chem. Phys.* **2009**, *210*, 823-831.

(137) van der Vlies, A. J.; O'Neil, C. P.; Hasegawa, U.; Hammond, N.; Hubbell, J. A. *Bioconjugate Chem.* **2010**, *21*, 653-662.

(138) Iha, R. K.; Wooley, K. L.; Nyström, A. M.; Burke, D. J.; Kade, M. J.; Hawker, C. J. *Chem. Rev.* **2009**, *109*, 5620-5686.

(139) Kelkar, S. S.; Reineke, T. M. *Bioconjugate Chem.* **2011**, *22*, 1879-1903.

(140) Li, X.; Guo, J.; Asong, J.; Wolfert, M. A.; Boons, G.-J. *J. Am. Chem. Soc.* **2011**, *133*, 11147-11153.

(141) O'Reilly, R. K.; Joralemon, M. J.; Wooley, K. L.; Hawker, C. J. *Chem. Mater.* **2005**, *17*, 5976-5988.

(142) An, Z.; Tang, W.; Wu, M.; Jiao, Z.; Stucky, G. D. *Chem. Commun.* **2008**, *44*, 6501-6503.

(143) Chalker, J. M.; Bernardes, G. J. L.; Davis, B. G. *Acc. Chem. Res.* **2011**, *44*, 730-741.

(144) Spicer, C. D.; Davis, B. G. *Chem. Commun.* **2011**, *47*, 1698-700.

(145) Chalker, J. M.; Wood, C. S. C.; Davis, B. G. *J. Am. Chem. Soc.* **2009**, *131*, 16346-16347.

(146) Simmons, R. L.; Yu, R. T.; Myers, A. G. *J. Am. Chem. Soc.* **2011**, *133*, 15870-15873.

(147) Kodama, K.; Fukuzawa, S.; Nakayama, H.; Sakamoto, K.; Kigawa, T.; Yabuki, T.; Matsuda, N.; Shirouzu, M.; Takio, K.; Yokoyama, S.; Tachibana, K. *Chembiochem* **2007**, *8*, 232-238.

(148) Li, N.; Lim, R. K. V.; Edwardraja, S.; Lin, Q. *J. Am. Chem. Soc.* **2011**, *133*, 15316–15319.

(149) Yusop, R. M.; Unciti-Broceta, A.; Johansson, E. M. V.; Sánchez-Martín, R. M.; Bradley, M. *Nat. Chem.* **2011**, *3*, 239-243.

(150) Spicer, C. D.; Triemer, T.; Davis, B. G. *J. Am. Chem. Soc.* **2012**, *134*, 800-803.

(151) Kataoka, K.; Miyazaki, H.; Bunya, M.; Okano, T.; Sakurai, Y. *J. Am. Chem. Soc.* **1998**, *120*, 12694-12695.

(152) Li, S.; Davis, E. N.; Anderson, J.; Lin, Q.; Wang, Q. *Biomacromolecules* **2009**, *10*, 113-118.

(153) Cambre, J. N.; Roy, D.; Gondi, S. R.; Sumerlin, B. S. *J. Am. Chem. Soc.* **2007**, *129*, 10348-10349.

(154) Roy, D.; Cambre, J. N.; Sumerlin, B. S. *Chem. Commun.* **2008**, *44*, 2477-2479.

(155) Vogel, N.; Hauser, C. P.; Schuller, K.; Landfester, K.; Weiss, C. K. *Macromol. Chem. Phys.* **2010**, *211*, 1355-1368.

(156) Mosiman, V. L.; Patterson, B. K.; Canterero, L.; Goolsby, C. L. *Cytometry* **1997**, *30*, 151-156.

(157) Kielhorn, J.; Melber, C.; Keller, D.; Mangelsdorf, I. *Int. J. Hyg. Environ. Health* **2002**, *205*, 417-432.

(158) Mosmann, T. *J. Immunol. Methods* **1983**, *65*, 55-63.

(159) Kim, T. W.; Park, J.-hyun; Hong, J.-I. *Bull. Korean Chem. Soc.* **2007**, *28*, 1221-1223.

(160) Meister, A.; Gilbert, H. F. *Advances in Enzymology and Related Areas of Molecular Biology*; Meister, A., Ed.; John Wiley & Sons, Inc.: Hoboken, NJ, USA, **1990**.

(161) Chan, W. C.; White, P. D. *Fmoc-Solid Phase Peptide Synthesis: A Practical Approach*; Oxford University Press: New York, **2000**.

(162) Díaz-Mochón, J. J.; Bialy, L.; Bradley, M. *Org. Lett.* **2004**, *6*, 1127-1129.

(163) Hatakeyama, T.; Hashimoto, T.; Kondo, Y.; Fujiwara, Y.; Seike, H.; Takaya, H.; Tamada, Y.; Ono, T.; Nakamura, M. *J. Am. Chem. Soc.* **2010**, *132*, 10674-10676.

(164) Xie, J.; Schultz, P. G. *Nat. Rev. Mol. Cell Biol.* **2006**, *7*, 775-782.

(165) Lu, W.; Lieber, C. M. *Nat. Mater.* **2007**, *6*, 841-850.

(166) Woodrow Wilson International Center for Scholars - Project on Emerging Nanotechnologies www.nanotechproject.org. Date: **03/2012**.

(167) Krug, H. F.; Wick, P. *Angew. Chem. Int. Ed.* **2011**, *50*, 1260-1278.

(168) Nel, A.; Xia, T.; Mädler, L.; Li, N. *Science* **2006**, *311*, 622-627.

(169) Lynch, I.; Cedervall, T.; Lundqvist, M.; Cabaleiro-Lago, C.; Linse, S.; Dawson, K. A. *Adv. Colloid Interface Sci.* **2007**, *134-135*, 167-174.

(170) Klein, J. *Proc. Natl. Acad. Sci. USA* **2007**, *104*, 2029-2030.

(171) Walczyk, D.; Bombelli, F. B.; Monopoli, M. P.; Lynch, I.; Dawson, K. A. *J. Am. Chem. Soc.* **2010**, *132*, 5761-5768.

(172) Cedervall, T.; Lynch, I.; Foy, M.; Berggård, T.; Donnelly, S. C.; Cagney, G.; Linse, S.; Dawson, K. A. *Angew. Chem. Int. Ed.* **2007**, *46*, 5754-5756.

(173) Monopoli, M. P.; Walczyk, D.; Campbell, A.; Elia, G.; Lynch, I.; Bombelli, F. B.; Dawson, K. A.; Baldelli Bombelli, F. *J. Am. Chem. Soc.* **2011**, *133*, 2525-2534.

(174) Lundqvist, M.; Stigler, J.; Cedervall, T.; Berggård, T.; Flanagan, M. B.; Lynch, I.; Elia, G.; Dawson, K. *ACS Nano* **2011**, *5*, 7503-7509.

(175) Lynch, I.; Dawson, K. A. *Nano Today* **2008**, *3*, 40-47.

(176) Hellstrand, E.; Lynch, I.; Andersson, A.; Drakenberg, T.; Dahlbäck, B.; Dawson, K. A.; Linse, S.; Cedervall, T. *FEBS J.* **2009**, *276*, 3372-3381.

(177) Zeng, Z.; Patel, J.; Lee, S.-H.; McCallum, M.; Tyagi, A.; Yan, M.; Shea, K. J. *J. Am. Chem. Soc.* **2012**, *134*, 2681-2690.

(178) Lundqvist, M.; Stigler, J.; Elia, G.; Lynch, I.; Cedervall, T.; Dawson, K. A. *Proc. Natl. Acad. Sci. USA* **2008**, *105*, 14265-14270.

(179) Cedervall, T.; Lynch, I.; Lindman, S.; Berggård, T.; Thulin, E.; Nilsson, H.; Dawson, K. A.; Linse, S. *Proc. Natl. Acad. Sci. USA* **2007**, *104*, 2050-2055.

(180) Doorley, G. W.; Payne, C. *Chem. Commun.* **2012**, *48*, 2961-2963.

(181) Wang, J.; Jensen, U. B.; Jensen, G. V.; Shipovskov, S.; Balakrishnan, V. S.; Otzen, D. E.; Pedersen, J. S.; Besenbacher, F.; Sutherland, D. S. *Nano Lett.* **2011**, *11*, 4985-4991.

(182) Nel, A. E.; Mädler, L.; Velegol, D.; Xia, T.; Hoek, E. M. V.; Somasundaran, P.; Klaessig, F.; Castranova, V.; Thompson, M. *Nat. Mater.* **2009**, *8*, 543-557.

(183) Kittler, S.; Greulich, C.; Gebauer, J. S.; Diendorf, J.; Treuel, L.; Ruiz, L.; Gonzalez-Calbet, J. M.; Vallet-Regi, M.; Zellner, R.; Köller, M.; Epple, M. *J. Mater. Chem.* **2010**, *20*, 512-518.

(184) Limbach, L. K.; Li, Y.; Grass, R. N.; Brunner, T. J.; Hintermann, M. A.; Muller, M.; Gunther, D.; Stark, W. J. *Environ. Sci. Technol.* **2005**, *39*, 9370-9376.

(185) Gessnera, A.; Lieskeb, A.; Paulkeb, B. R.; Müller, R. H. *Eur. J. Pharm. Biopharm.* **2002**, *54*, 165-170.

(186) Roach, P.; Farrar, D.; Perry, C. C. *J. Am. Chem. Soc.* **2005**, *127*, 8168-8173.

(187) Sahoo, S. K.; Parveen, S.; Panda, J. J. *Nanomed. Nanotechnol. Biol. Med.* **2007**, *3*, 20-31.

(188) Tabata, Y.; Ikada, Y. *Biomaterials* **1988**, *9*, 356-362.

(189) Zauner, W.; Farrow, N. A.; Haines, A. M. R. *J. Controlled Release* **2001**, *71*, 39-51.

(190) He, C.; Hu, Y.; Yin, L.; Tang, C.; Yin, C. *Biomaterials* **2010**, *31*, 3657-3666.

(191) Lorenz, M. R.; Kohnle, M.-V.; Dass, M.; Walther, P.; Höcherl, A.; Ziener, U.; Landfester, K.; Mailänder, V. *Macromol. Biosci.* **2008**, *8*, 711-27.

(192) Foster, K. A.; Yazdanian, M.; Audus, K. L. *J. Pharm. Pharmacol.* **2001**, *53*, 57-66.

(193) Alexander, L. M.; Pernagallo, S.; Livigni, A.; Sánchez-Martín, R. M.; Brickman, J. M.; Bradley, M. *Mol. BioSyst.* **2010**, *6*, 399-409.

(194) Manabe, M.; Tatarazako, N.; Kinoshita, M. *Aquat. Toxicol.* **2011**, *105*, 576-581.

(195) Desai, M. P.; Labhasetwar, V.; Walter, E.; Levy, R. J.; Amidon, G. L. *Pharm. Res.* **1997**, *14*, 1568-1573.

(196) Dausend, J.; Musyanovych, A.; Dass, M.; Walther, P.; Schrezenmeier, H.; Landfester, K.; Mailänder, V. *Macromol. Biosci.* **2008**, *8*, 1135-1143.

(197) Rejman, J.; Oberle, V.; Zuhorn, I. S.; Hoekstra, D. *Biochem. J.* **2004**, *377*, 159-169.

(198) Rothen-Rutishauser, B. M.; Schürch, S.; Haenni, B.; Kapp, N.; Gehr, P. *Environ. Sci. Technol.* **2006**, *40*, 4353-4359.

(199) Faunce, T. A.; White, J.; Matthaei, K. I. *Nanomed.* **2008**, *3*, 859-866.

(200) Ehrenberg, M. S.; Friedman, A. E.; Finkelstein, J. N.; Oberdörster, G.; McGrath, J. L. *Biomaterials* **2009**, *30*, 603-610.

(201) Baier, G.; Costa, C.; Zeller, A.; Baumann, D.; Sayer, C.; Araujo, P. H. H.; Mailänder, V.; Musyanovych, A.; Landfester, K. *Macromol. Biosci.* **2011**, *11*, 628-638.

(202) Patil, S.; Sandberg, A.; Heckert, E.; Self, W.; Seal, S. *Biomaterials* **2007**, *28*, 4600-4607.

(203) Deligiannia, D. D.; Katsalaa, N.; Ladasb, S.; Sotiropouloub, D.; Amedeec, J.; Missirlisa, Y. F. *Biomaterials* **2001**, *22*, 1241–1251.

(204) Rechendorff, K.; Hovgaard, M. B.; Foss, M.; Zhdanov, V. P.; Besenbacher, F. *Langmuir* **2006**, *22*, 10885-10888.

(205) Lewinski, N.; Colvin, V.; Drezek, R. *Small* **2008**, *4*, 26-49.

(206) Warheit, D. B. *Nano Lett.* **2010**, *10*, 4777-4782.

(207) Nemmar, A.; Vanbilloen, H.; Hoylaerts, M. F.; Hoet, P. H. M.; Verbruggen, A.; Nemery, B. *Am. J. Respir. Crit. Care Med.* **2001**, *164*, 1665-1668 .

(208) Choi, H. S.; Ashitate, Y.; Lee, J. H.; Kim, S. H.; Matsui, A.; Insin, N.; Bawendi, M. G.; Semmler-Behnke, M.; Frangioni, J. V.; Tsuda, A. *Nat. Biotechnol.* **2010**, *28*, 1300-1303.

(209) Oberdörster, G.; Elder, A.; Rinderknecht, A. *J. Nanosci. Nanotechnol.* **2009**, *9*, 4996-5007.

(210) Oberdörster, G.; Oberdörster, E.; Oberdörster, J. *Environ. Health Perspect.* **2005**, *113*, 823-839.

(211) Donaldson, K.; Tran, L.; Jimenez, L. A.; Duffin, R.; Newby, D. E.; Mills, N.; MacNee, W.; Stone, V. *Part. Fibre Toxicol.* **2005**, *2*, 10-24.

(212) Xia, T.; Kovochich, M.; Brant, J.; Hotze, M.; Sempf, J.; Oberley, T.; Sioutas, C.; Yeh, J. I.; Wiesner, M. R.; Nel, A. E. *Nano Lett.* **2006**, *6*, 1794-1807.

(213) Mantell, L. L.; Horowitz, S.; Davis, J. M.; Kazzaz, J. A. *Ann. N. Y. Acad. Sci.* **2006**, *887*, 171-180.

(214) Hornung, V.; Bauernfeind, F.; Halle, A.; Samstad, E. O.; Kono, H.; Rock, K. L.; Fitzgerald, K. A.; Latz, E. *Nat. Immunol.* **2008**, *9*, 847-856.

(215) Yazdi, A. S.; Guarda, G.; Riteau, N.; Drexler, S. K.; Tardivel, A.; Couillin, I.; Tschopp, J. *Proc. Natl. Acad. Sci. USA* **2010**, *107*, 19449-19454.

(216) Lunov, O.; Syrovets, T.; Loos, C.; Nienhaus, G. U.; Mailaender, V.; Landfester, K.; Rouis, M.; Simmet, T. *ACS Nano* **2011**, *5*, 9648-9657.

(217) Lu, S.; Duffin, R.; Poland, C.; Daly, P.; Murphy, F.; Drost, E.; Macnee, W.; Stone, V.; Donaldson, K. *Environ. Health Perspect.* **2009**, *117*, 241-247.

(218) Cho, W.-S.; Duffin, R.; Thielbeer, F.; Bradley, M.; Megson, I. L.; Macnee, W.; Poland, C. A.; Tran, C. L.; Donaldson, K. *Toxicol. Sci.* **2012**, *126*, 469-477.

(219) Asati, A.; Santra, S.; Kaittanis, C.; Perez, J. M. *ACS Nano* **2010**, *4*, 5321-5331.

(220) Ruizendaal, L.; Bhattacharjee, S.; Pournazari, K.; Rosso-Vasic, M.; de Haan, L. H. J.; Alink, G. M.; Marcelis, A. T. M.; Zuilhof, H. *Nanotoxicol.* **2009**, *3*, 339-347.

(221) Xia, T.; Kovochich, M.; Liong, M.; Zink, J. I.; Nel, A. E. *ACS Nano* **2008**, *2*, 85-96.

(222) Thevenot, P.; Cho, J.; Wavhal, D.; Timmons, R. B.; Tang, L. *Nanomed. Nanotechnol. Biol. Med.* **2008**, *4*, 226-236.

(223) Donaldson, K.; Borm, P. J.; Castranova, V.; Gulumian, M. *Part. Fibre Toxicol.* **2009**, *6*, 13-21.

(224) Wallace, W. E.; Keane, M. J.; Mike, P. S.; Hill, C. A.; Vallyathan, V.; Regad, E. D. *J. Toxicol. Environ. Health* **1992**, *37*, 391-409.

(225) Bielawski, J. *Biochim. Biophys. Acta* **1990**, *1035*, 214-217.

(226) Jiao, G.-S.; Han, J. W.; Burgess, K. *J. Org. Chem.* **2003**, *68*, 8264-8267.

(227) Bycroft, B. W.; Chan, W. C.; Chhabra, S. R.; Hone, N. D. *J. Chem. Soc., Chem. Commun.* **1993**, *29*, 778-779.

(228) Gude, M.; Ryf, J.; White, P. D. *Lett. Pept. Sci.* **2002**, *9*, 203-206.

(229) Cho, W.-S.; Duffin, R.; Poland, C. A.; Howie, S. E. M.; MacNee, W.; Bradley, M.; Megson, I. L.; Donaldson, K. *Environ. Health Perspect.* **2010**, *118*, 1699-1706.

Appendices

Publications:

Reprinted with permission from Thielbeer, F., Donaldson, K. and Bradley, M. *Bioconjugate Chem.* **2011**, *22*, 144-150. Copyright 2012 American Chemical Society.

Reprinted with permission from Thielbeer, F., *Synlett*, **2012**, *23*, 1703-1704. Copyright 2012 Thieme.

Reprinted with permission from Thielbeer, F., Chankeshwara, S. V. and Bradley, M. *Biomacromolecules* **2011**, *12*, 4386-4391. Copyright 2012 American Chemical Society.